

# Chemical abundances of planetary nebulae from optical recombination lines – II. Abundances derived from collisionally excited lines and optical recombination lines

Y. Liu,<sup>1,2\*</sup> X.-W. Liu,<sup>1</sup> M. J. Barlow<sup>3</sup> and S.-G. Luo<sup>1</sup>

<sup>1</sup>*Department of Astronomy, Peking University, Beijing 100871, China*

<sup>2</sup>*Center for Astrophysics, Guangzhou University, Guangzhou 510400, China*

<sup>3</sup>*Department of Physics and Astronomy, University College London, Gower Street, London WC1E 6BT*

Accepted 2004 June 22. Received 2004 June 22; in original form 2004 April 6

## ABSTRACT

In Paper I, we presented spectrophotometric measurements of emission lines from the ultraviolet (UV) to the far-infrared for 12 Galactic planetary nebulae (PNe) and derived nebular thermal and density structures using a variety of plasma diagnostics. The measurements and plasma diagnostic results are used in the current paper to determine elemental abundances in these nebulae. Abundance analyses are carried out using both strong collisionally excited lines (CELs) and weak optical recombination lines (ORLs) from heavy element ions.

Assuming electron temperatures and densities derived from H I recombination spectra (line and continuum), we are able to determine the ORL C abundance relative to hydrogen for all the PNe in our sample, N and O abundances for 11 of them and Ne abundances for nine of them. In all cases, ORL abundances are found to be systematically higher than the corresponding values deduced from CELs. In NGC 40, the discrepancy between the abundances derived from the two types of emission line reaches a factor of 17 for oxygen. For the other 10 PNe, the discrepancies for oxygen vary from 1.6 to 3.1. In general, collisionally excited infrared fine-structure lines, which have excitation energies less than  $10^3$  K and consequently emissivities that are insensitive to electron temperature and temperature fluctuations, yield ionic abundances comparable to those derived from optical/UV CELs. For a given nebula, the discrepancies between the ORL and CEL abundances are of similar magnitude for different elements. In other words, relative abundance ratios such as C/O, N/O and Ne/O deduced from the traditional method based on strong CELs are comparable to those yielded by ORLs, for a wide range of ORL to CEL oxygen abundance ratios, varying from near unity to over a factor of 20.

We have also determined ORL abundances relative to hydrogen for the third-row element magnesium for 11 nebulae in our sample. In strong contrast to the cases for second-row elements, Mg abundances derived from the Mg II 3d–4f  $\lambda 4481$  ORL are nearly constant for all the PNe analysed so far and agree within the uncertainties with the solar photospheric value.

In accordance with results from previous studies, the ORL to CEL abundance ratio is correlated with the difference between the electron temperatures derived from the [O III] forbidden-line ratio, on the one hand, and from the hydrogen recombination Balmer discontinuity, on the other. We find that the discrepancy between the ORL and CEL abundances is correlated with nebular absolute diameter, surface brightness, the electron density derived from [S II] CELs, and excitation class. The results confirm that the dichotomy of temperatures and heavy elemental abundances determined from the two types of emission line, which has been widely observed in PNe, is a strong function of nebular evolution, as first pointed out by Garnett and Dinerstein.

\*E-mail: liuyi@bac.pku.edu.cn

Our analyses show that temperature fluctuations and/or density inhomogeneities are incapable of explaining the large discrepancies between the heavy elemental abundances and electron temperatures determined from the two types of emission line. Our analyses support the bi-abundance model of Liu et al., who have proposed that PNe contain another previously unseen component of ionized gas which, highly enriched in heavy elements, has an electron temperature of  $\lesssim 10^3$  K and emits strongly in recombination lines but not in CELs. Our determinations of low average emission temperatures from the observed line intensity ratios of He I and O II ORLs lend further support to this scenario.

**Key words:** ISM: abundances – planetary nebulae: general.

## 1 INTRODUCTION

This paper is the second part of a work devoted to the study of chemical abundances for a sample of Galactic planetary nebulae (PNe) which, together with Liu et al. (2004, hereafter Paper I), focuses on the problem of optical recombination line (ORL) emission from heavy element ions (e.g.  $C^{2+}$ ,  $N^{2+}$ ,  $O^{2+}$  and  $Ne^{2+}$ ) in PNe and H II regions. A long-standing problem in nebular astrophysics is a dichotomy between abundance determinations, whereby heavy element abundances relative to hydrogen from weak ORLs (such as C II  $\lambda 4267$ , N II  $\lambda 4041$ , O II  $\lambda \lambda 4089, 4650$ ) are systematically higher than those from (much brighter) collisionally excited lines (CELs; often collectively referred to as forbidden lines) (e.g. Peimbert, Storey & Torres-Peimbert 1993; Liu et al. 1995, 2000, 2001b; Garnett & Dinerstein 2001a; Ruiz et al. 2003; Wesson, Liu & Barlow 2003; Peimbert et al. 2004; Tsamis et al. 2004). A further problem is a dichotomy between temperature determinations whereby electron temperatures ( $T_e$ ) derived from the Balmer jump of the H I recombination spectrum are systematically lower than those derived from the collisionally excited [O III] optical forbidden-line ratio (e.g. Liu & Danziger 1993; Liu et al. 2001b).

In Paper I, we presented deep, scanned, medium-resolution optical spectra for 12 PNe. The optical data, together with ultraviolet (UV) data obtained with the *International Ultraviolet Explorer* (IUE) and infrared data obtained with the *Infrared Space Observatory* (ISO), were used to study nebular thermal and density structures. Electron temperatures and densities were derived from a variety of CEL diagnostic ratios as well as from the H I recombination spectrum, specifically from the nebular continuum Balmer discontinuity and the high- $n$  Balmer decrement.

In this paper, we undertake a detailed chemical composition analysis and contrast heavy elemental abundances derived using the traditional method based on CELs, on the one hand, and from heavy element ORLs, on the other. We will investigate whether the current PN samples show the phenomenon observed in other PNe, whereby ORL heavy element abundances are systematically higher compared to those derived from the traditional method based on CELs and, if so, the magnitude and distribution of the discrepancies, their possible links to other nebular properties, and finally the possible physical causes of the discrepancies.

In Section 2 we present heavy element abundances derived from UV, optical and infrared (IR) CELs, and He, C, N, O and Ne abundances derived from ORLs. Mg abundances derived from an ORL are also presented in this section. The results derived from

the two types of emission line are compared in Section 3 and analysed in relation to other nebular properties in Section 4. Finally, in Section 5 we investigate possible physical causes of the abundance and temperature determination discrepancies in terms of nebular inhomogeneities in temperature, density and chemical composition.

## 2 ABUNDANCE ANALYSIS

### 2.1 Ionic abundances from CELs

Ionic abundance ratios,  $X^{i+}/H^+$ , derived from collisionally excited UV, optical and IR lines for the 12 PNe in our sample are presented in Table 1. Columns 1 and 2 list the ion name and the wavelength(s) of line(s) used to determine the ionic abundance.

The inclusion of UV to far-infrared (FIR) observational data increases significantly the number of ionic species whose abundances can be determined and thus the accuracy of total abundances of individual elements. For example, UV emission lines detected by the IUE have given us access to ionic species such as: C<sup>+</sup> – [C II]  $\lambda 2326$ , C<sup>2+</sup> – [C III]  $\lambda 1908$  and C<sup>3+</sup> – [C IV]  $\lambda 1550$ ; N<sup>2+</sup> – [N III]  $\lambda 1750$  and N<sup>3+</sup> – [N IV]  $\lambda 1486$ ; O<sup>+</sup> – [O II]  $\lambda 2470$ , O<sup>2+</sup> – [O III]  $\lambda 1663$  and O<sup>3+</sup> – [O IV]  $\lambda 1401$ ; Ne<sup>3+</sup> – [Ne IV]  $\lambda 2423$ . UV observation is essential for carbon as it has no CELs in the optical and IR [except for [C II] 158  $\mu$ m, which is however dominated by emission from the photodissociated regions (PDRs) rather than the ionized regions in most PNe]. Nitrogen abundance estimates also benefit greatly from the inclusion of UV lines in the analysis, because in the optical only the abundance of the trace species N<sup>+</sup> can be determined from the [N II]  $\lambda \lambda 5754, 6548, 6584$  emission lines. The inclusion of IR fine-structure lines detectable by the ISO increases not only the total number of ionic species whose abundances can be determined but, more importantly, the analysis of IR fine-structure lines provides a key to test the paradigm of temperature fluctuations as the cause of the nebular electron temperature and abundance determination dichotomies found when using the two types of emission line – ORLs versus CELs – thanks to the very low excitation energies ( $\lesssim 10^3$  K) of IR fine-structure lines.

Ionic abundances in Table 1 were derived using the FORTRAN code EQUIB, which solves the statistical balance equations for each ion and yields level populations and line emissivities for a specified ( $T_e, N_e$ ) appropriate to the zone in a nebula where the ion is expected to exist. Once the level populations are known, the ionic abundance can be determined using the equation

**Table 1.** Ionic abundances from CELs. Numbers in parentheses are powers of 10; values followed by ‘:’ were discarded when calculating the total abundances.

Ion	$\lambda$ (Å)	Hu 1–2	IC 3568	NGC 40	NGC 6210	NGC 6572	NGC 6720
C <sup>+</sup>	2326	2.28(−5)	–	5.56(−4)	–	2.51(−5)	7.75(−5)
C <sup>++</sup>	1908	2.90(−5)	1.15(−4)	1.02(−4)	9.51(−5)	4.98(−4)	2.41(−4)
C <sup>3+</sup>	1548	1.63(−5)	1.56(−5)	≤4.04(−5)	–	–	4.76(−5)
N <sup>+</sup>	6548,84 <sup>a</sup>	1.37(−5)	1.39(−7)	7.58(−5)	2.90(−6)	7.23(−6)	6.61(−5)
	122 μm <sup>b</sup>	–	5.31(−6):	1.93(−5):	–	–	–
	122 μm <sup>c</sup>	–	1.41(−5):	4.24(−5):	–	–	3.78(−5):
N <sup>++</sup>	1750	2.64(−5)	1.81(−5):	–	5.98(−5)	1.28(−4)	8.42(−5)
	57 μm <sup>b</sup>	≤1.42(−5):	2.65(−5)	8.62(−6)	–	4.11(−5):	–
	57 μm <sup>c</sup>	≤7.08(−5):	5.58(−5):	1.48(−5):	1.17(−4):	1.06(−4)	7.63(−5)
N <sup>3+</sup>	1487	4.56(−5)	–	–	–	–	–
N <sup>4+</sup>	1238	2.16(−5)	–	–	–	–	–
O <sup>+</sup>	2470	–	–	6.89(−4):	–	3.95(−5):	1.40(−4):
	3726,29 <sup>a</sup>	1.41(−5)	1.04(−6)	4.83(−4)	1.46(−5)	1.45(−5)	1.87(−4)
	7320,30 <sup>a,d</sup>	1.90(−5):	1.29(−6):	5.56(−4):	2.15(−5):	1.73(−5):	1.94(−4):
O <sup>++</sup>	1663	3.51(−5):	1.17(−4):	≤9.89(−5):	2.98(−4):	4.96(−4):	3.57(−4):
	4931	7.64(−5):	2.16(−4):	5.93(−5):	3.65(−4):	3.14(−4):	2.53(−4):
	4959	4.35(−5)	2.43(−4)	1.20(−5)	4.23(−4)	3.47(−4)	3.02(−4)
	52,88 μm <sup>b</sup>	≤2.04(−5):	1.86(−4):	1.24(−5)	–	1.67(−4):	–
	52,88 μm <sup>c</sup>	≤7.27(−5):	3.30(−4):	1.86(−5):	9.62(−4):	4.01(−4):	3.24(−4):
O <sup>3+</sup>	1401	9.42(−5):	–	–	–	–	–
	25.9 μm <sup>b</sup>	3.97(−5)	1.02(−6)	≤1.92(−8):	–	–	–
	25.9 μm <sup>c</sup>	6.86(−5):	1.35(−6):	≤2.29(−8):	–	–	1.40(−4)
Ne <sup>+</sup>	12.8 μm <sup>b</sup>	2.76(−6):	–	1.01(−4):	–	–	–
	12.8 μm <sup>c</sup>	2.79(−6)	–	1.01(−4)	–	–	–
Ne <sup>++</sup>	3868	1.13(−5)	4.88(−5)	5.33(−7)	9.72(−5)	7.94(−5)	1.08(−4)
	15.5 μm <sup>b</sup>	1.39(−5):	6.93(−5):	5.74(−7):	–	3.13(−6):	–
	15.5 μm <sup>c</sup>	1.44(−5):	6.83(−5):	5.79(−7):	–	3.43(−6):	1.07(−4):
	36.0 μm <sup>b</sup>	–	–	–	–	1.38(−5):	–
	36.0 μm <sup>c</sup>	–	–	–	–	1.74(−5):	1.89(−4):
Ne <sup>3+</sup>	4725	1.58(−5)	–	–	–	–	5.86(−5)
Ne <sup>4+</sup>	14.3 μm <sup>b</sup>	8.14(−6)	–	–	–	–	–
	14.3 μm <sup>c</sup>	8.85(−6):	–	–	–	–	–
	24.3 μm <sup>b</sup>	9.16(−6)	–	–	–	–	–
	24.3 μm <sup>c</sup>	1.49(−5):	–	–	–	–	2.07(−6)
Ne <sup>5+</sup>	7.65 μm	2.71(−6)	–	–	–	–	–
Mg <sup>3+</sup>	4.49 μm	9.43(−7)	–	–	–	–	–
Mg <sup>4+</sup>	2783	5.22(−6)	–	–	–	–	–
	5.61 μm	6.19(−6)	–	–	–	–	–
Si <sup>++</sup>	1889	5.53(−7)	–	1.35(−6)	4.86(−6)	1.76(−6)	–
S <sup>+</sup>	4068,76 <sup>e</sup>	3.33(−7):	–	1.17(−6):	1.59(−7):	1.28(−7):	1.01(−6):
	6716,31	2.96(−7)	5.35(−9)	1.24(−6)	2.08(−7)	1.25(−7)	1.23(−6)
S <sup>++</sup>	6312 <sup>f</sup>	7.08(−7)	4.38(−7)	1.34(−6)	2.77(−6)	2.14(−6)	2.89(−6)
	18.7 μm <sup>b</sup>	–	6.81(−7):	2.73(−6):	–	1.92(−7):	–
	18.7 μm <sup>c</sup>	–	7.03(−7):	2.69(−6):	–	3.22(−7):	–
	33.5 μm <sup>b</sup>	–	–	1.46(−6):	–	8.18(−7):	–
	33.5 μm <sup>c</sup>	–	–	2.17(−6):	–	2.45(−6):	3.76(−6):
S <sup>3+</sup>	10.5 μm <sup>b</sup>	9.57(−7):	1.04(−6):	–	–	–	–
	10.5 μm <sup>c</sup>	1.14(−6)	1.12(−6)	–	–	–	2.31(−6)
Cl <sup>++</sup>	5517,37	1.31(−8)	2.06(−8)	4.19(−8)	6.80(−8)	5.40(−8)	8.78(−8)
Cl <sup>3+</sup>	5323	2.42(−8):	–	–	–	2.28(−8):	–
	7531	2.14(−8)	2.39(−8)	–	5.47(−8)	2.05(−8)	2.29(−8)
Ar <sup>+</sup>	6.99 μm <sup>b</sup>	–	–	1.37(−6):	–	–	–
	6.99 μm <sup>c</sup>	–	–	1.38(−6)	–	–	–
Ar <sup>++</sup>	7135	2.39(−7)	4.79(−7)	4.68(−7)	9.66(−7)	1.18(−6)	1.86(−6)
	8.99 μm <sup>b</sup>	–	–	8.25(−7):	–	–	–
	8.99 μm <sup>c</sup>	–	–	8.31(−7):	–	–	–
Ar <sup>3+</sup>	4740	2.91(−7)	2.82(−7)	–	2.99(−7)	2.89(−7)	2.05(−7)
Ar <sup>4+</sup>	6435,7006	1.68(−7)	–	–	–	–	1.74(−8)
Ar <sup>5+</sup>	4.53 μm	1.03(−7)	–	–	–	–	–
Fe <sup>++g</sup>	4658	2.38(−8)	2.25(−8)	1.74(−7)	7.24(−8)	6.44(−8)	5.18(−8)
	22.9 μm	–	–	2.56(−7):	–	–	–
Fe <sup>3+</sup>	various	–	–	2.04(−6)	7.03(−7)	1.30(−6)	1.34(−6)

**Table 1** – *continued*

Ion	$\lambda$ (Å)	NGC 6741	NGC 6781	NGC 6790	NGC 6826	NGC 6884	NGC 7662
C <sup>+</sup>	2326	1.66(−4)	–	5.28(−6)	4.09(−5)	2.30(−5)	9.46(−6)
C <sup>++</sup>	1908	2.47(−4)	–	1.52(−4)	2.47(−4)	2.92(−4)	9.91(−5)
C <sup>3+</sup>	1548	1.32(−4)	–	–	–	4.85(−5)	1.21(−4)
N <sup>+</sup>	6548,84 <sup>a</sup>	4.50(−5)	5.61(−5)	1.28(−6)	2.46(−6)	4.77(−6)	6.98(−7)
	122 $\mu\text{m}^b$	–	–	–	–	–	–
N <sup>++</sup>	1750	1.29(−4)	6.80(−5):	2.80(−5)	7.74(−5)	1.06(−4)	8.21(−6):
	57 $\mu\text{m}^b$	4.03(−5):	–	–	5.59(−5)	2.41(−5):	1.73(−5)
	57 $\mu\text{m}^c$	5.66(−5):	1.74(−4)	–	8.68(−5):	8.34(−5)	3.96(−5):
N <sup>3+</sup>	1487	6.02(−5)	–	–	–	–	3.05(−5)
N <sup>4+</sup>	1238	1.73(−4)	–	–	–	–	1.15(−5)
O <sup>+</sup>	2470	1.87(−3):	–	–	–	–	4.28(−6):
	3726,29 <sup>d</sup>	1.03(−4)	1.57(−4)	4.63(−6)	2.48(−5)	1.07(−5)	3.18(−6)
O <sup>++</sup>	7320,30 <sup>a,d</sup>	1.13(−4):	1.50(−4):	4.11(−6):	4.26(−5):	1.17(−5):	4.70(−6):
	1663	2.48(−4):	–	2.27(−4):	3.05(−4):	4.49(−4):	7.62(−5):
	4931	2.91(−4):	–	2.21(−4):	2.70(−4):	3.09(−4):	1.72(−4):
	4959	2.56(−4)	2.73(−4)	2.44(−4)	3.29(−4)	3.62(−4)	1.79(−4)
	52,88 $\mu\text{m}^b$	1.03(−4):	–	–	2.86(−4):	1.26(−4):	1.80(−4):
	52,88 $\mu\text{m}^c$	1.39(−4):	6.23(−4):	1.52(−4):	4.03(−4):	3.64(−4):	3.49(−4):
O <sup>3+</sup>	1401	7.22(−4):	–	–	–	–	1.88(−4):
	25.9 $\mu\text{m}^b$	4.95(−5):	–	–	–	1.53(−5):	9.15(−5)
	25.9 $\mu\text{m}^c$	6.09(−5)	1.33(−5)	2.48(−6)	–	3.18(−5)	1.31(−4):
Ne <sup>+</sup>	12.8 $\mu\text{m}^b$	1.12(−5):	–	–	–	–	9.62(−7):
	12.8 $\mu\text{m}^c$	1.12(−5)	–	–	–	–	9.68(−7)
Ne <sup>++</sup>	3868	7.02(−5)	1.03(−4)	5.13(−5)	6.49(−5)	8.74(−5)	3.20(−5)
	15.5 $\mu\text{m}^b$	7.26(−5):	–	–	5.54(−5):	4.51(−5):	3.98(−5):
	15.5 $\mu\text{m}^c$	7.39(−5):	3.73(−4):	3.28(−5):	5.61(−5):	4.78(−5):	4.08(−5):
	36.0 $\mu\text{m}^b$	8.58(−5):	–	–	–	8.49(−5):	5.80(−5):
	36.0 $\mu\text{m}^c$	8.97(−5):	–	3.33(−5):	–	9.93(−5):	6.16(−5):
Ne <sup>3+</sup>	2423	6.64(−5):	–	–	–	2.91(−5):	3.08(−5):
	4725	8.42(−5)	–	1.43(−6)	–	5.21(−5)	4.30(−5)
Ne <sup>4+</sup>	14.3 $\mu\text{m}^b$	2.51(−6)	–	–	–	–	1.20(−6)
	14.3 $\mu\text{m}^c$	2.66(−6):	–	–	–	–	1.28(−6):
	24.3 $\mu\text{m}^b$	4.19(−6)	–	–	–	–	1.95(−6)
	24.3 $\mu\text{m}^c$	5.17(−6):	–	–	–	–	2.73(−6):
Mg <sup>3+</sup>	4.49 $\mu\text{m}$	1.43(−6)	–	–	–	–	8.50(−6)
Mg <sup>4+</sup>	2783	–	–	–	–	–	9.15(−7)
	5.61 $\mu\text{m}$	1.28(−6)	–	–	–	–	1.16(−6)
Si <sup>++</sup>	1889	–	–	–	2.14(−6)	9.44(−7)	4.78(−7)
S <sup>+</sup>	4068,76 <sup>e</sup>	1.25(−6):	8.08(−7):	5.14(−8):	4.71(−8):	2.09(−7):	6.20(−8):
	6716,31	1.34(−6)	9.35(−7)	7.10(−8)	5.06(−8)	1.43(−7)	4.80(−8)
S <sup>++</sup>	6312 <sup>f</sup>	2.71(−6)	2.78(−6)	8.50(−7)	1.82(−6)	1.89(−6)	9.51(−7)
	18.7 $\mu\text{m}^b$	2.57(−6):	–	–	1.37(−6):	1.29(−6):	1.26(−6):
	18.7 $\mu\text{m}^c$	2.89(−6):	–	–	1.42(−6):	1.86(−6):	1.40(−6):
	33.5 $\mu\text{m}^b$	3.88(−6):	–	–	2.01(−6):	–	6.51(−7):
	33.5 $\mu\text{m}^c$	5.61(−6):	–	–	3.11(−6):	–	1.34(−6):
S <sup>3+</sup>	10.5 $\mu\text{m}^b$	5.19(−7):	–	–	5.89(−7):	1.83(−6):	2.29(−6):
	10.5 $\mu\text{m}^c$	5.61(−7)	5.72(−6)	6.19(−7)	6.20(−7)	2.41(−6)	2.56(−6)
Cl <sup>++</sup>	5517,37	6.16(−8)	7.92(−8)	1.95(−8)	6.55(−8)	6.06(−8)	2.82(−8)
Cl <sup>3+</sup>	5323	–	–	2.32(−8):	–	–	5.39(−8):
	7531	2.29(−8)	–	2.25(−8)	1.08(−8)	4.85(−8)	6.15(−8)
Ar <sup>++</sup>	7135	1.42(−6)	1.61(−6)	3.25(−7)	1.11(−6)	9.96(−7)	4.32(−7)
	8.99 $\mu\text{m}^b$	8.67(−7):	–	–	6.01(−7):	9.01(−7):	4.68(−7):
	8.99 $\mu\text{m}^c$	8.79(−7):	–	1.63(−7):	6.05(−7):	9.43(−7):	4.77(−7):
Ar <sup>3+</sup>	4740	5.56(−7)	1.12(−7)	2.24(−7)	8.48(−8)	7.23(−7)	5.30(−7)
Ar <sup>4+</sup>	6435,7006	1.34(−7)	–	–	–	2.88(−8)	8.21(−8)
	7.91 $\mu\text{m}$	–	–	–	–	–	2.10(−6):
Ar <sup>5+</sup>	4.53 $\mu\text{m}$	2.37(−8)	–	–	–	–	1.77(−8)
Fe <sup>++g</sup>	4658	2.82(−7)	–	3.37(−8)	8.03(−8)	8.42(−8)	5.99(−8)
Fe <sup>3+</sup>	various	–	–	6.12(−8)	2.98(−7)	2.13(−7)	1.48(−7)

Notes. <sup>a</sup>Corrected for contributions from recombination excitation. <sup>b</sup>Assuming  $N_e$  derived from the [O III] 52- $\mu\text{m}$ /88- $\mu\text{m}$  ratio. <sup>c</sup>Assuming the average  $N_e$  yielded by various optical diagnostics. <sup>d</sup>Corrected for contribution from the [Ar IV]  $\lambda$ 7331.40 line assuming  $I(\lambda 7331.40)/I(\lambda 7262.76) = 0.196$ . <sup>e</sup>Corrected for contributions from O II V10 and C III V16 using a synthetic recombination line spectrum. <sup>f</sup>Corrected for contributions from the He II  $\lambda$ 6310.80 line using a synthetic recombination line spectrum. <sup>g</sup>Upper limit as the  $\lambda$ 4658 line could be contaminated by C IV  $\lambda$ 4658, especially in high-excitation PNe.

$$\frac{N(X^{m+})}{N(H^+)} = \frac{N_e h\nu_{42} \alpha_{\text{eff}}(H\beta)}{A_{ij} n_i E_{ij}} \frac{I(\lambda)}{I(H\beta)}$$

Here,  $I(\lambda)$  is the dereddened flux of an emission line of wavelength  $\lambda$  emitted by ion  $X^{m+}$  from upper level  $i$  to  $j$  following collisional excitation by electron impacts,  $A_{ij}$  is the Einstein spontaneous transition probability of the transition,  $n_i$  is the fractional population of upper level  $i$ ,  $E_{ij}$  is the photon energy of the emission line,  $\alpha_{\text{eff}}(H\beta)$  is the effective recombination coefficient of  $H\beta$  and  $h\nu_{42}$  is energy of an  $H\beta$  photon.

For nebular abundance analyses using the traditional method based on CELs,  $T_e(\text{N II})$  is generally assumed for singly ionized species and  $T_e(\text{O III})$  for ions of higher ionization degrees. However, electron temperatures derived from the  $[\text{N II}]$  and  $[\text{O II}]$  nebular to auroral line ratios can be overestimated due to contamination of the  $[\text{N II}]$  and  $[\text{O II}]$  auroral lines by recombination excitation (Rubin 1986; Liu et al. 2000). In Paper I, we presented  $T_e(\text{N II})$  deduced after correcting the effects of recombination excitation. In the current work, we have adopted the corrected  $T_e(\text{N II})$  for ionic species with ionization potentials lower than 20 eV (essentially all singly ionized species) and  $T_e(\text{O III})$  for ions with higher ionization potentials (essentially all ionic species other than those that are singly ionized). In calculating  $\text{N}^+/\text{H}^+$  and  $\text{O}^+/\text{H}^+$  from the measured intensities of the  $[\text{N II}]$  and  $[\text{O II}]$  nebular lines, we have also corrected for the recombination contributions to these lines. The various adopted  $T_e$  values are listed for each nebula in table 8 of Paper I.

For electron densities, we have adopted mean values deduced from various optical diagnostics, as listed in table 7 of Paper I. However, for FIR fine-structure lines with relatively low critical densities, such as the  $[\text{N II}]$  122- $\mu\text{m}$ ,  $[\text{N III}]$  57- $\mu\text{m}$  and  $[\text{O III}]$  52-, 88- $\mu\text{m}$  lines, densities deduced from the  $[\text{O III}]$  88- $\mu\text{m}/52\text{-}\mu\text{m}$  ratio were used for PNe with low densities [ $\log N_e([\text{Ar IV}]) < 3.9 \text{ cm}^{-3}$ ]. For a given nebula, the  $[\text{O III}]$  88- $\mu\text{m}/52\text{-}\mu\text{m}$  ratio typically yields a lower density compared to the mean value given by optical density-diagnostic line ratios, suggesting moderate density inhomogeneities (Liu et al. 2001a). For the majority of the other abundance diagnostic lines listed in Table 1, the differences between ionic abundances deduced assuming these two densities are negligible, owing to their high critical densities. For comparison, ionic abundances derived from IR fine-structure lines assuming the higher density yielded by optical density-diagnostics are also provided in Table 1.

## 2.2 Ionic abundances from ORLs

In the following subsections, we present ionic abundances for He, C, N, O, Ne and Mg derived for 11 PNe from ORLs. Electron temperatures derived from the H I recombination Balmer discontinuity were adopted in the calculations. For the electron density, the mean values deduced from various optical diagnostics have been assumed for each nebula, i.e. the same as those adopted for the CEL abundance analysis. As pointed out in Paper I, for the nebulae in our sample, the high-order H I Balmer lines yield densities comparable to those given by the CEL optical density-diagnostic ratios. Ionic abundances relative to hydrogen deduced from ORLs depend only weakly on electron temperature, and are essentially independent of electron density under the low-density conditions prevailing in most nebulae.

The ionic abundances deduced from ORLs for each nebula are presented in Tables 2–12, respectively. The atomic data used are the same as described by Liu et al. (2000), except for  $\text{He}^+/\text{H}^+$  and

**Table 2.** Ionic abundances from ORLs – Hu 1–2. We assume  $T_e = 18900 \text{ K}$  and  $N_e = 4500 \text{ cm}^{-3}$ . Numbers in parentheses are powers of 10.

Ion	$\lambda_0$ (Å)	Multiplet	$I_{\text{obs}}$	$X^{i+}/\text{H}^+$
$\text{He}^+$	5875.66	V11	8.27	0.040
	4471.50	V14	3.19	0.047
	6678.16	V46	2.11	0.052
		Mean		0.043
$\text{He}^{++}$	4685.68	3.4	96.9	0.088
	<b>Sum</b>			0.131
$\text{C}^{++}$	4267.15	V6	0.109	1.05(−4)
$\text{C}^{+3}$	4647.42,50.25,51.47	V1	0.123	3.37(−5)
	4186.90	V18	0.142	1.52(−4):
		Mean		3.37(−5)
$\text{N}^{++}$	5666.63	V3	0.063	2.35(−4)
	5676.02	V3	0.038	3.22(−4)
	5679.56	V3	0.143	2.88(−4)
	5686.21	V3	0.027	3.10(−4)
	5710.77	V3	0.021	3.51(−4)
		V3	0.294	2.84(−4)
	4601.48	V5	0.016	1.76(−4)
	4613.87	V5	0.023	4.27(−4)
	4621.39	V5	0.023	3.19(−4)
	4630.54	V5	0.092	3.41(−4)
	4643.09	V5	0.016	1.82(−4)
		V5	0.192	2.96(−4)
	4788.13	V20	0.009	1.80(−4)
	4803.29	V20	0.014	1.55(−4)
	V20	0.035	1.64(−4)	
	5940.24,1.65	V28	0.021	1.35(−4)
		3d–4f transitions		
	4041.31,3.53	V39a,b	0.023	1.06(−4)
	4176.16	V43a	0.014	2.44(−4)
	4241.24,78	V48a	0.035	4.23(−4)
	4431.82,2.74,3.48	V55a,a,b	0.019	3.48(−4)
		Sum	0.080	1.06(−4)
		Mean		1.06(−4)
$\text{N}^{+3}$	4378.99,9.20	V18	0.199	8.85(−5)
$\text{O}^{++}$	4649.13,50.84	V1	0.049	7.06(−5)
	4676.24	V1	0.065	5.07(−4)
		V1	0.101	7.06(−5)
	4349.43	V2	0.015	7.08(−5)
		V2	0.042	7.08(−5)
	4129.32,32.80	V19	0.021	3.35(−4)
	4153.40	V19	0.024	3.03(−4)
		V19	0.066	3.17(−4)
		3d–4f transitions		
	4273–78	V53c,67	0.022	1.79(−4)
	4315–20	V2,53a,63c,78b	0.048	2.57(−4)
	4609.44,10.20	V92a,c	0.027	5.02(−4)
		Sum	0.213	2.32(−4)
		Mean		7.07(−5)
$\text{Mg}^{++}$	4481.21	V4	0.035	3.34(−5)

$\text{N}^{2+}/\text{H}^+$ . For He I lines, we have adopted the emissivities given in Benjamin, Skillman & Smits (1999) who combined the effective recombination coefficients calculated by Smits (1996) for some selected He I lines and the collisional excitation rates from the  $2s^3S$  metastable level of Sawey & Berrington (1993). For  $\text{N}^{2+}/\text{H}^+$ , the more recent calculations of the effective recombination coefficients for N II lines by Kisielius & Storey (2002) have been used, except

**Table 3.** Ionic abundances from ORLs – IC 3568. We assume  $T_e = 9490$  K and  $N_e = 2000 \text{ cm}^{-3}$ . Numbers in parentheses are powers of 10.

Ion	$\lambda_0$	Multiplet	$I_{\text{obs}}$	$X^{i+}/H^+$
He <sup>+</sup>	5875.66	V11	13.8	0.094
	4471.50	V14	5.20	0.101
	6678.16	V46	3.72	0.092
		Mean		0.095
He <sup>++</sup>	4685.68	3.4	1.26	0.001
	Sum			0.096
C <sup>++</sup>	7231.32	V3	0.040	9.75(−5)
	7236.42,7.17	V3	0.084	1.02(−4)
		V3	0.136	1.00(−4)
	4267.15	V6	0.315	3.00(−4)
	6461.95	V17.04	0.043	3.96(−4)
		Mean		3.00(−4)
C <sup>+3</sup>	4647.42,50.25,51.47	V1	0.171	5.24(−5)
N <sup>++</sup>	5666.63	V3	0.028	1.28(−4)
	5676.02	V3	0.009	9.19(−5)
	5679.56	V3	0.024	6.00(−5)
	5686.21	V3	0.021	2.92(−4)
		V3	0.087	1.04(−4)
	4630.54	V5	0.026	1.18(−4)
		V5	0.062	1.18(−4)
	Mean		1.10(−4)	
N <sup>+3</sup>	4378.99,9.20	V18	0.056	2.36(−5)
O <sup>++</sup>	4661.63	V1	0.068	5.17(−4)
	4676.24	V1	0.062	5.60(−4)
		V1	0.666	5.37(−4)
	4317.14	V2	0.058	7.68(−4)
	4319.63	V2	0.047	5.77(−4)
	4366.89	V2	0.079	9.90(−4)
		V2	0.359	6.68(−4)
	4414.90,16.97	V5	0.045	5.68(−4)
		V5	0.049	5.68(−4)
	4072.16	V10	0.097	4.06(−4)
	4075.86	V10	0.126	3.66(−4)
		V10	0.366	3.82(−4)
	4132.80	V19	0.034	6.22(−4)
		V19	0.128	6.22(−4)
		3d–4f transitions		
	4088.27,9.29,7.15	V48a,c	0.061	4.26(−4)
	4083.90	V48b	0.028	8.69(−4)
	4273–78	V67	0.077	5.47(−4)
	4281–84	V53,67	0.030	7.57(−4)
	4303.82,61,4.08	V53a,67	0.035	6.58(−4)
4294.78,92	V53b	0.021	6.59(−4)	
4609.44,10.20	V92a,c	0.042	6.66(−4)	
	Sum	0.619	5.85(−4)	
	Mean		5.34(−4)	
Ne <sup>++</sup>	3694.21	V1	0.094	2.84(−4)
	3766.26	V1	0.053	3.78(−4)
	3777.14	V1	0.044	3.40(−4)
		V1	0.300	3.18(−4)
	3829.75	V39	0.039	3.14(−4)
		V39	0.066	3.14(−4)
		3d–4f transitions		
	4457.05,24	V61d,66c	0.026	3.04(−4)
		Mean		3.12(−4)
	Mg <sup>++</sup>	4481.21		0.042

**Table 4.** Ionic abundances from ORLs – NGC 40. We assume  $T_e = 7020$  K and  $N_e = 1200 \text{ cm}^{-3}$ . Numbers in parentheses are powers of 10.

Ion	$\lambda_0$	Multiplet	$I_{\text{obs}}$	$X^{i+}/H^+$
He <sup>+</sup>	5875.66	V11	9.20	0.062
	4471.50	V14	3.15	0.061
	6678.16	V46	2.52	0.059
		Mean		0.062
He <sup>++</sup>	4685.68	3.4	0.044	3.40(−5)
	Sum			0.062
C <sup>++</sup>	7231.32	V3	0.360	8.55(−4)
	7236.42,7.17	V3	0.595	7.07(−4)
		V3	0.955	7.56(−4)
	3918.98	V4	0.200	1.26(−2)
	3920.69	V4	0.404	1.26(−2)
		V4	0.604	1.26(−2)
	4267.15	V6	0.667	5.96(−4)
	4491.13,22		0.015	6.68(−4)
	6151.43	V16.04	0.032	7.21(−4)
	6461.95	V17.04	0.068	5.90(−4)
	5342.40	V17.06	0.050	8.50(−4)
		Mean		5.96(−4)
	N <sup>++</sup>	5666.63	V3	0.042
5676.02		V3	0.013	1.42(−4)
5679.56		V3	0.088	2.24(−4)
5686.21		V3	0.014	1.99(−4)
5710.77		V3	0.009	1.91(−4)
		V3	0.167	2.04(−4)
3994.99		V12	0.024	3.35(−4)
5927.81		V28	0.012	4.24(−4)
5931.78		V28	0.033	5.07(−4)
5940.24,1.65		V28	0.047	3.24(−4)
		V28	0.102	3.87(−4)
		3d–4f transitions		
4035.08		V39a	0.038	3.94(−4)
4043.53,1.31		V39a,b	0.073	2.55(−4)
4176.16		V43a	0.021	2.80(−4)
4236.91,7.05		V48a,b	0.018	1.57(−4)
4241.24,78		V48a	0.023	2.18(−4)
4431.82,2.74,3.48	V55a,b	0.010	1.35(−4)	
4442.02	V55a	0.008	2.97(−4)	
4552.53	V58a	0.023	8.56(−4)	
4530.41	V58b	0.015	1.39(−4)	
	Sum	0.245	2.25(−4)	
	Mean		2.15(−4)	
O <sup>++</sup>	4638.86	V1	0.043	4.23(−4)
	4349.43	V2	0.037	1.97(−4)
	4366.89	V2	0.023	2.91(−4)
		V2	0.120	2.25(−4)
		3d–4f transitions		
	4088.27,9.29,7.15	V48a,c	0.022	1.45(−4)
4273–78	V67	0.039	2.59(−4)	
	Sum	0.228	2.02(−4)	
	Mean		2.14(−4)	
Mg <sup>++</sup>	4481.21	V4	0.023	2.09(−5)

for lines from 3d–4f configurations, for which we have adopted the same atomic data as used by Liu et al. (2000).

### 2.2.1 He<sup>+</sup>/H<sup>+</sup> and He<sup>2+</sup>/H<sup>+</sup>

Singly and doubly ionized helium abundances were derived from the He I  $\lambda 4471$ ,  $\lambda 5876$  and  $\lambda 6678$  and He II  $\lambda 4686$  recombination

**Table 5.** Ionic abundances from ORLs – NGC 6210. We assume  $T_e = 9300$  K and  $N_e = 4400 \text{ cm}^{-3}$ . Numbers in parentheses are powers of 10.

Ion	$\lambda_0$	Multiplet	$I_{\text{obs}}$	$X^{i+}/H^+$	
He <sup>+</sup>	5875.66	V11	13.9	0.093	
	4471.50	V14	5.22	0.101	
	6678.16	V46	4.03	0.099	
		Mean		0.096	
He <sup>++</sup>	4685.68	3.4	1.49	0.001	
	Sum			0.097	
C <sup>++</sup>	7231.32	V3	0.038	9.25(−5)	
	7236.42,7.17	V3	0.089	1.07(−4)	
		V3	0.136	1.00(−4)	
	3918.98,20.69	V4	0.033	6.09(−4)	
	4267.15	V6	0.336	3.20(−4)	
	6151.43	V16.04	0.019	4.39(−4)	
	6461.95	V17.04	0.034	3.13(−4)	
	5342.40	V17.06	0.045	8.04(−4)	
		Mean		3.20(−4)	
	C <sup>+3</sup>	4647.42,50.25,51.47	V1	0.141	4.31(−5)
		4186.90	V18	0.069	1.04(−4)
		Mean		4.31(−5)	
N <sup>++</sup>	5666.63	V3	0.028	1.31(−4)	
	5676.02	V3	0.010	1.07(−4)	
	5679.56	V3	0.048	1.19(−4)	
	5686.21	V3	0.014	1.89(−4)	
	5710.77	V3	0.006	1.18(−4)	
		V3	0.107	1.27(−4)	
	4607.16	V5	0.015	2.67(−4)	
	4630.54	V5	0.019	8.85(−5)	
		V5	0.076	1.45(−4)	
	3994.99	V12	0.017	2.03(−4)	
	4788.13	V20	0.008	1.77(−4)	
	4803.29	V20	0.013	1.64(−4)	
		V20	0.035	1.77(−4)	
	5940.24,1.65	V28	0.020	1.42(−4)	
		V28	0.037	1.42(−4)	
		3d–4f transitions			
	4035.08	V39a	0.017	1.91(−4)	
	4041.31,3.53,4.78	V39a,b	0.022	7.83(−5)	
	4176.16	V43a	0.006	8.53(−5)	
	4236.91,7.05	V48a,b	0.018	1.66(−4)	
	4241.24,78	V48a	0.030	3.06(−4)	
	4431.82,2.74,3.48	V55a,b	0.017	2.59(−4)	
	4442.02	V55a	0.010	4.03(−4)	
	4552.53	V58a	0.017	6.75(−4)	
	4530.41	V58b	0.020	1.92(−4)	
		Sum	0.176	1.86(−4)	
		Mean		1.63(−4)	
	N <sup>+3</sup>	4378.99,9.20	V18	0.078	3.26(−5)
	O <sup>++</sup>	4638.86	V1	0.101	9.76(−4)
		4649.13,50.84	V1	0.502	8.40(−4)
		4661.63	V1	0.150	1.14(−3)
		4673.73	V1	0.028	1.36(−3)
4676.24,7.07		V1,91	0.114	1.00(−3)	
4696.35		V1,89a	0.016	1.14(−3)	
		V1	1.17	9.46(−4)	
4319.63		V2	0.052	6.42(−4)	
4324.79,5.76,7.59		V2,63b,75c	0.022	1.32(−3)	
4349.43		V2	0.119	6.36(−3)	
4366.53,79,89,9.28		V2,26,75a	0.070	8.21(−4)	
		V2	0.399	7.44(−4)	
4414.90		V5	0.062	1.22(−3)	
4416.97		V5	0.070	2.47(−3)	

**Table 5 – continued**

Ion	$\lambda_0$	Multiplet	$I_{\text{obs}}$	$X^{i+}/H^+$
Ne <sup>++</sup>	4452.37	V5	0.011	1.92(−3)
		V5	0.160	1.89(−4)
	3945.04	V6	0.006	1.22(−3)
	3954.36	V6	0.015	1.41(−3)
	3982.71	V6	0.007	1.42(−3)
		V6	0.064	1.37(−3)
	4071.23,2.16	V48a,10	0.292	1.13(−3)
	4083.9,4.65,5.11	V48b,21,10	0.107	1.38(−3)
	4092.93,4.14	V10	0.040	1.14(−3)
		V10	1.14	1.19(−3)
	3907.46	V11	0.015	1.46(−3)
		V11	0.027	9.67(−4)
	3842.82,3.51	V12,13	0.007	1.25(−3)
	3847.89	V12	0.007	1.65(−3)
	3851.03,47	V12,13	0.011	1.35(−3)
	3856.13,7.17	V12,13	0.026	3.47(−3)
	3882.19,45,3.13	V12,11	0.034	8.24(−4)
		V12	0.096	1.26(−3)
	4129.32	V19	0.020	3.13(−3)
	4132.80	V19	0.073	1.35(−3)
	4153.30	V19	0.103	1.33(−3)
	4156.53	V19	0.059	4.78(−3)
		V19	0.275	1.34(−3)
	4108.75-12.02	V48c,20,21	0.033	1.05(−3)
		V20	0.229	1.05(−3)
	4699.22	V25	0.014	2.09(−3)
	4705.35	V25	0.014	1.33(−3)
		V25	0.030	1.71(−3)
	4890.86	V28	0.015	1.33(−3)
	4906.83	V28	0.034	1.38(−3)
	4924.53	V28	0.070	1.66(−3)
		V28	0.121	1.54(−3)
		3d–4f transitions		
4087.15,8.27,9.29	V48c,a	0.161	1.12(−3)	
4046.11,7.8,8.21	V50a,b	0.014	1.57(−3)	
4061.21,22,75,2.94	V46c,50a	0.023	1.65(−3)	
4303.61,83,4.08	V53a,65a	0.089	1.65(−3)	
4315-7.7	V2,53a,62c,78b	0.098	1.03(−3)	
4294.78,92	V53b	0.052	1.63(−3)	
4305.39,7.23,9.0	V53b,55,63c	0.023	9.53(−4)	
4273-78	V53c,67a,b	0.150	1.06(−3)	
4281-89	V53b,c,67c,78a,b	0.073	1.03(−3)	
4291.25,86,2.21,95	V55,78c	0.061	2.15(−3)	
4371.25,62	V76b	0.015	1.32(−3)	
4312.11,3.44	V78a	0.028	1.37(−3)	
4477.90	V88	0.013	1.33(−3)	
4669.27,43	V89b	0.009	2.03(−3)	
4609.44,10.20	V92a,c	0.077	1.22(−3)	
4602.13	V92b	0.030	1.56(−3)	
	Sum	1.38	1.30(−3)	
	Mean		1.29(−3)	
Ne <sup>++</sup>	3664.07	V1	0.039	2.73(−4)
	3694.21	V1	0.126	3.71(−4)
	3766.26	V1	0.054	3.89(−4)
	3777.14	V1	0.039	3.01(−4)
		V1	0.323	3.44(−4)
		V1	0.007	1.05(−4)
	4772.93	3d–4f transitions		
	4217.17,9.75	V52a,b	0.043	4.93(−4)
	4231.64,3.85	V52a,b	0.013	5.05(−4)
	4250.64	V52b	0.004	5.15(−4)
	4391.99,2.00	V55e	0.045	4.70(−4)
	4409.30	V55e	0.044	6.83(−4)

**Table 5** – *continued*

Ion	$\lambda_0$	Multiplet	$I_{\text{obs}}$	$X^{i+}/H^+$
	4397.99	V57b	0.018	5.39(−4)
	4428.61	V60c	0.033	1.14(−3)
	4430.94	V61a	0.018	1.91(−3)
	4457.05,24	V61d,66c	0.010	1.11(−4)
	4413.22	V65	0.012	5.31(−4)
	4421.39	V66c	0.005	5.37(−4)
		Sum	0.238	5.45(−4)
		Mean		3.44(−4)
Mg <sup>++</sup>	4481.21	V4	0.020	1.90(−5)

lines, respectively. Case A recombination was assumed for the triplet He I lines,  $\lambda 4471$  and  $\lambda 5876$ , and case B for the singlet  $\lambda 6678$  line. He<sup>+</sup>/H<sup>+</sup> abundance ratios derived from the three He I lines were then averaged, weighted by 1 : 3 : 1, roughly the intrinsic intensity ratios of the three lines. Only the He II  $\lambda 4686$  line was used to calculate He<sup>2+</sup>/H<sup>+</sup> abundance ratio.

For the low surface brightness nebula NGC 6781, assuming  $T_e = 10\,200$  K and  $N_e = 240$  cm<sup>−3</sup>, as derived from the [O III] optical forbidden-line ratio and optical density-diagnostic ratios, then the observed intensities of the He I  $\lambda\lambda 4471$ , 5876 and 6678 lines yield He<sup>+</sup>/H<sup>+</sup> = 0.115, 0.115 and 0.108, respectively, which, weighted by 1 : 3 : 1, give an average He<sup>+</sup>/H<sup>+</sup> ionic abundance ratio of 0.113. Similarly, from the observed intensity of the He II  $\lambda 4686$  line, we obtain He<sup>2+</sup>/H<sup>+</sup> = 0.007.

### 2.2.2 C<sup>2+</sup>/H<sup>+</sup> and C<sup>3+</sup>/H<sup>+</sup>

C<sup>2+</sup>/H<sup>+</sup> abundance ratios have been derived from C II ORLs for all the PNe in our sample. The upper levels of multiplets V3 and V4 can cascade directly to the C II 2p<sup>2</sup>P<sup>o</sup> ground level and thus their emissivities depend strongly on the optical depths of C II resonance lines. Here we have assumed case B recombination for multiplets V3 and V4.

For several nebulae in our sample, C<sup>2+</sup>/H<sup>+</sup> abundances derived from multiplets V3 and V4 differ significantly from the value yielded by multiplet V6. Multiplet V3 is found to yield values smaller than those given by multiplet V6 at 4267 Å, the emissivity of the latter is essentially case-insensitive, suggesting that for multiplet V4 there is some departure from case B recombination. Similar phenomena have been observed previously in NGC 6153 (Liu et al. 2000), and in M 1–42 and M 2–36 (Liu et al. 2001b). In some PNe, the multiplet V4 doublet is partially affected by line blending with the He II line at 3923.48 Å. For six PNe in our sample, C<sup>2+</sup>/H<sup>+</sup> abundance ratios derived from multiplet V4 are higher than those derived from multiplet V6. Kaler (1972) suggests that that V4 is mainly excited by fluorescence by starlight such that its strength reflects the abundance of C<sup>+</sup>/H<sup>+</sup> rather than C<sup>++</sup>/H<sup>+</sup> in the nebula. The suggestion is however not supported by the recent careful measurements for NGC 6153, M 1–42 and M 2–36, where in all cases multiplet V4 yields compatible or even slightly lower C<sup>++</sup>/H<sup>+</sup> abundance ratios compared to those derived from multiplet V6.

In NGC 6153, several high-excitation C II ORLs, including two lines from the 4f–ng series which feeds the 3d–4f  $\lambda 4267$  line,  $\lambda 6462$  ( $n = 6$ ) and  $\lambda 5342$  ( $n = 7$ ), as well as 4p–5d  $\lambda 6259$  and 4d–6f  $\lambda 6151$ , were detected by Liu et al. (2000). The observed intensities relative to  $\lambda 4267$  were in good agreement with the predictions of recombination theory. These high-excitation lines have also been detected

**Table 6.** Ionic abundances from ORLs – NGC 6572. We assume  $T_e = 11\,000$  K and  $N_e = 15\,000$  cm<sup>−3</sup>. Numbers in parentheses are powers of 10.

Ion	$\lambda_0$	Multiplet	$I_{\text{obs}}$	$X^{i+}/H^+$	
He <sup>+</sup>	5875.66	V11	16.6	0.103	
	4471.50	V14	5.93	0.109	
	6678.16	V46	3.99	0.098	
		Mean		0.103	
He <sup>++</sup>	4685.68	3.4	0.412	3.47(−4)	
	Sum			0.104	
C <sup>++</sup>	7231.32	V3	0.098	2.38(−4)	
	7236.42,7.17	V3	0.227	2.75(−4)	
		V3	0.325	2.62(−4)	
	3918.98,20.69	V4	0.061	1.01(−3)	
	4267.15	V6	0.517	5.12(−4)	
	6151.43	V16.04	0.026	5.89(−4)	
	6461.95	V17.04	0.056	5.34(−4)	
	5342.40	V17.06	0.026	1.02(−4)	
		Mean		5.12(−4)	
	C <sup>3+</sup>	4647.42,50.25,51.47	V1	0.142	4.29(−5)
	4186.90	V18	0.059	8.61(−5)	
		Mean		4.29(−5)	
	N <sup>++</sup>	5666.63	V3	0.034	1.52(−4)
5676.02		V3	0.011	1.13(−4)	
5679.56		V3	0.056	1.36(−4)	
5686.21		V3	0.014	1.93(−4)	
5710.77		V3	0.011	2.21(−4)	
		V3	0.127	1.47(−4)	
4601.48		V5	0.010	1.36(−4)	
4607.16		V5	0.020	3.40(−4)	
4613.87		V5	0.015	3.30(−4)	
4621.39		V5	0.017	2.80(−4)	
4630.54		V5	0.048	2.14(−4)	
		V5	0.142	2.62(−4)	
3994.99		V12	0.020	2.10(−4)	
4788.13		V20	0.011	2.38(−4)	
		V20	0.046	2.38(−4)	
5927.81		V28	0.007	2.39(−4)	
5931.78		V28	0.013	2.05(−4)	
5940.24,1.65		V28	0.013	9.32(−5)	
		V28	0.037	1.41(−4)	
		3d–4f transitions			
		4035.08	V39a	0.013	1.52(−4)
		4043.53,4.78	V39a	0.012	1.01(−4)
		4041.31	V39b	0.027	1.87(−4)
	4176.16	V43a	0.002	3.11(−4)	
	4241.24,78	V48a	0.024	2.56(−4)	
	4236.91,7.05	V48a,b	0.022	2.12(−4)	
	4442.02	V55a	0.009	3.64(−4)	
	4431.82,2.74,3.48	V55a,b	0.014	2.25(−4)	
	4552.53	V58a	0.011	4.60(−4)	
		Sum	0.210	2.32(−4)	
		Mean		2.05(−4)	
N <sup>3+</sup>	4378.99,9.20	V18	0.039	1.65(−5)	
O <sup>++</sup>	4638.86	V1	0.034	3.25(−4)	
	4661.63	V1	0.081	5.94(−4)	
	4673.73	V1	0.013	6.38(−4)	
	4676.24,7.07	V1,91	0.057	4.89(−4)	
	4696.35	V1,89a	0.009	5.96(−4)	
		V1	0.659	5.19(−4)	
	4315–18	V2,53a,63c,78b	0.045	4.67(−4)	
	4319.63	V2	0.030	3.57(−4)	
	4349.43	V2	0.095	4.96(−4)	
	4366.89	V2	0.076	8.76(−4)	

**Table 6** – *continued*

Ion	$\lambda_0$	Multiplet	$I_{\text{obs}}$	$X^{i+}/H^+$
		V2	0.325	5.91(−4)
	4414.90	V5	0.055	9.26(−4)
	4416.97	V5	0.026	7.91(−4)
	4452.37	V5	0.007	1.10(−3)
		V5	0.089	9.00(−4)
	4072.16,1.23	V10,48a	0.283	1.11(−3)
	4085.11,3.9,4.65	V10,48b,26	0.037	4.86(−4)
	4092.93,4.14	V10	0.018	5.21(−4)
		V10	0.476	4.97(−4)
	3907.46	V11	0.007	7.29(−4)
		V11	0.021	7.29(−4)
	3851.03,47	V12,13	0.006	6.70(−4)
	3882.19,45,3.13	V12,11	0.014	3.47(−4)
		V12	0.034	4.44(−4)
	4132.80	V19	0.050	9.36(−4)
	4153.30	V19	0.049	6.31(−4)
		V19	0.160	7.85(−4)
	4110.79,08.75,09.29,12.02	V20,48c,21	0.017	5.64(−4)
		V20	0.122	5.64(−4)
	4699.22	V25	0.009	1.44(−3)
	4705.35	V25	0.010	9.49(−4)
		V25	0.021	1.18(−3)
	4890.86	V28	0.010	8.80(−4)
	4906.83	V28	0.019	7.83(−4)
		V28	0.063	8.16(−4)
		3d–4f transitions		
	4088.27,9.29,7.15	V48a,c	0.072	5.43(−4)
	4083.90	V48b	0.028	8.69(−4)
	4273–78	V67	0.066	5.03(−4)
	4061.21,22,75,2.94	V50a,46c	0.016	1.23(−3)
	4281–84	V53,67	0.009	2.42(−4)
	4284–89	V53c,78b	0.016	5.23(−4)
	4303.82,61,4.08	V53a,65a	0.036	7.14(−4)
	4294.78,92	V53b	0.017	5.86(−4)
	4307.23,5.39,9.00	V53b,55,63c	0.017	7.95(−4)
	4291–93	V55,78c	0.017	6.40(−4)
	4371.25,62	V76b	0.007	7.05(−4)
	4312.11,3.44	V78a	0.009	4.67(−4)
	4477.90	V88	0.006	6.77(−4)
	4602.13	V92b	0.010	5.79(−4)
	4609.44,10.20,11.07	V92a,c	0.036	6.13(−4)
		Sum	0.617	6.30(−4)
		Mean		5.62(−4)
Ne <sup>++</sup>	3694.21	V1	0.067	1.95(−4)
	3766.26	V1	0.029	2.05(−4)
	3777.14	V1	0.021	1.62(−4)
		V1	0.180	1.90(−4)
		3d–4f transitions		
	4219.75	V52a	0.021	3.93(−4)
	4391.99	V55e	0.026	2.71(−4)
	4409.30	V55e	0.024	3.77(−4)
	4428.61,30.94	V60c,61a	0.021	5.33(−4)
	4457.05,24	V61d,66c	0.009	1.10(−4)
		Sum	0.105	2.40(−4)
		Mean		2.15(−4)
Mg <sup>++</sup>	4481.21	V4	0.030	2.92(−5)

in M 1–42 and M 2–36, with intensities relative to  $\lambda 4267$  that are within 40 per cent of the predicted values (Liu et al. 2001b). For the case of NGC 3242, Tsamis et al. (2004) find excellent agreement between recombination theory and the observed relative intensities

**Table 7.** Ionic abundances from ORLs – NGC 6720. We assume  $T_e = 9100$  K and  $N_e = 500 \text{ cm}^{-3}$ . Numbers in parentheses are powers of 10.

Ion	$\lambda_0$ (Å)	Multiplet	$I_{\text{obs}}$	$X^{i+}/H^+$
He <sup>+</sup>	5875.66	V11	13.4	0.093
	4471.50	V14	5.01	0.098
	6678.16	V46	3.68	0.091
		Mean		0.094
He <sup>++</sup>	4685.68	3.4	21.6	0.017
	Sum			0.111
C <sup>++</sup>	7231.32	V3	0.092	2.26(−4)
	7236.42,7.17	V3	0.257	3.15(−4)
		V3	0.349	2.85(−4)
	3918.98,20.69	V4	0.084	1.58(−3)
	4267.15	V6	0.892	8.58(−4)
	6151.43	V16.04	0.028	6.35(−4)
	6461.95	V17.04	0.077	7.18(−4)
	5342.40	V17.06	0.082	1.49(−3)
	4802.70	V17.08	0.050	1.52(−3)
	4292.21,29		0.060	4.17(−3)
		Mean		8.58(−4)
C <sup>+3</sup>	4647.42,50.25,51.47	V1	0.184	5.63(−5)
	4186.90	V18	0.169	2.55(−4)
		Mean		5.63(−5)
N <sup>++</sup>	5666.63	V3	0.042	1.95(−4)
	5676.02	V3	0.011	1.13(−4)
	5679.56	V3	0.064	1.58(−4)
	5686.21	V3	0.006	8.85(−5)
	5710.77	V3	0.011	2.28(−4)
		V3	0.142	1.69(−4)
	4607.16	V5	0.013	2.27(−4)
	4630.54	V5	0.049	2.25(−4)
		V5	0.118	2.25(−4)
	3994.99	V12	0.019	2.29(−4)
	4779.72	V20	0.005	1.88(−4)
	4788.13	V20	0.022	5.03(−4)
		V20	0.036	1.88(−4)
	5927.81,31.78	V28	0.038	4.12(−4)
	5940.24,1.65	V28	0.027	1.87(−4)
		V28	0.048	1.87(−4)
		3d–4f transitions		
	4035.08	V39a	0.029	3.27(−4)
	4043.53,4.78	V39a	0.054	4.36(−4)
	4041.31	V39b	0.033	2.22(−4)
	4176.16	V43a	0.018	2.57(−4)
	4241.24,78	V48a	0.078	7.85(−4)
	4236.91,7.05	V48a,b	0.022	2.09(−4)
	4442.02	V55a	0.022	8.83(−4)
	4431.82,2.74,3.48	V55a,b	0.057	8.66(−4)
	4552.53	V58a	0.024	9.65(−4)
	4530.41	V58b	0.021	2.09(−4)
		Sum	0.286	3.05(−4)
		Mean		2.00(−4)
N <sup>+3</sup>	4378.99,9.20	V18	0.116	4.84(−5)
O <sup>++</sup>	4638.86	V1	0.059	5.83(−4)
	4649.13,50.84	V1	0.365	6.22(−4)
	4661.63	V1	0.149	1.16(−3)
	4673.73	V1	0.026	1.30(−3)
	4676.24	V1	0.080	7.24(−4)
	4696.35	V1,89a	0.015	1.09(−3)
		V1	0.820	6.78(−4)
	4315–18	V2,53a,63c,78b	0.100	1.12(−3)
	4319.63	V2	0.020	2.53(−4)
	4325.76	V2	0.020	1.24(−3)

**Table 7** – *continued*

Ion	$\lambda_0$ (Å)	Multiplet	$I_{\text{obs}}$	$X^{i+}/H^+$
	4349.43	V2	0.066	3.63(−4)
	4366.89,53,79	V2,75a	0.044	5.43(−4)
		V2	0.392	7.59(−4)
	4414.90	V5	0.099	1.64(−3)
	4416.97	V5	0.034	1.02(−3)
		V5	0.148	1.48(−3)
	4072.16,1.23	V10,48a	0.223	8.74(−4)
	4085.11,7.15,6.58,71	V10,48c,46b	0.062	8.76(−4)
		V10	0.836	8.74(−4)
	3882.19,45,3.13	V12,11	0.024	5.97(−4)
		V11,12	0.062	5.97(−4)
	4132.80	V19	0.040	7.47(−4)
	4153.30	V19	0.111	1.45(−3)
		V19	0.258	1.26(−3)
	4107-4112	V20,46a,48c,21	0.032	7.51(−4)
		V20	0.162	7.51(−4)
	4705.35	V25	0.016	1.47(−3)
		V25	0.026	1.47(−3)
	4890.86	V28	0.023	2.01(−3)
	4906.83	V28	0.056	2.29(−3)
		V28	0.174	2.24(−3)
		3d–4f transitions		
	4088.27,9.29	V48a	0.080	8.10(−4)
	4083.90,4.65	V48b,21	0.058	2.05(−3)
	4273-78	V67	0.136	1.10(−3)
	4281-84	V53,67	0.025	7.34(−4)
	4303.82,61,4.08	V53a,67	0.153	3.28(−3)
	4294.78,92	V53b	0.054	1.94(−3)
	4307.23	V53b	0.023	2.23(−3)
	4285-89	V53c,78b	0.018	6.59(−4)
	4291-93	V55,78c	0.060	2.46(−3)
	4357-59.4	V63a,18,26	0.013	1.73(−3)
	4331.13,2.71,3.88	V65b	0.011	6.67(−4)
	4353.59,4.18	V76c	0.014	1.35(−3)
	4312.11,3.44	V78a	0.033	1.90(−3)
	4609.44,10.20	V92a,c	0.036	6.61(−4)
	4613.14,68	V92b	0.014	1.83(−3)
		Sum	0.827	9.01(−4)
		Mean		7.32(−4)
Ne <sup>++</sup>	3694.21	V1	0.080	2.40(−4)
	3777.14	V1	0.037	2.88(−4)
		V1	0.235	2.54(−4)
	3829.75	V39	0.042	3.38(−4)
		V39	0.0	3.38(−4)
		3d–4f transitions		
	4217.17,9.75	V52a,b	0.027	3.09(−4)
	4391.99	V55e	0.031	3.19(−4)
	4409.30	V55e	0.029	4.51(−4)
	4428.61	V60c	0.020	5.11(−4)
	4457.05	V61d	0.015	3.62(−4)
		Sum	0.168	3.85(−4)
		Mean		3.26(−4)
Mg <sup>++</sup>	4481.21	V4	0.027	2.58(−5)

of five C II recombination lines. Several C II lines have been detected for 10 PNe in the current sample and  $C^{2+}/H^+$  abundance ratios derived from them are in reasonable agreement with those derived from the  $\lambda 4267$  line.

For NGC 6781, only the strongest C II  $\lambda 4267$  ORL has been detected. The measured flux yields  $C^{2+}/H^+ = 9.05 \times 10^{-4}$  for  $T_e = 10\,200$  K and  $N_e = 240\text{ cm}^{-3}$ .

**Table 8.** Ionic abundances from ORLs – NGC 6741. We assume  $T_e = 15\,300$  K and  $N_e = 5100\text{ cm}^{-3}$ . Numbers in parentheses are powers of 10.

Ion	$\lambda_0$ (Å)	Multiplet	$I_{\text{obs}}$	$X^{i+}/H^+$
He <sup>+</sup>	5875.66	V11	13.0	0.071
	4471.50	V14	4.58	0.075
	6678.16	V46	3.18	0.079
		Mean		0.073
He <sup>++</sup>	4685.68	3.4	36.2	0.032
	Sum			0.105
C <sup>++</sup>	7231.32	V3	0.087	1.95(−4)
	7236.42,7.17	V3	0.339	3.81(−4)
		V3		1.95(−4)
	3918.98,20.69	V4	0.059	6.75(−4)
	4267.15	V6	0.617	6.29(−4)
	6151.43	V16.04	0.036	7.98(−4)
	6461.95	V17.04	0.053	5.46(−4)
	5342.40	V17.06	0.040	7.75(−4)
		Mean		6.29(−4)
C <sup>+3</sup>	4647.42,50.25,51.47	V1	0.250	7.16(−5)
	4186.90	V18	0.089	1.10(−4)
		Mean		7.16(−5)
N <sup>++</sup>	5666.63	V3	0.039	1.63(−4)
	5686.21	V3	0.015	1.90(−4)
	5710.77	V3	0.012	2.28(−4)
		V3	0.167	1.78(−4)
	6482.05	V8	0.018	3.87(−4)
		Mean		1.98(−4)
N <sup>+3</sup>	4378.99,9.20	V18	0.158	6.97(−5)
O <sup>++</sup>	4661.63	V1	0.055	3.82(−4)
	4673.73	V1	0.020	8.94(−4)
	4676.24	V1	0.055	4.50(−4)
		V1	0.656	4.90(−4)
	4317.14,70,9.63	V2,53a	0.116	6.76(−4)
	4349.43	V2	0.105	5.32(−4)
	4366.89,53,79	V2,75a	0.072	8.17(−4)
		V2	0.372	6.59(−4)
	4132.80	V19	0.038	7.04(−4)
	4153.30	V19	0.061	7.93(−4)
		V19	0.156	7.59(−4)
		3d–4f transitions		
	4088.27,9.29,7.15	V48a,c	0.073	5.59(−4)
	4083-85	V10,48b,21	0.056	7.46(−4)
	4273-78	V53c,67a,b,c	0.123	9.60(−4)
	4303.61,83,4.08	V53a,65a	0.042	8.66(−4)
		Sum	0.772	8.06(−4)
		Mean		4.90(−4)
Ne <sup>++</sup>	3694.21	V1	0.096	2.84(−4)
	3709.62	V1	0.058	4.36(−4)
		V1	0.315	3.27(−4)
	3829.75	V39	0.055	4.47(−4)
		V39	0.092	4.47(−4)
		3d–4f transitions		
	4409.30	V55e	0.042	6.49(−4)
		Mean		3.27(−4)
Mg <sup>++</sup>	4481.21	V4	0.067	6.83(−5)

For all 12 PNe analysed here, we have adopted the  $C^{2+}/H^+$  abundance ratios derived from the  $\lambda 4267$  line alone.

$C^{3+}/H^+$  abundance ratios have been derived from C III multiplets V1 and V18. Their average values are adopted in the current analysis.

**Table 9.** Ionic abundances from ORLs – NGC 6790. We assume  $T_e = 15\,000\text{ K}$  and  $N_e = 40\,000\text{ cm}^{-3}$ . Numbers in parentheses are powers of 10.

Ion	$\lambda_0$ (Å)	Multiplet	$I_{\text{obs}}$	$X^{i+}/H^+$
He <sup>+</sup>	5875.66	V11	17.1	0.087
	4471.50	V14	6.42	0.100
	6678.16	V46	4.08	0.097
		Mean		0.091
He <sup>++</sup>	4685.68	3.4	3.83	0.003
	Sum			0.094
C <sup>++</sup>	7231.32	V3	0.044	1.01(−4)
	7236.42,7.17	V3	0.210	2.66(−4)
		V3	0.254	2.07(−4)
	3918.98,20.69	V4	0.034	3.99(−4)
	4267.15	V6	0.465	4.76(−4)
	6151.43	V16.04	0.023	5.12(−4)
	6461.95	V17.04	0.044	4.40(−4)
C <sup>+</sup>	4647.42,50.25,51.47	V1	0.497	1.43(−4)
	4186.90	V18	0.160	2.01(−4)
		Mean		1.43(−4)
N <sup>++</sup>	5666.63	V3	0.009	3.67(−5)
	5676.02,9.56	V3	0.024	4.36(−5)
		V3	0.039	4.15(−5)
	4630.54	V5	0.014	5.47(−5)
		V5	0.032	5.47(−5)
		3d–4f transitions		
	4035.08	V39a	0.008	1.05(−4)
	4041.31,3.53,4.78	V39a,b	0.014	5.85(−5)
	4176.16	V43a	0.006	6.21(−5)
	4241.24,78	V48a	0.007	8.26(−5)
4431.82,2.74,3.48	V55a,b	0.004	7.54(−5)	
	Sum	0.063	7.47(−5)	
	Mean		4.15(−5)	
N <sup>+</sup>	4378.99,9.20	V18	0.262	1.16(−5)
O <sup>++</sup>	4649.13,50.84	V1	0.227	3.50(−4)
	4661.63	V1	0.056	3.92(−4)
	4673.73	V1	0.019	8.47(−4)
	4676.24	V1	0.042	3.38(−4)
	4696.35	V1	0.011	8.44(−4)
		V1	0.532	3.97(−4)
	4317.14,70,9.63	V2,53a	0.061	3.50(−4)
	4349.43	V2	0.061	3.08(−4)
	4366.89,53.79	V2,75a	0.048	5.45(−4)
		V2	0.223	3.90(−4)
	4414.90	V5	0.059	8.22(−4)
	4416.97	V5	0.032	8.03(−4)
		V5	0.097	8.15(−4)
	4083-87	V10,21,46b,48b	0.031	4.25(−4)
	4092.93,4.14	V10	0.012	3.44(−4)
		V10	0.390	4.02(−4)
	3882.19,45,3.13	V12,11	0.017	4.09(−4)
		V12,11	0.043	4.09(−4)
	4132.80	V19	0.026	4.83(−4)
	4153.30	V19	0.049	6.39(−4)
	V19	0.119	5.85(−4)	
4110.79,8.75,9.29	V20,48c	0.012	4.26(−4)	
	V20	0.092	4.26(−4)	
4705.35	V25	0.007	6.44(−4)	
	V25	0.011	6.44(−4)	
4890.86	V28	0.013	1.12(−3)	
4906.83	V28	0.028	1.13(−3)	
4924.53	V28	0.025	5.91(−4)	
	V28	0.072	9.24(−4)	

**Table 9 – continued**

Ion	$\lambda_0$ (Å)	Multiplet	$I_{\text{obs}}$	$X^{i+}/H^+$	
		3d–4f transitions			
		4088.27,9.29,7.15	V48a,c	0.077	6.24(−4)
		4273-78	V67	0.058	4.78(−4)
		4281-84	V53,67	0.026	7.66(−4)
		4303.82,61,4.08	V53a,67	0.030	6.36(−4)
		4294.78,92	V53b	0.016	4.29(−4)
		4312.11,3.44	V78a	0.011	6.27(−4)
		4284-89	V78b,53c,67c	0.033	1.17(−3)
		4489.49,91.23	V86a,b	0.021	1.10(−3)
		4602.13	V92b	0.012	7.31(−4)
		4609.44,10.20	V92a,c	0.036	6.59(−4)
		Sum	0.553	6.05(−4)	
		Mean		4.22(−4)	
Ne <sup>++</sup>		V1	0.048	1.37(−4)	
		V1	0.012	8.23(−5)	
		V1	0.122	1.26(−4)	
		3d–4f transitions			
		4217.17,9.75	V52a,b	0.019	2.20(−4)
		4391.99	V55e	0.030	3.06(−4)
		4409.59	V55e	0.014	2.23(−4)
		4428.61	V60c	0.007	2.40(−4)
		4457.05,24	V61d,66c	0.013	1.48(−4)
			Sum	0.106	2.42(−4)
	Mean		1.26(−4)		
Mg <sup>++</sup>	4481.21	V4	0.024	2.41(−5)	

### 2.2.3 N<sup>2+</sup>/H<sup>+</sup> and N<sup>3+</sup>/H<sup>+</sup>

N<sup>2+</sup>/H<sup>+</sup> ratios derived from N II ORLs are presented in Tables 2–12 for 11 PNe. Lines from 3s–3p, 3p–3d and 3d–4f configurations, both singlet and triplet multiplets, have been detected. The emissivity of multiplet V5 is very sensitive to the optical depths of the N II resonance lines  $2p^2\ ^3P^o - 2pnl\ ^3S, ^3D$  and case B recombination was assumed. This multiplet has been detected in eight PNe. For seven of them, the N<sup>2+</sup>/H<sup>+</sup> abundance ratios derived from it agree with those derived from 3d–4f lines. The only exception is Hu 1–2 where V5 yields a much higher N<sup>2+</sup>/H<sup>+</sup> abundance ratio. Multiplet V3 is less sensitive to optical depth effects and has been detected in 11 PNe. For six of these, N<sup>2+</sup>/H<sup>+</sup> abundance ratios derived from it are however somewhat lower than those derived from 3d–4f lines, suggesting that there might be some departure from case B to case A recombination.

Our adopted N<sup>2+</sup>/H<sup>+</sup> ratios for each PN are listed in Table 13 and are average values of results derived from individual lines of various electron configurations. For Hu 1–2, only the average value derived from the 3d–4f transitions was used.

The N<sup>3+</sup>/H<sup>+</sup> abundance ratio has been determined from the N III multiplet V18  $\lambda 4379$  line only.

### 2.2.4 O<sup>2+</sup>/H<sup>+</sup>

O<sup>2+</sup>/H<sup>+</sup> abundance ratios for 11 PNe have been derived from O II ORLs from 3–3 transitions and the 3d–4f configuration. The relative intensities of individual multiplets, both doublets or quartets, as well as lines from the 3d–4f group closely resemble those observed in NGC 7009 (Liu et al. 1995), NGC 6153 (Liu et al. 2000) and M 1–42 and M 2–36 (Liu et al. 2001b). The agreement between the

**Table 10.** Ionic abundances from ORLs – NGC 6826. We assume  $T_e = 9650$  K and  $N_e = 1800 \text{ cm}^{-3}$ . Numbers in parentheses are powers of 10.

Ion	$\lambda_0$ (Å)	Multiplet	$I_{\text{obs}}$	$X^{i+}/H^+$	
He <sup>+</sup>	5875.66	V11	14.3	0.097	
	4471.50	V14	5.19	0.101	
	6678.16	V46	4.07	0.101	
		Mean		0.099	
He <sup>++</sup>	4685.68	3.4	1.26	2.24(−3)	
	Sum			0.099	
C <sup>++</sup>	7231.32	V3	0.192	4.65(−4)	
	7236.42,7.17	V3	0.340	4.12(−4)	
		V3	0.534	4.31(−4)	
	3918.98	V4	0.107	5.80(−3)	
	3920.69	V4	0.156	4.22(−3)	
		V4	0.263	4.75(−3)	
	4267.15	V6	0.574	5.49(−4)	
	6151.43	V16.04	0.0242	6.42(−4)	
	6461.95	V17.04	0.0578	5.38(−4)	
	5342.38	V17.06	0.0409	7.36(−4)	
	4802.70	V17.08	0.0143	4.36(−4)	
		Mean		5.49(−4)	
	N <sup>++</sup>	5666.63	V3	0.0307	1.41(−4)
		5676.02	V3	0.0203	2.10(−4)
		5679.56	V3	0.0472	1.16(−4)
5686.21		V3	0.0109	1.51(−4)	
5710.77		V3	0.0109	2.27(−4)	
		V3	0.116	1.38(−4)	
4630.54		V5	0.0489	2.24(−4)	
		V5	0.118	2.24(−4)	
3994.99		V12	0.0200	2.36(−4)	
4788.13		V20	0.0135	2.99(−4)	
4803.28		V20	0.0204	2.53(−4)	
		V20	0.0525	2.69(−4)	
5927.81		V28	0.0101	3.49(−4)	
5931.78		V28	0.0222	3.41(−4)	
5941.65,40.24		V28	0.0245	1.71(−4)	
		V28	0.0623	2.40(−4)	
		3d–4f transitions			
4035.08		V39a	0.0174	1.97(−4)	
4043.53		V39a	0.0349	2.32(−4)	
4041.31		V39b	0.0229	1.98(−4)	
4176.16		V43a	0.0106	1.51(−4)	
4241.24,77		V48a	0.0262	2.65(−4)	
4237.05,36.91	V48a,b	0.0126	1.26(−4)		
4179.67,8.86	V50a	0.0102	1.04(−3)		
4432.73,33.48,31.82	V55a,b	0.0161	2.45(−4)		
4530.41	V58b	0.0110	1.09(−4)		
	Sum	0.191	1.90(−4)		
	Mean		2.16(−4)		
O <sup>++</sup>	4649.13,50.84	V1	0.370	6.16(−4)	
	4661.63	V1	0.107	8.09(−4)	
	4673.73	V1	0.0201	9.80(−4)	
	4676.23	V1	0.0735	6.61(−4)	
		V1	0.820	6.60(−4)	
	4317.14	V2	0.0904	1.203(−3)	
	4319.63	V2	0.0448	5.52(−4)	
	4349.43	V2	0.0850	4.52(−4)	
	4366.89	V2	0.0479	5.96(−4)	
		V2	0.274	5.08(−4)	
	4414.90	V5	0.0233	4.51(−4)	
		V5	0.0388	4.51(−4)	
	4072.16	V10	0.114	4.78(−4)	
	4085.11	V10	0.0216	4.85(−4)	
4092.93	V10	0.0186	5.71(−4)		

**Table 10 – continued**

Ion	$\lambda_0$ (Å)	Multiplet	$I_{\text{obs}}$	$X^{i+}/H^+$	
	3882.45	V10	0.467	4.88(−4)	
		V11	0.00451	6.89(−4)	
		V11	0.0197	6.89(−4)	
	3882.19,3.13	V12	0.0241	6.89(−4)	
		V12	0.0526	6.89(−4)	
		V25	0.0066	6.10(−4)	
	4705.35	V25	0.0109	6.10(−4)	
		3d–4f transitions			
		4089.29,8.27	V48a	0.0735	6.51(−4)
			V48b	0.0115	3.64(−4)
4083.90		V48c	0.0201	6.70(−4)	
4087.15		V53,67,78	0.0324	5.39(−4)	
4281–86		V53a,65a	0.0540	1.006(−3)	
4303.82,61,4.08		V53b	0.0173	5.46(−4)	
4294.78,92		V53b,63c	0.0120	5.94(−4)	
4307.23,9.00,9.00		V53c,67	0.0524	3.72(−4)	
4273–78		V76b	0.0113	1.033(−3)	
4371.62,25		V92a,c	0.0300	4.80(−4)	
4609.44,10.20,11.07	Sum	0.598	5.67(−4)		
	Mean		5.68(−4)		
Ne <sup>++</sup>	3694.21	V1	0.0405	1.22(−4)	
		V1	0.0143	1.11(−4)	
		V1	0.112	1.19(−4)	
	3777.14	V39	0.0268	2.13(−4)	
		V39	0.0447	2.13(−4)	
	3d–4f transitions				
	4219.74	V52a	0.0117	2.18(−4)	
		V55e	0.0341	3.53(−4)	
	4391.99,2.00	V55e	0.0206	3.21(−4)	
	4409.30	V57b	0.00726	2.18(−4)	
4397.99	V60c,61b	0.0114	2.70(−4)		
4428.64,52,52	Sum	0.0851	2.93(−4)		
	Mean		2.08(−4)		
Mg <sup>++</sup>	4481.21	V4	0.0338	3.23(−5)	

$O^{2+}/H^+$  abundance ratios derived from the 3p–3d lines and from the 3d–4f transitions is excellent.

$O^{2+}/H^+$  abundance ratios derived from individual 3–3 multiplets and from co-added 3d–4f transitions were averaged (a few values were excluded either because of low signal-to-noise ratio or because they are affected by line blending). The adopted values are given in Table 13.

### 2.2.5 Ne<sup>2+</sup>/H<sup>+</sup>

A few Ne II multiplets, including V1 and some transitions from the 3d–4f configuration, have been detected in nine PNe in our sample. Note that Ne II has a doublet ground-state  $2p^5P^o$ . Therefore, case B recombination has been assumed for doublets and case A for quartets. The Ne<sup>2+</sup>/H<sup>+</sup> abundance ratios derived from individual 3–3 multiplets were averaged with the value derived from the co-added 3d–4f transitions and the results adopted in the further analysis.

### 2.2.6 Mg<sup>2+</sup>/H<sup>+</sup>

Mg<sup>2+</sup>/H<sup>+</sup> abundance ratios have been derived from the Mg II  $3d^2D-4f^2F^o$   $\lambda 4481$  line for 11 PNe. Barlow et al. (2003) point out that the Mg II line at 4481.21 Å is the strongest and easiest to measure

**Table 11.** Ionic abundances from ORLs – NGC 6884. We assume  $T_e = 11\,550\text{ K}$  and  $N_e = 7400\text{ cm}^{-3}$ . Numbers in parentheses are powers of 10.

Ion	$\lambda_0$ (Å)	Multiplet	$I_{\text{obs}}$	$X^{i+}/H^+$	
He <sup>+</sup>	5875.66	V11	13.6	0.084	
	4471.50	V14	4.99	0.090	
	6678.16	V46	3.08	0.076	
		Mean		0.084	
He <sup>++</sup>	4685.68	3.4	18.3	0.015	
	Sum			0.099	
C <sup>++</sup>	7231.32	V3	0.118	2.85(−4)	
	7236.42,7.17	V3	0.297	3.58(−4)	
		V3	0.415	3.35(−4)	
	3918.98,20.69	V4	0.084	1.34(−3)	
	4267.15	V6	0.751	7.44(−4)	
	6151.43	V16.04	0.028	6.28(−4)	
	6461.95	V17.04	0.078	7.54(−4)	
	5342.40	V17.06	0.028	5.24(−4)	
		Mean		7.44(−4)	
	C <sup>+3</sup>	4647.42,50.25,51.47	V1	0.319	9.57(−5)
		4186.90	V18	0.182	2.60(−4)
		Mean		9.57(−5)	
N <sup>++</sup>	5666.63	V3	0.030	1.33(−4)	
	5676.02	V3	0.010	9.60(−5)	
	5679.56	V3	0.126	3.02(−4)	
	5686.21	V3	0.010	1.29(−4)	
		V3	0.109	1.25(−4)	
	4607.16	V5	0.030	4.98(−4)	
	4613.87	V5	0.023	5.12(−4)	
	4621.39	V5	0.047	7.80(−4)	
	4630.54	V5	0.046	2.02(−4)	
		V5	0.110	2.02(−4)	
	4788.13	V20	0.014	3.21(−4)	
		V20	0.063	3.21(−4)	
		3d–4f transitions			
	4041.31	V39b	0.045	3.13(−4)	
	4176.16	V43a	0.021	3.18(−4)	
	4236.91,7.05	V48a,b	0.023	2.26(−4)	
	4241.24,78	V48a	0.027	2.89(−4)	
	4442.02	V55a	0.007	2.76(−4)	
		Sum		2.90(−4)	
		Mean		2.35(−4)	
	N <sup>+3</sup>	4378.99,9.20	V18	0.240	1.03(−4)
	O <sup>++</sup>	4661.63	V1	0.107	7.90(−4)
		4673.73	V1	0.042	1.98(−3)
4676.24		V1	0.084	7.24(−4)	
4696.35		V1.89a	0.012	8.10(−4)	
		V1	1.23	9.72(−4)	
4315.20		V2,53a,63c,78b	0.117	6.63(−4)	
4344.46		V2.65c	0.060	6.58(−4)	
4349.43		V2	0.129	6.81(−4)	
4366.89		V2	0.079	9.90(−4)	
		V2	0.363	6.68(−4)	
4414.90		V5	0.089	1.60(−3)	
4416.97		V5	0.024	7.80(−4)	
		V5	0.072	7.80(−4)	
4085.11,3.90,4.65		V10,48a,21	0.039	5.13(−4)	
		V10	0.491	5.13(−4)	
4132.80		V19	0.053	9.85(−4)	
4153.30		V19	0.068	8.81(−4)	
		V19	0.190	9.27(−4)	
4110.79	V20	0.024	1.02(−3)		
	V20	0.220	1.02(−3)		
	3d–4f transitions				
4088.27,9.29,7.15	V48a,c	0.121	8.84(−4)		

**Table 11 – continued**

Ion	$\lambda_0$ (Å)	Multiplet	$I_{\text{obs}}$	$X^{i+}/H^+$	
	4083.90	V48b	0.028	8.69(−4)	
	4273-78	V67	0.129	9.57(−4)	
	4281-84	V53,67	0.057	1.55(−3)	
	4303.82,61,4.08	V53a,67	0.051	9.99(−4)	
	4294.78,92	V53b	0.028	9.05(−4)	
	4307.23	V53b	0.022	1.94(−3)	
	4285-89	V53c,78b	0.040	1.31(−3)	
	4331-35	V63b,65b	0.023	9.41(−4)	
	4371.25,62	V76b	0.015	1.42(−3)	
	4609.44,10.20	V92a,c	0.072	1.20(−4)	
		Sum	0.981	9.71(−4)	
		Mean		8.36(−4)	
	Ne <sup>++</sup>	3694.21	V1	0.113	3.28(−4)
		3709.62	V1	0.058	4.36(−4)
		3766.26	V1	0.079	5.58(−4)
3777.14		V1	0.060	4.52(−4)	
		V1	0.410	4.31(−4)	
		3d–4f transitions			
4219.75		V52a	0.036	6.64(−4)	
4231.64		V52b	0.007	5.35(−4)	
4233.85		V52b	0.009	6.99(−4)	
4391.99		V55e	0.045	4.70(−4)	
4409.30		V55e	0.043	6.63(−4)	
4397.99		V57b	0.022	6.60(−4)	
4428.61		V60c	0.019	6.56(−4)	
4457.05,24		V61d,66c	0.042	4.87(−4)	
		Sum	0.256	5.88(−4)	
	Mean		5.10(−4)		
Mg <sup>++</sup>	4481.21	V4	0.038	3.78(−5)	

ORLs from a third-row element ion. Given the similarity of atomic structure of Mg II and C II, we have assumed that the Mg II  $\lambda 4481$  line has an effective recombination coefficient equal to that of the C II 3d–4f  $\lambda 4267$  line.

### 2.3 Total elemental abundances from CELs and from ORLs

The total elemental abundances for each PN in our sample derived from CELs and from ORLs are listed in Table 13. The procedures used to calculate total elemental abundances from determined ionic abundance ratios are very similar to those described by Liu et al. (2000). For most elements, we have used the ionization correction factor (ICF) formulae given by Kingsburgh & Barlow (1994), except for a few cases described below. The ICFs adopted for individual elements are also listed in Table 13.

Except for NGC 40, a total He/H abundance for each PN was obtained by simply taking the sum of the ionic abundances of singly and doubly ionized species,  $\text{He}/\text{H} = \text{He}^+/\text{H}^+ + \text{He}^{2+}/\text{H}^+$ . Given the very low excitation class (E.C.) of NGC 40 (E.C. = 0.18; see Section 4), we expect a significant amount of neutral helium to be present within the hydrogen ionized region. In order to correct for the unseen He<sup>0</sup>, we have adopted the helium ICF formula adopted by Zhang & Liu (2003) in their analysis of M 2–24:

$$\frac{\text{He}}{\text{H}} = \frac{\text{S}^+ + \text{S}^{2+}}{\text{S}^{2+}} \frac{\text{He}^+}{\text{H}^+}.$$

For a wide range of E.C.s, Mg<sup>2+</sup> is the dominant ionic stage of magnesium in a nebula, given the very large ionization potential

**Table 12.** Ionic abundances from ORLs – NGC 7662. We assume  $T_e = 12\,200$  K and  $N_e = 3200\text{ cm}^{-3}$ . Numbers in parentheses are powers of 10.

Ion	$\lambda_0$ (Å)	Multiplet	$I_{\text{obs}}$	$X^{i+}/H^+$	
He <sup>+</sup>	5875.66	V11	9.61	0.060	
	4471.50	V14	3.10	0.057	
	6678.16	V46	2.64	0.066	
He <sup>++</sup>	4685.68	Mean		0.060	
	Sum	3.4	44.5	0.038	
C <sup>++</sup>	7231.32	V3	0.054	1.29(−4)	
	7236.42,7.17	V3	0.339	4.07(−4)	
		V3	0.393	3.14(−4)	
	3918.98,20.69	V4	0.037	5.66(−4)	
	4267.15	V6	0.465	4.66(−4)	
	6151.43	V16.04	0.020	4.52(−4)	
	6461.95	V17.04	0.061	5.94(−4)	
	5342.40	V17.06	0.027	5.07(−4)	
		Mean		4.66(−4)	
	C <sup>+3</sup>	4647.42,50.25,51.47	V1	0.622	1.85(−4)
		4186.90	V18	0.277	3.87(−4)
		Mean		1.85(−4)	
N <sup>++</sup>	5666.63	V3	0.014	6.37(−5)	
	5676.02,9.56	V3	0.034	6.52(−5)	
	5686.21	V3	0.008	1.12(−4)	
		V3	0.063	7.15(−5)	
	3994.99	V12	0.007	7.15(−5)	
	4788.13	V20	0.004	9.74(−5)	
		V20	0.019	9.74(−5)	
		3d–4f transitions			
	4041.31,3.53,4.78	V39a,b	0.016	6.18(−5)	
	4241.24,78	V48a	0.009	9.59(−5)	
	Sum	0.032	7.41(−5)		
	Mean		7.86(−5)		
N <sup>+3</sup>	4378.99,9.20	V18	0.140	6.07(−5)	
O <sup>++</sup>	4661.63	V1	0.056	4.08(−4)	
	4676.24	V1	0.034	2.98(−4)	
		V1	0.422	3.30(−4)	
	4315–20	V2,53a,63c,78b	0.066	3.72(−4)	
	4349.43	V2	0.054	2.85(−4)	
	4366.89	V2	0.079	9.90(−4)	
		V2	0.182	3.33(−4)	
	3954.36	V6	0.005	3.89(−4)	
		V6	0.020	3.89(−4)	
	4083–87	V10,48b,21	0.033	4.34(−4)	
	4092.93	V10	0.014	4.40(−4)	
		V10	0.418	4.36(−4)	
	3882.19,45,3.13	V12,11	0.012	2.83(−4)	
		V12,11	0.029	2.83(−4)	
	4132.80	V19	0.019	3.44(−4)	
	4153.30	V19	0.026	3.36(−4)	
		V19	0.070	3.39(−4)	
	4110.79	V20	0.015	6.26(−4)	
		V20	0.136	6.26(−4)	
		3d–4f transitions			
4088.27,9.29,7.15	V48a,c	0.076	5.60(−4)		
4083.90	V48b	0.028	8.69(−4)		
4273–78	V67	0.068	5.06(−4)		
4281–89	V53,67,78	0.025	3.69(−4)		
4303.82,61,4.08	V53a,67	0.040	7.34(−4)		
4294.78,92	V53b	0.022	7.42(−4)		
4307.23	V53b	0.009	7.74(−4)		
4312.11,3.44	V78b	0.013	6.84(−4)		
4466.42,59	V86b	0.016	1.54(−3)		
4609.44,10.20	V92a,c	0.043	7.24(−4)		

**Table 12 – continued**

Ion	$\lambda_0$ (Å)	Multiplet	$I_{\text{obs}}$	$X^{i+}/H^+$
		Sum	0.627	6.27(−4)
		Mean		3.52(−4)
Ne <sup>++</sup>	3694.21	V1	0.075	2.18(−4)
	3709.62	V1	0.044	3.30(−4)
	3777.14	V1	0.017	1.29(−4)
		V1	0.232	2.43(−4)
		3d–4f transitions		
	4419.75	V52a	0.013	2.35(−4)
	4391.99	V55e	0.018	1.88(−4)
	4397.99	V57b	0.008	2.32(−4)
	4428.61	V60c	0.012	4.03(−4)
	4421.39	V66c	0.005	5.69(−4)
		Sum	0.093	2.13(−4)
		Mean		2.28(−4)
Mg <sup>++</sup>	4481.21	V4	0.018	1.85(−5)

interval between 15 eV for Mg<sup>+</sup> and 80 eV for Mg<sup>2+</sup>. For an ORL abundance analysis, Mg<sup>2+</sup> abundances have been determined from the Mg II  $\lambda$ 4481 line for 11 PNe in our sample, and we have simply assumed that

$$\frac{\text{Mg}}{\text{H}} = \frac{\text{Mg}^{2+}}{\text{H}^+}.$$

The assumption should be fairly accurate, except possibly for the cases of high-excitation PNe Hu 1–2, NGC 6741 and 7662, where the total magnesium abundance determined in this way may have underestimated the real value.<sup>1</sup>

Mg<sup>3+</sup>/H<sup>+</sup> and Mg<sup>4+</sup>/H<sup>+</sup> abundances have been determined for several nebulae in our sample using IR fine-structure lines. However, only a tiny fraction of magnesium exists in the form of Mg<sup>3+</sup> and Mg<sup>4+</sup>. Thus, a very large ICF is required to calculate total magnesium abundance from Mg<sup>3+</sup>/H<sup>+</sup> and Mg<sup>4+</sup>/H<sup>+</sup> determined from observations. No reliable ICF formula based on ionic abundances of other elements determinable from observations is available for this purpose. We have therefore refrained from giving total CEL magnesium abundances in the current work.

For chlorine, we have adopted the prescription of Liu et al. (2000) who, based on the similarities between the ionization potentials of individual chlorine ionic stages and those of the corresponding ionic stages of sulphur, assume

$$\frac{\text{Cl}}{\text{H}} = \frac{\text{S}}{\text{S}^{2+} + \text{S}^{3+}} \frac{\text{Cl}^{2+} + \text{Cl}^{3+}}{\text{H}^+}.$$

For iron, when only Fe<sup>2+</sup> was measurable, the total elemental abundance was calculated assuming

$$\frac{\text{Fe}}{\text{H}} = \frac{\text{N}}{\text{N}^+} \frac{\text{Fe}^{2+}}{\text{H}^+}.$$

When both Fe<sup>2+</sup> and Fe<sup>3+</sup> were measured, the total elemental abundance was derived assuming

$$\frac{\text{Fe}}{\text{H}} = \frac{\text{N}}{\text{N}^+ + \text{N}^{2+}} \frac{\text{Fe}^{2+} + \text{Fe}^{3+}}{\text{H}^+}.$$

Finally, in cases where ionic abundances for a given ion have been determined from both collisionally excited optical forbidden

<sup>1</sup> In the detailed photoionization model of NGC 7662 constructed by Harrington et al. (1982), Mg<sup>2+</sup> accounts for 60 per cent of the ionic concentration.

**Table 13.** Total elemental abundances from CELs and from ORLs with adopted ICFs.

Ion	ORLs A(X <sup>+i</sup> )	ICF	A(X)	CELs A(X <sup>+i</sup> )	ICF	A(X)
Humason 1–2						
He <sup>+</sup>	0.043					
He <sup>++</sup>	0.088					
He			0.131			
C <sup>+</sup>				2.28(−5)		
C <sup>++</sup>	1.05(−4)	1.786		2.90(−5)		
C <sup>3+</sup>	3.37(−5)			1.63(−5)		
C		2.191	4.85(−4)		2.191	1.49(−4)
N <sup>+</sup>				1.37(−5)		
N <sup>++</sup>	1.06(−4)			2.64(−5)		
N <sup>3+</sup>	8.85(−5)			4.56(−5)		
N <sup>4+</sup>				2.16(−5)		
N		1.490	2.90(−4)			1.07(−4)
O <sup>+</sup>				1.41(−5)		
O <sup>++</sup>	7.07(−5)			4.35(−5)		
O <sup>3+</sup>				3.97(−5)		
O		2.766	1.96(−4)		1.236	1.20(−4)
Ne <sup>+</sup>				2.79(−6)		
Ne <sup>++</sup>				1.13(−5)		
Ne <sup>3+</sup>				1.58(−5)		
Ne <sup>4+</sup>				8.65(−6)		
Ne <sup>5+</sup>				2.71(−6)		
Ne						4.13(−5)
Mg <sup>++</sup>	3.34(−5)					
Mg			3.34(−5) <sup>a</sup>			
S <sup>+</sup>				2.96(−7)		
S <sup>++</sup>				7.08(−7)		
S <sup>3+</sup>				1.14(−6)		
S					1.739	3.73(−6)
Cl <sup>++</sup>				1.31(−8)		
Cl <sup>3+</sup>				2.14(−8)		
Cl					2.018	6.96(−8)
Ar <sup>++</sup>				2.39(−7)		
Ar <sup>3+</sup>				2.91(−7)		
Ar <sup>4+</sup>				1.68(−7)		
Ar <sup>5+</sup>				1.03(−7)		
Ar					1.146	9.18(−7)
Fe <sup>++</sup>				2.38(−8)		
Fe					7.832	1.86(−7)
IC 3568						
He <sup>+</sup>	0.095					
He <sup>++</sup>	0.001					
He			0.096			
C <sup>++</sup>	3.00(−4)			1.15(−4)		
C <sup>3+</sup>	5.24(−5)			1.56(−5)		
C		1.004	3.54(−4)		1.004	1.31(−4)
N <sup>+</sup>				1.39(−7)		
N <sup>++</sup>	1.10(−4)	1.005		2.65(−5)	1.215	
N <sup>3+</sup>	2.36(−5)					
N			1.34(−4)			3.23(−5)
O <sup>+</sup>				1.04(−6)		
O <sup>++</sup>	5.34(−4)	1.008		2.43(−4)		
O <sup>3+</sup>				1.02(−6)		
O			5.39(−4)			2.45(−4)
Ne <sup>++</sup>	3.12(−4)			4.88(−5)		
Ne		1.008	3.15(−4)		1.008	4.92(−5)
Mg <sup>++</sup>	3.99(−5)					
Mg			3.99(−5)			

**Table 13 – continued**

Ion	ORLs A(X <sup>+i</sup> )	ICF	A(X)	CELs A(X <sup>+i</sup> )	ICF	A(X)
S <sup>+</sup>				5.35(−9)		
S <sup>++</sup>				4.38(−7)		
S <sup>3+</sup>				1.12(−6)		
S					1.213	1.90(−6)
Cl <sup>++</sup>				2.06(−8)		
Cl <sup>3+</sup>				2.39(−8)		
Cl					1.218	5.32(−8)
Ar <sup>++</sup>				4.79(−7)		
Ar <sup>3+</sup>				2.82(−7)		
Ar					1.004	7.64(−7)
Fe <sup>++</sup>				2.25(−8)		
Fe					232.6	5.23(−6)
NGC 40						
He <sup>+</sup>	0.062	1.925				
He <sup>++</sup>	3.40(−5):					
He			0.119			
C <sup>+</sup>				5.56(−4)		
C <sup>++</sup>	5.96(−4)	6.848		1.02(−4)		
C <sup>3+</sup>				≤4.04(−5)		
C		1.000	4.08(−3)		1.000	6.98(−4)
N <sup>+</sup>				7.58(−5)		
N <sup>++</sup>	2.15(−4)	9.794		8.62(−6)		
N		1.000	2.11(−3)		1.000	8.45(−5)
O <sup>+</sup>				4.83(−4)		
O <sup>++</sup>	2.14(−4)	41.27		1.20(−5)		
O <sup>3+</sup>				≤1.92(−8)		
O		1.000	8.83(−3)		1.000	4.95(−4)
Ne <sup>+</sup>				1.01(−4)		
Ne <sup>++</sup>				5.33(−7)		
Ne					1.000	1.02(−4)
Mg <sup>++</sup>	2.09(−5)					
Mg			2.09(−5)			
S <sup>+</sup>				1.24(−6)		
S <sup>++</sup>				1.34(−6)		
S					1.000	2.58(−6)
Cl <sup>++</sup>				4.19(−8)		
Cl					1.925	8.07(−8)
Ar <sup>++</sup>				4.68(−7)		
Ar					1.870	8.75(−7)
Fe <sup>++</sup>				1.74(−7)		
Fe <sup>3+</sup>				2.04(−6)		
Fe					1.000	2.21(−6)
NGC 6210						
He <sup>+</sup>	0.096					
He <sup>++</sup>	0.001					
He			0.097			
C <sup>++</sup>	3.20(−4)			9.51(−5)		
C <sup>3+</sup>	4.31(−5)					
C		1.035	3.76(−4)		1.174	1.12(−4)
N <sup>+</sup>				2.90(−6)		
N <sup>++</sup>	1.63(−4)	1.048		5.98(−5)	1.200	
N <sup>3+</sup>	3.26(−5)					
N			2.04(−4)			7.47(−5)
O <sup>+</sup>				1.46(−5)		
O <sup>++</sup>	1.29(−3)			4.23(−4)		
O		1.042	1.34(−3)		1.007	4.41(−4)
Ne <sup>++</sup>	3.44(−4)			9.72(−5)		
Ne		1.042	3.58(−4)		1.042	1.01(−4)
Mg <sup>++</sup>	1.90(−5)					
Mg			1.90(−5)			

**Table 13** – *continued*

Ion	ORLs A(X <sup>+i</sup> )	ICF	A(X)	CELs A(X <sup>+i</sup> )	ICF	A(X)
S <sup>+</sup>				2.08(−7)		
S <sup>++</sup>				2.77(−6)		
S					2.183	6.50(−6)
Cl <sup>++</sup>				6.80(−8)		
Cl <sup>3+</sup>				5.47(−8)		
Cl					1.033	1.28(−7)
Ar <sup>++</sup>				9.66(−7)		
Ar <sup>+3</sup>				2.99(−7)		
Ar					1.040	1.32(−6)
Fe <sup>++</sup>				7.24(−8)		
Fe <sup>3+</sup>				7.03(−7)		
Fe					1.191	9.23(−7)
NGC 6572						
He <sup>+</sup>	0.103					
He <sup>++</sup>	3.47(−4)					
He			0.104			
C <sup>+</sup>				2.51(−5)		
C <sup>++</sup>	5.12(−4)	1.050		4.98(−4)	1.084	
C <sup>3+</sup>	4.29(−5)					
C		1.000	5.81(−4)		1.000	5.65(−4)
N <sup>+</sup>				7.23(−6)		
N <sup>++</sup>	2.05(−4)	1.062		1.17(−4)	1.080	
N <sup>3+</sup>	1.65(−5)					
N			2.34(−4)			1.34(−4)
O <sup>+</sup>				1.45(−5)		
O <sup>++</sup>	5.62(−4)	1.042		3.47(−4)		
O		1.002	5.87(−4)		1.002	3.62(−4)
Ne <sup>++</sup>	2.15(−4)			7.94(−5)		
Ne		1.044	2.24(−4)		1.044	8.29(−5)
Mg <sup>++</sup>	2.92(−5)					
Mg			2.92(−5)			
S <sup>+</sup>				1.25(−7)		
S <sup>++</sup>				2.14(−6)		
S					2.054	4.65(−6)
Cl <sup>++</sup>				5.40(−8)		
Cl <sup>3+</sup>				2.05(−8):		
Cl					2.174	1.17(−7)
Ar <sup>++</sup>				1.18(−6)		
Ar <sup>+3</sup>				2.89(−7)		
Ar					1.057	1.55(−6)
Fe <sup>++</sup>				6.44(−8)		
Fe <sup>3+</sup>				1.30(−6)		
Fe					1.076	1.47(−6)
NGC 6720						
He <sup>+</sup>	0.094					
He <sup>++</sup>	0.017					
He			0.111			
C <sup>+</sup>				7.75(−5)		
C <sup>++</sup>	8.58(−4)	1.322		2.41(−4)		
C <sup>3+</sup>	5.63(−5)			4.76(−5)		
C		1.057	1.26(−3)		1.057	3.87(−4)
N <sup>+</sup>				6.61(−5)		
N <sup>++</sup>	2.00(−4)	1.823		8.03(−5)	1.242	
N <sup>3+</sup>	4.84(−5)					
N			4.13(−4)			1.66(−4)
O <sup>+</sup>				1.87(−4)		
O <sup>++</sup>	7.32(−4)	2.083		3.02(−4)		
O <sup>3+</sup>				1.40(−4)		
O		1.000	1.52(−3)		1.000	6.29(−4)

**Table 13** – *continued*

Ion	ORLs A(X <sup>+i</sup> )	ICF	A(X)	CELs A(X <sup>+i</sup> )	ICF	A(X)
Ne <sup>++</sup>	3.26(−4)	1.562		1.08(−4)		
Ne <sup>3+</sup>				5.86(−5)		
Ne <sup>4+</sup>				2.07(−6)		
Ne			5.09(−4)			1.69(−4)
Mg <sup>++</sup>	2.58(−5)					
Mg			2.58(−5)			
S <sup>+</sup>				1.23(−6)		
S <sup>++</sup>				2.89(−6)		
S <sup>3+</sup>				2.31(−6)		
S					1.133	7.28(−6)
Cl <sup>++</sup>				8.78(−8)		
Cl <sup>3+</sup>				2.29(−8)		
Cl					1.401	1.55(−7)
Ar <sup>++</sup>				1.86(−6)		
Ar <sup>+3</sup>				2.05(−7)		
Ar <sup>+4</sup>				1.74(−8)		
Ar					1.663	3.46(−6)
Fe <sup>++</sup>				5.18(−8)		
Fe <sup>3+</sup>				1.34(−6)		
Fe					1.133	1.58(−6)
NGC 6741						
He <sup>+</sup>	0.073					
He <sup>++</sup>	0.032					
He			0.105			
C <sup>+</sup>				1.66(−4)		
C <sup>++</sup>	6.29(−4)	1.672		2.47(−4)		
C <sup>3+</sup>	7.16(−5)			1.32(−4)		
C		1.739	1.95(−3)		1.739	9.48(−4)
N <sup>+</sup>				4.50(−5)		
N <sup>++</sup>	1.98(−4)			1.29(−4)		
N <sup>3+</sup>	6.97(−5)			6.02(−5)		
N <sup>4+</sup>				1.73(−4)		
N		2.152	5.76(−4)			4.07(−4)
O <sup>+</sup>				1.03(−4)		
O <sup>++</sup>	4.90(−4)	1.640		2.56(−4)		
O <sup>3+</sup>				6.09(−5)		
O		1.677	1.35(−3)		1.677	7.04(−4)
Ne <sup>+</sup>				1.12(−5)		
Ne <sup>++</sup>	3.27(−4)			7.02(−5)		
Ne <sup>3+</sup>				8.42(−5)		
Ne <sup>4+</sup>				3.19(−6)		
Ne		2.404	7.86(−4)			1.69(−4)
Mg <sup>++</sup>	6.83(−5)					
Mg			6.83(−5) <sup>a</sup>			
S <sup>+</sup>				1.34(−6)		
S <sup>++</sup>				2.71(−6)		
S <sup>3+</sup>				5.61(−7)		
S					1.173	5.41(−6)
Cl <sup>++</sup>				6.16(−8)		
Cl <sup>3+</sup>				2.29(−8)		
Cl					1.654	1.40(−7)
Ar <sup>++</sup>				1.42(−6)		
Ar <sup>+3</sup>				5.56(−7)		
Ar <sup>+4</sup>				1.34(−7)		
Ar <sup>+5</sup>				2.37(−8)		
Ar					1.124	2.37(−6)
Fe <sup>++</sup>				2.82(−7)		
Fe					9.049	2.55(−6)

Table 13 – continued

Ion	ORLs A(X <sup>+i</sup> )	ICF	A(X)	CELs A(X <sup>+i</sup> )	ICF	A(X)
NGC 6781						
He <sup>+</sup>	0.113					
He <sup>++</sup>	0.007					
He			0.120			
C <sup>++</sup>	9.05(−4)					
C		1.624	1.47(−3)			
N <sup>+</sup>				5.61(−5)		
N <sup>++</sup>				1.74(−4)		
N					1.031	2.37(−4)
O <sup>+</sup>				1.57(−4)		
O <sup>++</sup>				2.73(−4)		
O <sup>3+</sup>				1.33(−5)		
O						4.43(−4)
Ne <sup>++</sup>				1.03(−4)		
Ne					1.624	1.67(−4)
S <sup>+</sup>				9.35(−7)		
S <sup>++</sup>				2.78(−6)		
S <sup>3+</sup>				5.72(−6)		
S					1.000	9.44(−6)
Cl <sup>++</sup>				7.92(−8)		
Cl					3.394	2.69(−7)
Ar <sup>++</sup>				1.61(−6)		
Ar <sup>+3</sup>				1.12(−7)		
Ar					1.310	2.26(−6)
NGC 6790						
He <sup>+</sup>	0.091					
He <sup>++</sup>	0.003					
He			0.094			
C <sup>+</sup>				5.28(−6)		
C <sup>++</sup>	4.76(−4)	1.035		1.52(−4)	1.300	
C <sup>3+</sup>	1.43(−4)					
C		1.011	6.42(−4)		1.011	2.05(−4)
N <sup>+</sup>				1.28(−6)		
N <sup>++</sup>	4.15(−5)	1.046		2.80(−5)	1.280	
N <sup>3+</sup>	1.16(−5)					
N			5.50(−5)			3.71(−5)
O <sup>+</sup>				4.63(−6)		
O <sup>++</sup>	4.22(−4)	1.029		2.44(−4)		
O <sup>3+</sup>				2.48(−6)		
O			4.34(−4)			2.51(−4)
Ne <sup>++</sup>	1.26(−4)	1.028		5.13(−5)		
Ne <sup>3+</sup>				1.43(−6)		
Ne		1.019	1.32(−4)		1.019	5.37(−5)
Mg <sup>++</sup>	2.41(−5)					
Mg			2.41(−5)			
S <sup>+</sup>				7.10(−8)		
S <sup>++</sup>				8.50(−7)		
S <sup>3+</sup>				6.19(−7)		
S					1.267	1.95(−6)
Cl <sup>++</sup>				1.95(−8)		
Cl <sup>3+</sup>				2.25(−8)		
Cl					1.329	5.58(−8)
Ar <sup>++</sup>				3.25(−7)		
Ar <sup>+3</sup>				2.24(−7)		
Ar					1.036	5.69(−7)
Fe <sup>++</sup>				3.37(−8)		
Fe <sup>++</sup>				6.12(−8)		
Fe					1.267	1.20(−7)

Table 13 – continued

Ion	ORLs A(X <sup>+i</sup> )	ICF	A(X)	CELs A(X <sup>+i</sup> )	ICF	A(X)
NGC 6826						
He <sup>+</sup>	0.099					
He <sup>++</sup>	2.24(−5)					
He			0.099			
C <sup>+</sup>				4.09(−5)		
C <sup>++</sup>	5.49(−4)	1.166		2.47(−4)		
C		1.000	6.40(−4)		1.000	2.88(−4)
N <sup>+</sup>				2.46(−6)		
N <sup>++</sup>	2.16(−4)	1.037		6.67(−5)		
N		1.000	2.24(−4)		1.000	6.92(−5)
O <sup>+</sup>				2.48(−5)		
O <sup>++</sup>	5.68(−4)	1.081		3.07(−4)		
O		1.000	6.14(−4)		1.000	3.32(−4)
Ne <sup>++</sup>	2.08(−4)			6.05(−5)		
Ne		1.081	2.25(−4)		1.081	6.54(−5)
Mg <sup>++</sup>	3.23(−5)					
Mg			3.23(−5)			
S <sup>+</sup>				5.06(−8)		
S <sup>++</sup>				1.73(−6)		
S <sup>3+</sup>				6.20(−7)		
S					1.000	2.40(−6)
Cl <sup>++</sup>				6.55(−8)		
Cl <sup>3+</sup>				1.08(−8)		
Cl					1.022	7.79(−8)
Ar <sup>++</sup>				8.58(−7)		
Ar <sup>+3</sup>				8.48(−8)		
Ar					1.037	9.78(−7)
Fe <sup>++</sup>				8.03(−8)		
Fe <sup>3+</sup>				2.98(−7)		
Fe					1.000	3.78(−7)
NGC 6884						
He <sup>+</sup>	0.084					
He <sup>++</sup>	0.015					
He			0.099			
C <sup>+</sup>				2.30(−5)		
C <sup>++</sup>	7.44(−4)	1.079		2.92(−4)		
C <sup>3+</sup>	9.57(−5)			4.85(−5)		
C		1.056	9.49(−4)		1.056	3.84(−4)
N <sup>+</sup>				4.77(−6)		
N <sup>++</sup>	2.35(−4)	1.050		9.47(−5)		1.438
N <sup>3+</sup>	1.03(−4)					
N			3.50(−4)			1.41(−4)
O <sup>+</sup>				1.07(−5)		
O <sup>++</sup>	8.36(−4)	1.117		3.62(−4)		
O <sup>3+</sup>				3.18(−5)		
O			9.34(−4)			4.05(−4)
Ne <sup>++</sup>	5.10(−4)	1.596		8.74(−5)		
Ne <sup>3+</sup>				5.21(−5)		
Ne		1.027	8.36(−4)		1.027	1.43(−4)
Mg <sup>++</sup>	3.78(−5)					
Mg			3.78(−5)			
S <sup>+</sup>				1.43(−7)		
S <sup>++</sup>				1.89(−6)		
S <sup>3+</sup>				2.41(−6)		
S					1.417	6.30(−6)
Cl <sup>++</sup>				6.06(−8)		
Cl <sup>3+</sup>				4.85(−8)		
Cl					1.464	1.60(−7)

**Table 13** – *continued*

Ion	ORLs		CELs			
	A(X <sup>+i</sup> )	ICF	A(X)	A(X <sup>+i</sup> )	ICF	A(X)
Ar <sup>++</sup>				9.96(−7)		
Ar <sup>+3</sup>				7.23(−7)		
Ar <sup>+4</sup>				2.88(−8)		
Ar					1.035	1.81(−6)
Fe <sup>++</sup>				8.42(−8)		
Fe <sup>3+</sup>				2.13(−7)		
Fe					1.417	4.21(−7)
NGC 7662						
He <sup>+</sup>	0.060					
He <sup>++</sup>	0.038					
He			0.098			
C <sup>+</sup>				9.46(−6)		
C <sup>++</sup>	4.66(−4)	1.095		9.91(−5)		
C <sup>3+</sup>	1.85(−4)			1.21(−4)		
C		2.073	1.44(−3)		2.073	4.76(−4)
N <sup>+</sup>				6.98(−7)		
N <sup>++</sup>	7.86(−5)			1.73(−5)		
N <sup>3+</sup>	6.07(−5)			3.05(−5)		
N <sup>4+</sup>				1.15(−5)		
N		1.255	1.75(−4)			6.00(−5)
O <sup>+</sup>				3.18(−6)		
O <sup>++</sup>	3.52(−4)	1.529		1.79(−4)		
O <sup>3+</sup>				9.15(−5)		
O		1.223	6.58(−4)		1.223	3.35(−4)
Ne <sup>+</sup>				9.68(−7)		
Ne <sup>++</sup>	2.28(−4)	1.798		3.20(−5)		
Ne <sup>3+</sup>				2.30(−5)		
Ne <sup>4+</sup>				1.58(−6)		
Ne			4.10(−4)			5.75(−5)
Mg <sup>++</sup>	1.85(−5)					
Mg			1.85(−5) <sup>a</sup>			
S <sup>+</sup>				4.80(−8)		
S <sup>++</sup>				9.51(−7)		
S <sup>3+</sup>				2.56(−6)		
S					2.034	7.24(−6)
Cl <sup>++</sup>				2.82(−8)		
Cl <sup>3+</sup>				5.72(−8)		
Cl					2.062	1.85(−7)
Ar <sup>++</sup>				4.26(−7)		
Ar <sup>+3</sup>				5.30(−7)		
Ar <sup>+4</sup>				8.21(−8)		
Ar <sup>+5</sup>				1.77(−8)		
Ar					1.012	1.06(−6)
Fe <sup>++</sup>				5.99(−8)		
Fe <sup>3+</sup>				1.48(−7)		
Fe					3.334	6.93(−7)

Note. <sup>a</sup>Lower limit owing to the possible existence of Mg<sup>3+</sup> and Mg<sup>4+</sup> in this high-excitation nebula.

lines (such as [O III]  $\lambda$ 4959) and from IR fine-structure lines (such as [O III] 52 and 88  $\mu$ m), the results were averaged with equal weight. For the IR fine-structure lines, ionic abundances deduced using  $N_e$  derived from the [O III] 88- $\mu$ m/52- $\mu$ m ratio were adopted for PNe with  $\log N_e([\text{Ar IV}]) < 3.9 \text{ cm}^{-3}$ .

In Table 14 we present total elemental abundances relative to hydrogen derived from ORLs and from CELs, given in units where  $\log N(\text{H}) = 12$ , for He, C, N, O, Ne, Mg, S, Cl, Ar and Fe for the 12 PNe in our sample. For comparison, results for several other Galactic PNe previously analysed by our group in the context of the current ongoing programme are also given. They are NGC 7009 (Liu et al.

1995), NGC 6153 (Liu et al. 2000), M 1–42 and M 2–36 (Liu et al. 2001b), NGC 7027 (Zhang, Liu & Luo, in preparation), M 2–24 (Zhang & Liu 2003) and NGC 6543 (Wesson & Liu 2004). For the 12 PNe in the current sample, heavy element abundances derived from the traditional method based on CEL analysis are compared to values published in the literature in Table 15. For completeness, helium abundances, all based on ORL analysis, are also included in the table.

Peimbert & Torres-Peimbert (1983) defined type I PNe, believed to represent the high-mass end of the population of PN progenitor stars, as those having  $\text{He}/\text{H} \geq 0.125$  and  $\text{N}/\text{O} \geq 0.5$  by number. Kingsburgh & Barlow (1994) refined the type I classification to refer to those PNe which have N/O ratios larger than the original (C+N)/O ratios of the parent galaxy interstellar medium (ISM) out of which they formed, implying that any nitrogen in excess of this value must be primary in origin, e.g. produced via hot bottom burning of carbon brought up by the third dredge-up. For the Milky Way, this type I criterion translates into  $\text{N}/\text{O} \geq 0.74$ . If we adopt abundances derived from CELs, then based on this criterion Hu 1–2, M 1–42 and M 2–24 listed in Table 14 can be classified as type I PNe. If we adopt the original less stringent definition given by Peimbert & Torres-Peimbert (1983), then NGC 6741 can be added to the list. The average elemental abundances derived from ORLs and from CELs for non-type I and type I PNe are presented in Table 14.

For comparison, we also list the mean heavy elemental abundances for type I and non-type I PNe derived by Kingsburgh & Barlow (1994) for a large sample of Galactic PNe, all based on the traditional method of CEL analysis, as well as the solar photospheric abundances taken from Grevesse, Noels & Sauval (1996), except for oxygen and carbon, for which we have adopted the more recent values given in Allende Prieto, Lambert & Asplund (2001, 2002), respectively, and for magnesium for which the value was taken from Holweger (2001). The average C, O and Ar abundances for the 16 non-type I Galactic PNe listed in Table 14 are lower than those obtained by Kingsburgh & Barlow (1994) by 0.17, 0.03 and 0.13 dex, respectively. For N and Ne our average values for non-type I PNe are 0.06 and 0.04 dex higher than those obtained by Kingsburgh & Barlow (1994), respectively. The average abundances of sulphur from these two samples agree very well.

### 3 COMPARISON OF TEMPERATURES AND ABUNDANCES DERIVED FROM CELS AND FROM ORLS

#### 3.1 Elemental abundances

In Table 16, we present the abundance discrepancy factors (ADFs) between ionic abundance derived from ORLs to those deduced from CELs, for O<sup>2+</sup>, C<sup>2+</sup>, N<sup>2+</sup> and Ne<sup>2+</sup>. For all PNe and all ionic species, we find that the ADF is always larger than one, i.e. ionic abundances derived from ORLs are systematically higher than the corresponding CEL values. In the case of O<sup>2+</sup> where data are available for all except one PN (NGC 6781), the ADFs range from 1.6 to 3.1 for 10 of them. However, for one object, NGC 40, ADF(O<sup>2+</sup>) amounts to a very high value of 17.8. Similar results are found for three other ionic species. The large discrepancies seen in NGC 40 are comparable to those previously found in the Galactic bulge PN M 1–42 (Liu et al. 2001b).

Previous detailed spectroscopic analyses of PNe using ORLs have been focused on a small group of PNe previously known (e.g. NGC 7009; Liu et al. 1995) or newly discovered (e.g. NGC 6153 and M 1–42; Liu et al. 2000, 2001b) to exhibit extraordinarily rich and prominent permitted emission lines from ionized C, N, O and Ne.

**Table 14.** Elemental abundances, relative to H, derived from ORLs and from CELs, in units where  $\log N(\text{H}) = 12.0$ . A ‘(I)’ following the PN name indicates a type I nebula (see text).

PN	ID		He	C	N	O	Ne	Mg	S	Cl	Ar	Fe
Hu 1–2 (I)	(1)	ORLs	11.12	8.69	8.46	8.29		7.52				
		CELs		8.17	8.03	8.08	7.62		6.57	4.84	5.96	5.27
IC 3568	(2)	ORLs	10.98	8.55	8.13	8.73	8.50	7.60				
		CELs		8.12	7.51	8.39	7.69		6.28	4.73	5.88	6.72
NGC 40	(3)	ORLs	11.08	9.61	9.32	9.95		7.32				
		CELs		8.84	7.93	8.69	8.01		6.41	4.91	5.94	6.35
NGC 6210	(4)	ORLs	10.99	8.57	8.31	9.13	8.55	7.28				
		CELs		8.05	7.87	8.64	8.01		6.81	5.10	6.12	5.97
NGC 6572	(5)	ORLs	11.02	8.76	8.37	8.77	8.35	7.47				
		CELs		8.75	8.13	8.56	7.92		6.67	5.07	6.19	6.17
NGC 6720	(6)	ORLs	11.05	9.10	8.62	9.18	8.71	7.41				
		CELs		8.59	8.22	8.80	8.23		6.86	5.19	6.54	6.20
NGC 6741	(7)	ORLs	11.02	9.29	8.76	9.13	8.90	7.83				
		CELs		8.98	8.61	8.85	8.23		6.73	5.15	6.38	6.41
NGC 6781	(8)	ORLs	11.08	9.17								
		CELs			8.38	8.65	8.22		6.97	5.43	6.35	
NGC 6790	(9)	ORLs	10.97	8.81	7.74	8.64	8.12	7.38				
		CELs		8.31	7.57	8.40	7.73		6.29	4.75	5.75	5.08
NGC 6826	(10)	ORLs	11.00	8.81	8.35	8.79	8.35	7.51				
		CELs		8.46	7.84	8.52	7.82		6.38	4.89	5.99	5.58
NGC 6884	(11)	ORLs	11.00	8.98	8.54	8.97	8.92	7.58				
		CELs		8.58	8.15	8.61	8.16		6.80	5.20	6.26	5.62
NGC 7662	(12)	ORLs	10.99	9.16	8.24	8.82	8.61	7.27				
		CELs		8.68	7.78	8.52	7.76		6.86	5.27	6.02	5.84
M 1–42 <sup>a</sup> (I)	(a)	ORLs	11.17	9.35	9.59	9.79	9.40	7.72				
		CELs		7.80	8.68	8.63	8.12		7.08	5.26	6.56	
M 2–24 <sup>b</sup> (I)	(b)	ORLs	11.03	8.77	8.55	9.16	9.03	8.38				
		CELs			8.09	7.92	8.37		6.13		5.66	6.08
M 2–36 <sup>a</sup>	(c)	ORLs	11.13	9.41	9.17	9.64	9.16	7.63				
		CELs		8.73	8.42	8.85	8.57		7.47	5.42	6.66	
NGC 6153 <sup>c</sup>	(d)	ORLs	11.14	9.40	9.31	9.66	9.29	7.59				
		CELs		8.44	8.36	8.70	8.23		7.21	5.62	6.43	
NGC 6543 <sup>d</sup>	(e)	ORLs	11.07	8.90	8.85	9.30	8.67	7.39				
		CELs		8.50	8.52	8.86	8.27		7.09	6.51	5.40	
NGC 7009 <sup>e</sup>	(f)	ORLs	11.04	8.97	8.71	9.28	9.88	7.47				
		CELs		8.12	8.10	8.61	8.24		6.98		6.27	
NGC 7027 <sup>f</sup>	(g)	ORLs	11.00	9.23	8.63	8.69	8.47	7.39				
		CELs		9.02	8.21	8.56	8.12		6.61	5.12	6.26	5.58
Mean non-type I		ORLs	11.04	9.14	8.81	9.30	9.05	7.50				
		CELs		8.64	8.20	8.66	8.14		6.90	5.56	6.25	6.16
Mean type I		ORLs	11.11	9.04	9.18	9.42	9.25	8.04				
		CELs		8.03	8.37	8.32	8.13		6.76	5.10	6.22	5.84
KB 94 non-type I <sup>g</sup>			11.05	8.81	8.14	8.69	8.10	–	6.91	–	6.38	
KB 94 type I <sup>g</sup>			11.11	8.48	8.72	8.65	8.09	–	6.91	–	6.42	
Solar <sup>h</sup>			10.99	8.39	7.97	8.69	8.09	7.54	7.21	5.50	6.56	7.51

Notes.<sup>a</sup>From Liu et al. (2001b) except for Mg which is taken from Barlow et al. (2003). <sup>b</sup>From Zhang & Liu (2003). <sup>c</sup>From Liu et al. (2000) except for Mg which is taken from Barlow et al. (2003). <sup>d</sup>From Wesson & Liu (2004). <sup>e</sup>From Liu et al. (1995) for He, C, N & O abundances and Luo et al. (2001) for Ne, Barlow et al. (2003) for Mg. The CEL abundances of S and Ar are from Kingsburgh & Barlow (1994). <sup>f</sup>From Zhang et al. (in preparation). <sup>g</sup>Average abundances for PNe from Kingsburgh & Barlow (1994). <sup>h</sup>Solar photospheric abundances from Grevesse et al. (1996), except for C and O which are taken from Allende Prieto et al. (2002, 2001), respectively, and for Mg which is from Holweger (2001).

The main purpose of these studies was to establish the recombination nature of these faint lines and their fidelity as nebular abundance tracers. High-quality measurements show that the observed relative intensities of those permitted emission lines are indeed in good agreement with the predictions of recombination theory and that the very high heavy elemental abundances derived from them, assuming recombination excitation, cannot be caused by observational errors, blending by unknown lines or by contamination by other possible excitation mechanisms such as radiative charge transfer, radiative fluorescence or high-temperature di-electronic recombination. The

analyses have shown that, for a given nebula, C, N, O and Ne abundances derived from ORLs are all systematically higher than the corresponding CEL values by a similar factor, ranging from approximately 5 (NGC 7009) to 20 (M 1–42). Liu et al. (2000) have shown that the very high ORL abundances observed in these extreme nebulae are most likely caused by cold, metal-rich ionized gas embedded in the nebula, possibly produced by the evaporation of planetesimals now engulfed by the expanding nebula and ionized and stripped off by the intense UV radiation fields and stellar winds from the remnant white dwarf central star (Liu 2003).

**Table 15.** Comparison of heavy element abundances derived from the traditional method based on CEL analysis and values published in the literature, in units where  $\log N(\text{H}) = 12.0$ . Helium abundances, all based on ORL analysis, are also included in the table. The following references are cited: AC83, Aller & Czyzak (1983); AK87, Aller & Keyes (1987); AHF96, Aller, Hyung & Feibelman (1996); AKC85, Aller, Keyes & Czyzak (1985); BMGK83, Baessgen et al. (1983); BPMT94, Balick et al. (1994); B88, Barker (1988); B87, Barker (1987); B86, Barker (1986); B82, Barker (1982); B80, Barker (1980); B78a, Barker (1978a); B78b, Barker (1978b); CSPT83, Clegg et al. (1983); GMC97, Guerrero, Manchado & Chu (1997), where CS denotes central star, HR hollow ring, IR inner ring, OR outer ring, IH inner halo, and OH outer halo; HF83, Harrington & Feibelman (1983); HSAL82, Harrington et al. (1982); HM77, Hawley & Miller (1977); HA97a, Hyung & Aller (1997a); HA97b, Hyung & Aller (1997b); HAF97, Hyung, Aller & Feibelman (1997); HAF94, Hyung et al. (1994); KSK90, Kaler, Shaw & Kwitter (1990), where A denotes 30 arcsec south of the centre and B denotes centre; KH98, Kwitter & Henry (1998); M98, Mal' Kov (1998); MP, Manchado & Pottasch (1989); MCW89, Middlemass, Clegg & Walsh (1989); PTP87, Peimbert & Torres-Peimbert (1987); PBBF01, Pottasch et al. (2001); PHAB03, Pottasch et al. (2003a); PBBF03, Pottasch et al. (2003b); SCT87, Sabbadin, Cappellaro & Turatto (1987).

PN	Reference	He	C	N	O	Ne	S	Cl	Ar	Fe
Hu 1–2	Present	11.12	8.17	8.03	8.08	7.62	6.57	4.84	5.96	5.27
	PHAB03	11.10	8.21	8.28	8.20	7.69	6.62	5.04	6.04	
	PTP87	11.17		8.34	8.20	7.56			5.90	
	AC83	11.20	8.08	8.50	8.05	7.83	6.48	5.18	6.20	
	SCT87	11.20		8.81	7.49	7.64	6.49			
	M98	11.19	8.08	8.18	8.04	7.77	6.89		5.94	
IC 3568	Present	10.98	8.12	7.51	8.39	7.69	6.28	4.73	5.88	6.72
	HF83(M) <sup>a</sup>	10.99	8.46	7.70	8.57	7.90	7.00			
	KH98	11.04	7.99	8.37	8.50	7.61				
	B78a,b	10.99		7.17	8.41	7.79	7.70			
NGC 40	Present	11.08	8.84	7.93	8.69	8.01	6.41	4.91	5.94	6.35
	PBBF03	$\geq 10.66$	9.28	8.11	8.72	8.15	6.75		6.53	5.79
	CSPT83	$\geq 10.64$	9.00	8.38	8.92		6.59			
	AC83	$\geq 10.5$		7.99	8.78		$\geq 6.6$	$\geq 5.0$	$\geq 5.8$	
NGC 6210	Present	10.99	8.05	7.87	8.64	8.01	6.81	5.10	6.12	5.97
	AC83	11.01		7.69	8.70	7.98	7.33	5.00	6.29	
	KH98	11.04	7.97	8.16	8.64	7.85				
	B78a,b	11.03		7.57	8.60	8.04	7.70			
NGC 6572	Present	11.02	8.75	8.13	8.56	7.92	6.67	5.07	6.19	6.17
	HAF94(M) <sup>a</sup>	10.97	8.13	7.98	8.49	7.74	6.53	4.78	6.30	
	HAF94	11.04	8.33	7.79	8.54	7.76	6.33	4.83	6.28	
	BMGK83(M) <sup>a</sup>	11.00	8.70	8.12	8.63	8.32	6.90			
	B78a	11.07		7.77	8.44	7.78	6.02			
NGC 6720	Present	11.05	8.59	8.22	8.80	8.23	6.86	5.19	6.54	6.20
	GMC97(CS)	11.15		8.15	8.77	8.78	6.08		6.35	
	GMC97(HR)	11.15		8.00	8.71	8.59	6.26		6.31	
	GMC97(IR)	11.11		8.26	8.81	8.75	6.58		5.82	
	GMC97(OR)	11.12		8.32	8.76	8.31	6.68		6.34	
	GMC97(IH)	10.99		8.11	8.90	8.41			6.41	
	GMC97(OH)	11.16		7.85	8.65	8.15				
	B87	11.04	9.09	8.36	9.05	8.26			6.38	
	B80,82	11.04	8.59	8.34	8.79	8.20	6.99		6.57	
	HM77	11.06		8.40	8.97	8.40	6.65			
	KH98	11.04	8.81	8.40	8.77	8.00				
NGC 6741	Present	11.02	8.98	8.61	8.85	8.23	6.73	5.15	6.38	6.41
	PBBF01	11.04	8.81	8.45	8.82	8.26	7.04		6.69	
	HA97b(M) <sup>a</sup>	11.04	8.90	8.15	8.65	8.00	6.76		6.54	
	HA97b	11.04	8.86	8.38	8.73	8.11	6.90		6.49	
	AKC85	11.04	9.08	8.72	8.73	8.20	6.49		6.56	
NGC 6781	Present	11.08		8.38	8.65	8.22	6.97	5.43	6.35	
	KSK90(A)	11.01		8.34	8.79	7.99				
	KSK90(B)	11.14		7.85	8.30	7.41				
	AK87	11.11		8.35	8.64	7.83	7.0		6.60	

Similar detailed spectroscopic analyses contrasting heavy elemental abundances determined from weak ORLs and those derived from the traditional method based on bright CELs have now been carried out for a significant number of PNe. Garnett & Dinerstein

(2001a) determined  $\text{O}^{++}/\text{H}^{+}$  abundance ratios for 10 bright disc PNe from  $\text{O II}$  ORLs and found that they were systematically higher than the CEL values by a factor of up to 6. In a parallel study using an almost identical technique as employed here, Tsamis et al.

Table 15 – continued

PN	Reference	He	C	N	O	Ne	S	Cl	Ar	Fe
NGC 6790	Present	10.97	8.31	7.57	8.40	7.73	6.29	4.75	5.75	5.08
	AHF96(M80) <sup>a</sup>	11.00	8.51	7.81	8.73	8.06	6.79	5.23	6.30	
	AHF96(M) <sup>a</sup>	11.04	8.86	7.74	8.88	7.99	6.65	4.84	5.93	
	AHF96	11.04	8.9:	7.78	8.79	7.87	6.64	4.89	5.95	
	AC83	11.02		7.98	8.60	7.86	6.40	4.85	6.17	
NGC 6826	Present	11.00	8.46	7.84	8.52	7.82	6.38	4.89	5.99	5.58
	B88	10.97	8.53	7.71	8.60	7.96	6.77		6.11	
	BPMT94	10.99		7.92	8.68	7.93	6.69	4.79	6.20	
	MCW89	11.00		7.62	8.39	7.55				
	MP89	11.11		7.76	8.60	7.76			5.48	
	AC83	11.03		7.47	8.38	7.98	6.17	5.04	6.05	
	KH98	11.00	8.12	7.95	8.59	7.70				
NGC 6884	Present	11.00	8.58	8.15	8.61	8.16	6.80	5.20	6.26	5.62
	HAF97(M) <sup>a</sup>	11.00	9.00	8.48	9.00	8.41	6.95	5.30	6.60	
	HAF97	10.99	9.06	8.47	8.95	8.43	6.81	5.24	6.42	
	AC83	11.07		7.86	8.66	7.99	7.03	5.32	6.57	
	B78a	11.09		8.06	8.84		6.56			
NGC 7662	Present	10.99	8.68	7.78	8.52	7.76	6.86	5.27	6.02	5.84
	PBBF01	10.92	8.56	7.83	8.62	7.81	6.82		6.32	
	HA97a(M) <sup>a</sup>	10.97	8.65	7.67	8.54	7.80	6.85		6.30	
	HA97a	10.97	8.98	8.19	8.85	7.96	6.67		6.11	
	B86	10.97	8.83	8.04	8.63	7.96	6.62		6.18	
	AC83	11.07	8.60	7.87	8.57	7.80	6.83	4.72	6.32	
	HSAL82(M) <sup>a</sup>	10.97	8.79	7.78	8.56	7.85	7.18			
KB94 non-type I <sup>b</sup>		11.05	8.81	8.14	8.69	8.10	6.91	–	6.38	
KB94 type I <sup>b</sup>		11.11	8.48	8.72	8.65	8.09	6.91	–	6.42	
Solar <sup>c</sup>		10.99	8.39	7.97	8.69	8.09	7.21	5.50	6.56	7.51

Notes. <sup>a</sup>Values based on photoionization models. <sup>b</sup>Average abundances for Galactic PNe from Kingsburgh & Barlow (1994). <sup>c</sup>Solar photospheric abundances from Grevesse et al. (1996), except for C and O which are taken from Allende Prieto et al. (2002, 2001), respectively, and for Mg which is from Holweger (2001).

(2004) determined ORL C, N, O and Ne abundances for a sample of 12 Galactic and three Magellanic Cloud PNe and found that they are higher than those derived from CEL values by factors of  $\sim 2$ –16. Including results from the current work for our sample of 12 Galactic disc PNe, all these studies show that the problem of abundance discrepancies between values derived from ORLs and from CELs is a ubiquitous phenomenon amongst PNe and is present for all abundant second-row elements, including C, N, O and Ne. In all cases, the abundances determined from ORLs are systematically higher than the corresponding CEL values.

A histogram showing the distribution of the logarithm of the ADF, for  $O^{++}/H^+$ , is plotted in Fig. 1 for 23 PNe, including 18 out of 19 nebulae listed in Table 14 for which  $ADF(O^{++}/H^+)$  has been determined (i.e. except for NGC 6781) and the five other nebulae mentioned above and studied by Liu et al. (2001b) (NGC 3242, 3918, 5315, 5882 and 6644). The discrepancy ranges from 0.20 to 1.34 dex and peaks at  $\sim 0.25$  dex, or about a factor of 2. Fig. 1 shows that nebulae with ADFs larger than 10 are relatively rare, contributing only about 5–10 per cent of the population. A similar result was obtained from the independent sample of Tsamis et al. (2004), where two nebulae, NGC 2022 and LMC N 66, are found to have an ADF over 10 out of a sample of 15 PNe. On the other hand, Fig. 1 shows that there is clearly a continuous distribution of ADFs from nearly unity (i.e. no discrepancy) up to 20. Excluding those very few peculiar nebulae, such as Abell 30 (Wesson, Liu & Barlow 2003), which were previously known to contain H-deficient knots, the most extreme nebula found so far from a large spectroscopic

survey of over a hundred PNe is Hf 2–2 whose ADF reaches 84 for  $O^{++}/H^+$ , a value of almost two orders of magnitude (Liu 2003).

Ionic abundance ratios,  $C^{2+}/O^{2+}$  and  $N^{2+}/O^{2+}$ , calculated using either ORL/ORL or CEL/CEL ratios, are compared in Fig. 2. This shows that the abundance ratios of two heavy element ions derived from the same type of emission line are in good agreement, within a factor of  $\pm 0.30$  dex in most cases. This is consistent with the findings of earlier studies for a limited number of nebulae, that is, for a given nebula, ORL to CEL abundance discrepancy factors are of comparable magnitude for all (second-row) elements analysed (Liu et al. 1995, 2000, 2001b; Mathis, Torres-Peimbert & Peimbert 1998; Luo, Liu & Barlow 2001; Tsamis et al. 2003a, 2004). Given the fact that the emissivities of all recombination lines have only a weak and similar power-law dependence on electron temperature, ionic abundance ratios  $C^{2+}/O^{2+}$  and  $N^{2+}/O^{2+}$  derived from ORLs are essentially independent of the physical conditions in the nebula and thus should be highly reliable.

In Fig. 2, three combinations of diagnostic lines have been used to determine CEL  $C^{2+}/O^{2+}$  and  $N^{2+}/O^{2+}$  abundance ratios. For most objects, the individual determinations are in good agreement. There are however some notable exceptions, such as NGC 40 (ID = 3) and NGC 6210 (ID = 4). NGC 6210 has an angular diameter of  $\sim 16.2$  arcsec (see table 1 in Paper I), so normalization of line fluxes in different bands could be a problem, especially for the UV wavelength region observed with the *IUE*. NGC 40, with a diameter of about 50 arcsec, is much larger than the *IUE* large aperture. In this case, normalization of UV lines could be a

**Table 16.** ORL to CEL abundance discrepancy factor (ADFs) and heavy elemental abundance ratios,  $X^{2+}/O^{2+}$ , derived purely from ORLs or purely from CELs.

		Sun	Hu 1–2	IC 3568	NGC 40	NGC 6210	NGC 6572	NGC 6720
ADF( $O^{2+}$ )	(ORL/OPT)	–	1.6	2.2	17.8	3.1	1.6	2.4
ADF( $O^{2+}$ )	(ORL/UV)	–	2.0	4.6	$\geq 2.2$	4.3	1.1	2.1
ADF( $O^{2+}$ )	(ORL/IR)	–	3.4	2.9	17.3	1.3	1.4	2.3
ADF( $C^{2+}$ )	(ORL/UV)	–	3.6	2.6	5.8	3.4	1.0	3.6
ADF( $N^{2+}$ )	(ORL/UV)	–	4.0	6.1	–	2.7	1.6	2.4
ADF( $N^{2+}$ )	(ORL/IR)	–	$\geq 7.5$	4.2	24.9	1.4	1.9	2.6
ADF( $Ne^{2+}$ )	(ORL/OPT)	–	–	6.4	–	3.5	2.7	3.0
$C^{2+}/O^{2+}$	(ORLs)	0.50	1.5	0.56	2.8	0.25	0.91	1.17
$C^{2+}/O^{2+}$	(UV/UV)	0.50	0.83	0.98	$\geq 1.0$	0.32	1.00	0.68
$C^{2+}/O^{2+}$	(UV/OPT)	0.50	0.67	0.47	8.5	0.22	1.44	0.80
$N^{2+}/O^{2+}$	(ORLs)	0.19	1.5	0.21	1.0	0.13	0.36	0.27
$N^{2+}/O^{2+}$	(UV/UV)	0.19	0.75	0.15	–	0.20	0.26	0.24
$N^{2+}/O^{2+}$	(IR/IR)	0.19	$\leq 0.70$	0.14	0.70	0.12	0.63	0.24
$Ne^{2+}/O^{2+}$	(ORLs)	–	–	0.58	–	0.27	0.38	0.45
$Ne^{2+}/O^{2+}$	(CELs)	–	0.26	0.27	0.04	0.23	0.23	0.36
$10^4 \times O^{2+}/H^+$	(Opt CELs)	–	0.435	2.43	0.120	4.23	3.47	3.02
$10^4 \times O^{2+}/H^+$	(IR CELs)	–	0.205 <sup>a</sup>	1.86	0.124	9.62	4.01	3.24

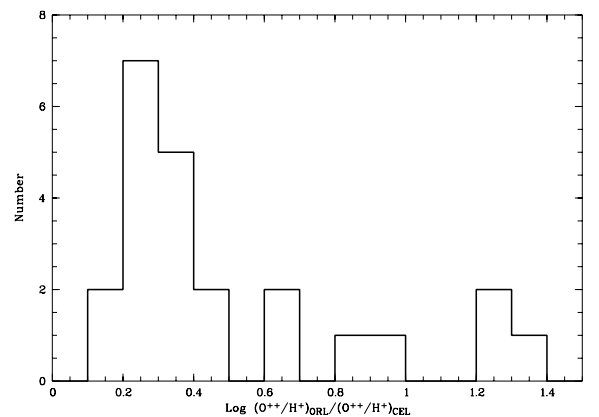
  

		Sun	NGC 6741	NGC 6781	NGC 6790	NGC 6826	NGC 6884	NGC 7662
ADF( $O^{2+}$ )	(ORL/OPT)	–	1.9	–	1.7	1.9	2.3	2.0
ADF( $O^{2+}$ )	(ORL/UV)	–	2.0	–	1.9	1.9	1.9	4.6
ADF( $O^{2+}$ )	(ORL/IR)	–	3.5	–	2.8	2.0	2.3	2.0
ADF( $C^{2+}$ )	(ORL/UV)	–	2.5	–	3.1	2.2	2.5	4.7
ADF( $N^{2+}$ )	(ORL/OPT)	–	1.5	–	1.5	2.8	2.2	9.6
ADF( $N^{2+}$ )	(ORL/IR)	–	3.5	–	–	2.5	2.8	2.0
ADF( $Ne^{2+}$ )	(ORL/OPT)	–	4.7	–	2.5	3.4	5.8	7.1
$C^{2+}/O^{2+}$	(ORLs)	0.50	1.28	–	1.13	0.97	0.89	1.32
$C^{2+}/O^{2+}$	(UV/UV)	0.50	1.00	–	0.67	0.81	0.65	1.30
$C^{2+}/O^{2+}$	(UV/OPT)	0.50	0.96	–	0.62	0.80	0.81	0.55
$N^{2+}/O^{2+}$	(ORLs)	0.19	0.40	–	0.10	0.38	0.28	0.22
$N^{2+}/O^{2+}$	(UV/UV)	0.19	0.52	–	0.12	0.25	0.24	0.11
$N^{2+}/O^{2+}$	(IR/IR)	0.19	0.39	0.28	–	0.20	0.19	0.10
$Ne^{2+}/O^{2+}$	(ORLs)	–	0.67	–	0.30	0.37	0.61	0.65
$Ne^{2+}/O^{2+}$	(CELs)	–	0.27	0.38	0.21	0.20	0.24	0.18
$10^4 \times O^{2+}/H^+$	(Opt CELs)	–	2.56	2.73	2.44	3.07	3.62	1.79
$10^4 \times O^{2+}/H^+$	(IR CELs)	–	1.39	6.23	1.52	2.86	3.64	1.80

Note. <sup>a</sup>Derived from the [O III] 88- $\mu$ m line.

problem, but this should not affect  $C^{2+}/O^{2+}$  and  $N^{2+}/O^{2+}$  derived from the  $\lambda 1908/\lambda 1663$  and  $\lambda 1750/\lambda 1663$  intensity ratios, respectively. In NGC 40,  $\lambda 1908/\lambda 1663$  yields an ionic ratio significantly lower than that derived from the other two pairs of diagnostic line ratios. For NGC 40 and 6210, the UV N III]  $\lambda 1750$  and O III]  $\lambda 1663$  intercombination lines were only marginally detected, so ionic abundances determined from them are therefore quite uncertain (see Table 1). In addition, NGC 40 has a WC 8 Wolf–Rayet central star. One possibility is that our measurements of UV lines in this nebula have been contaminated by emission/absorption from the stellar winds.

$N^{2+}/O^{2+}$  abundance ratios derived for NGC 7662, Hu 1–2 and NGC 6826 from the three pairs of collisionally excited diagnostic line ratios are in good agreement with each other and are lower than the ORL values by approximately a factor of 2. There is a possibility that some of the N II ORLs used to determine  $N^{2+}/O^{2+}$  abundance ratios are enhanced by fluorescence excitation. Grandi (1976) suggests that in the Orion nebula multiplets V3, V5 and V30 of N II are fluorescently excited by the He I  $\lambda 508.6$  resonance line. On the



**Figure 1.** Histogram of logarithmic ADF for  $O^{2+}/H^+$  ionic abundance for a sample of 23 PNe (see text for details).

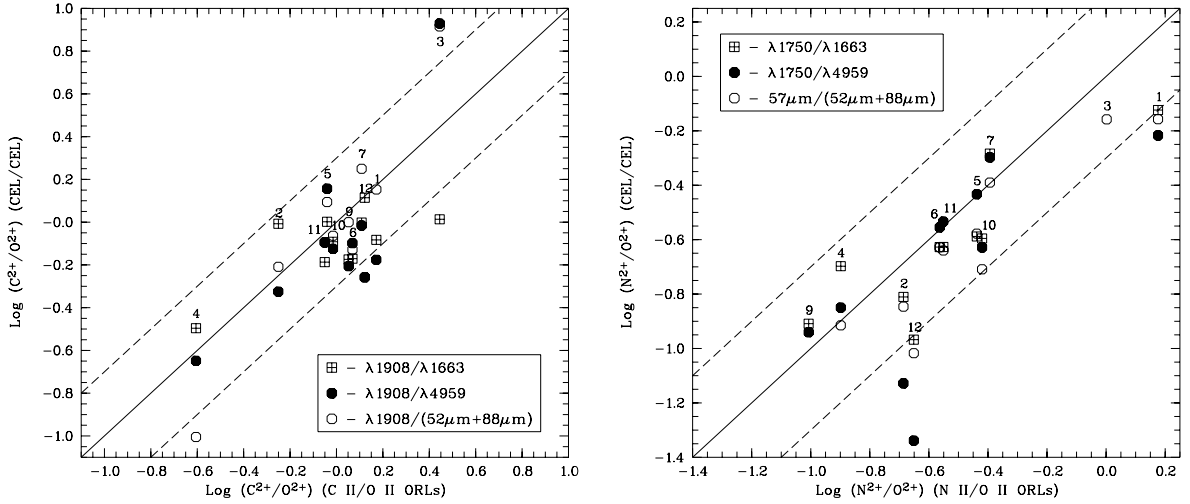


**Figure 2.** Comparison of  $C^{2+}/O^{2+}$  (left) and  $N^{2+}/O^{2+}$  (right) ionic abundance ratios derived from ORLs and from UV, optical and IR CELs. The dashed lines represent ADFs of  $\pm 0.3$  dex. Each nebula is labelled by an ID number listed in Table 14. Data points with identical abscissa values are for the same PN.

other hand, Liu et al. (2001b) show that the relative intensities of N II ORLs observed in PNe M 1–42 and M 2–36 are inconsistent with fluorescence by the He I  $\lambda 508.6$  line and suggest that continuum fluorescence by starlight is probably more plausible. It should be noted however that N II lines from large orbital angular momentum spectral terms, such as those from the 3d–4f configuration, are unlikely affected by any fluorescence processes. For objects in our sample, ORL  $N^{2+}/H^+$  abundances for IC 3568, NGC 40 could unfortunately be derived from multiplets V3 and V5 only (Tables 3 and 4). For Hu 1–2,  $N^{2+}/H^+$  abundances determined from multiplets V3 and V5 are significantly higher than those derived from multiplet V20 and from 3d–4f transitions. The ORL  $N^{2+}/H^+$  abundance ratio adopted here for Hu 1–2 was based on the 3d–4f lines only.

### 3.2 N and O ionic abundances derived from UV, optical and IR CELs

Collisionally excited IR fine-structure lines have excitation energies of only a few hundred Kelvin, much smaller than nebular electron temperatures determined from optical forbidden-line temperature-diagnostic ratios such as the [O III]  $\lambda 4959/\lambda 4363$  nebular to auroral line ratio (typically of the order of  $\sim 10^4$  K) and of the excitation energies of optical/UV CELs (typically  $\gtrsim$  a few eV, or equivalently  $\gtrsim$  a few times  $10^4$  K). Thus, unlike UV or optical CELs, ionic abundance ratios  $X^{i+}/H^+$  derived from IR fine-structure lines are insensitive to uncertainties in electron temperature determinations and to the presence of possible temperature fluctuations. Fig. 3 compares  $O^{2+}/H^+$  abundance ratios derived from the UV O III]  $\lambda\lambda 1661, 1665$

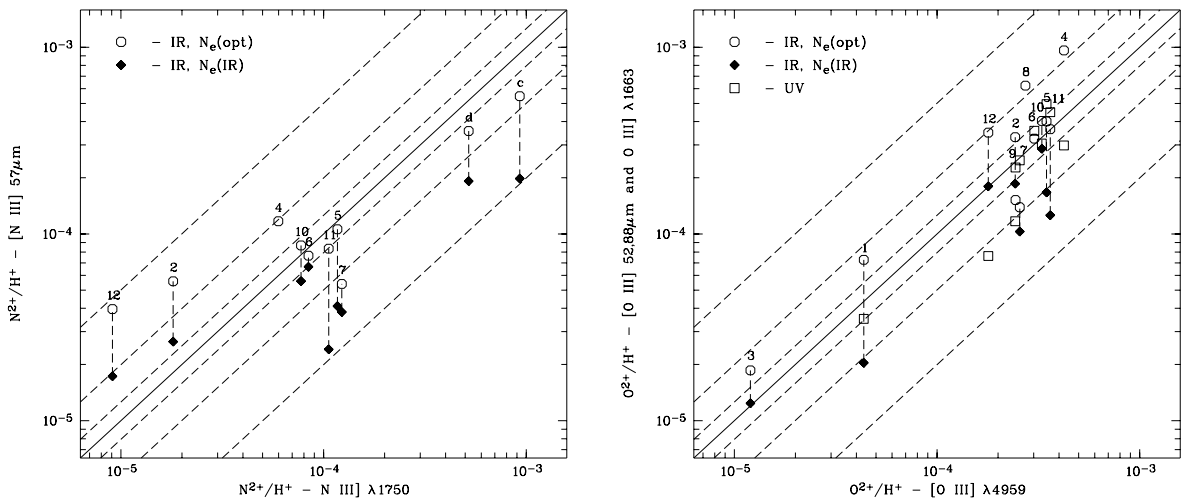


**Figure 3.** Comparison of  $N^{2+}/H^+$  abundance ratios derived from the N III] UV  $\lambda 1750$  intercombination line and from the IR [N III] 57- $\mu\text{m}$  fine-structure line, and  $O^{2+}/H^+$  ratios derived from the UV O III]  $\lambda 1663$  intercombination line, the [O III] optical  $\lambda 4959$  forbidden line, and from the IR 52- and 88- $\mu\text{m}$  fine-structure lines. Open and filled symbols represent IR ionic abundances derived assuming, respectively, the average electron density derived from optical density-diagnostic ratios and that deduced from the [O III] 88- $\mu\text{m}$ /52- $\mu\text{m}$  IR fine-structure line ratio. Nebulae are labelled by the IDs listed in Table 14. Data points with identical abscissa values are for the same PN. The dashed lines represent abundance discrepancy factors of  $\pm 0.1$ ,  $\pm 0.3$  and  $\pm 0.7$  dex, respectively.

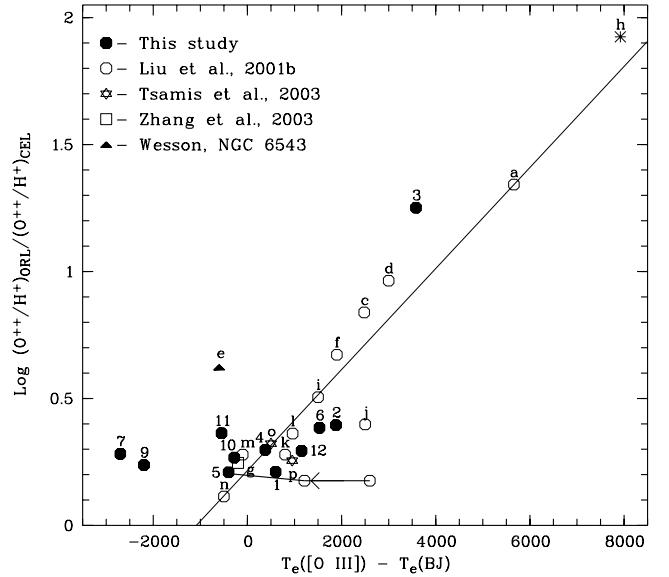
intercombination lines, the optical [O III]  $\lambda 4959$  forbidden line, and from the FIR [O III] 52- and 88- $\mu\text{m}$  fine-structure lines. Also compared in the figure are  $\text{N}^{2+}/\text{H}^+$  abundance ratios derived from the UV N III  $\lambda 1750$  intercombination line and from the FIR [N III] 57- $\mu\text{m}$  fine-structure line. Given that FIR fine-structure lines have relatively low critical densities ( $\sim$  a few times  $10^3 \text{ cm}^{-3}$ ), ionic abundances derived from them are however sensitive to the electron densities adopted. We have therefore plotted in Fig. 3  $\text{N}^{2+}/\text{H}^+$  and  $\text{O}^{2+}/\text{H}^+$  ionic abundance ratios derived adopting, respectively, the average electron density deduced from optical diagnostic line ratios (such as the [S II]  $\lambda 6731/\lambda 6716$  and [Cl III]  $\lambda 5537/\lambda 5517$  doublet ratios) and the electron density deduced from FIR fine-structure line ratios (such as the [O III] 88- $\mu\text{m}/52\text{-}\mu\text{m}$  ratio). The average electron densities derived from optical forbidden-line ratio are normally higher than values derived from FIR fine-structure line ratios and this has been attributed to modest density inhomogeneities within nebulae (Liu et al. 2001a).

Fig. 3 shows that, for the majority of PNe in our sample, FIR fine-structure lines yield ionic abundances very similar to those derived from UV or optical CELs. Tsamis et al. (2004) obtain a similar result from an independent sample. The result is consistent with previous detailed analysis for a few extreme nebulae, such as NGC 6153 (Liu et al. 2000), M 1-42 and M 2-36 (Liu et al. 2001b) where it is found that within the observational uncertainties, UV, optical and IR CELs all yield comparable ionic abundances, regardless of the large differences in excitation energy and critical density amongst the diagnostic lines in different wavebands.

In NGC 40, the  $\text{O}^{2+}/\text{H}^+$  abundance ratio derived from the O III  $\lambda 1663$  intercombination line is much higher than the values derived from the [O III] optical forbidden lines and FIR fine-structure lines. Again, measurement uncertainties or contaminations by emission/absorption from the WC 8 Wolf-Rayet stellar winds may contribute to the large discrepancy. Note that for NGC 40, if we adopt the  $\text{O}^{2+}/\text{H}^+$  ratio derived from the IR fine-structure lines instead of the optical CEL  $\text{O}^{2+}/\text{H}^+$  ratio (assuming the electron density derived from the [O III] 88- $\mu\text{m}/52\text{-}\mu\text{m}$  FIR fine-structure line ratio), then the ADF for  $\text{O}^{2+}/\text{H}^+$  between the ORL and CEL ionic abundances remains essentially unchanged, decreasing slightly from 17.8 to 17.3. However, if we adopt  $\text{O}^{2+}/\text{H}^+$  derived from the IR lines assuming the higher electron density deduced from optical forbidden-line ratios, then the discrepancy factor drops to 14.5. For comparison, the ADFs for  $\text{N}^{2+}/\text{H}^+$ , using the values derived from N II ORLs and the [N III] 57- $\mu\text{m}$  FIR fine-structure line, are 24.9 and 14.5 for the two cases where the  $\text{N}^{2+}/\text{H}^+$  ratio is derived from the IR line assuming the electron density determined from the [O III] 88- $\mu\text{m}/52\text{-}\mu\text{m}$  ratio, or from optical forbidden-line ratios, respectively. In both cases, the ORL abundances of N and O deduced for NGC 40 remain however much higher than the corresponding values deduced from IR fine-structure CELs.

### 3.3 Electron temperatures

The discrepancy between ORL and CEL abundances has been found to be strongly correlated with another long-standing discrepancy in nebular astrophysics: the dichotomy of  $T_e$  derived from the [O III] forbidden-line ratio and from the hydrogen recombination continuum Balmer discontinuity (Peimbert 1971; Liu & Danziger 1993). Nebulae previously found to show abnormally high ORL heavy elemental abundances all have a ‘normal’ forbidden-line electron temperature no different from that normally found for an ionized gaseous nebula, i.e. around  $1 \times 10^4 \text{ K}$ , yet they all exhibit a very low Balmer jump temperature,  $T_e(\text{BJ})$ . As the ORL to CEL abun-



**Figure 4.** ADFs for  $\text{O}^{2+}/\text{H}^+$  plotted against  $T_e([\text{O III}]) - T_e(\text{BJ})$ , the difference between the electron temperature derived from the [O III]  $\lambda 4959/\lambda 4363$  nebular to auroral line ratio and from the nebular continuum Balmer jump. The solid line gives the linear fit obtained by Liu et al. (2001b). Nebulae with IDs ‘1–12’ and ‘a–g’ are listed in Table 14: ‘h’, Hf 2–2; ‘i’, NGC 3242; ‘j’, NGC 3918; ‘k’, NGC 5315; ‘l’, NGC 5882; ‘m’, NGC 6644; ‘n’, M42; ‘o’, M17; ‘p’, NGC 3576. For NGC 6572 (‘5’), three independent measurements of  $T_e([\text{O III}]) - T_e(\text{BJ})$  are plotted separately, connected by a line and a left arrow (see text for more details).

dance discrepancy increases,  $T_e(\text{BJ})$  decreases rapidly (Liu et al. 2001b). The most extreme PN found so far is Hf 2–2, whose ADF reaches 84 and  $T_e(\text{BJ})$  drops to 900 K, a factor of 10 lower than its  $T_e([\text{O III}])$  of 8820 K (Liu 2003).

$T_e([\text{O III}])$  and  $T_e(\text{BJ})$  have both been measured for 11 PNe in our sample (Paper I). Amongst these objects, NGC 40 has the largest difference between the two temperatures,  $T_e(\text{BJ}) = 7020$ , about 3580 K lower than  $T_e([\text{O III}]) = 10600 \text{ K}$ .

In Fig. 4, ADFs for  $\text{O}^{2+}/\text{H}^+$  ionic abundances derived from O II ORLs and from the [O III] optical forbidden lines are plotted against  $T_e([\text{O III}]) - T_e(\text{BJ})$  for 23 PNe and three H II regions. Electron temperatures for the 11 PNe in the current sample are taken from table 8 of Paper I. Data for NGC 7027 and 6543 are from Zhang et al. (in preparation) and Wesson & Liu (2004), respectively. Measurements for the other PNe and the H II region M42 (the Orion nebula) are taken from Liu et al. (2001b). Data for the other two H II regions, M17 and NGC 3576, are taken from Tsamis et al. (2003a). Finally, data for the most extreme PN Hf 2–2 are taken from Liu (2003) and our unpublished results. The linear fit obtained by Liu et al. (2001b) for a smaller sample of nebulae is also overplotted in the figure.

Excluding NGC 40, the  $\text{O}^{2+}/\text{H}^+$  ADFs deduced for the other 10 PNe in our sample (filled circles in Fig. 4) fall in a narrow range between 1.6 and 3.1, and the corresponding values of  $T_e([\text{O III}]) - T_e(\text{BJ})$  vary from  $-2700$  to  $1900 \text{ K}$ . Amongst them, NGC 6790 and 6741 have ADFs of 1.7 and 1.9, respectively, yet both nebulae are found to have a  $T_e(\text{BJ})$  significantly higher than  $T_e([\text{O III}])$ , by  $\sim 2200$  and  $2700 \text{ K}$ , respectively. NGC 6572 has been previously discussed by Liu et al. (1999) and Liu et al. (2001b). This compact, high-density PN has one of the smallest ADFs amongst the PNe analysed so far,  $\text{ADF}(\text{O}^{2+}) = 0.20 \text{ dex}$  (current work) and  $0.18 \text{ dex}$  (Liu et al. 2001b). The Balmer jump temperature of NGC 6572

was first determined by Peimbert (1971), who found that  $T_e(\text{BJ}) = 8700_{-900}^{+1050}$  K. From a medium-resolution spectrum obtained with the European Southern Observatory (ESO) 1.52-m telescope in 1992 May, Liu et al. (1999) derived a Balmer jump temperature of 7800 K. A much higher value of 9090 K was determined by Liu et al. (2001b) using newly obtained high-quality spectra. Our own spectrum yields a Balmer jump temperature of 11 000 K, which is 400 K higher than the  $[\text{O III}]$  forbidden-line temperature of 10 600 K. As noted by Liu et al. (2001b), NGC 6572 is one of a rare class of PN known to have a variable spectrum (Mendez, Manchado & Herrero 1988; Feibelman, Aller & Hyung 1992; Hyung et al. 1994). It is unclear whether the wide range of Balmer jump temperature found for NGC 6572 from these independent studies represents intrinsic variations. The differences between the individual determinations seem to be too large to be simply attributed to measurement uncertainties.

#### 4 CORRELATIONS OF ABUNDANCE AND TEMPERATURE DETERMINATION DISCREPANCIES WITH OTHER NEBULAR PROPERTIES

In this section, we investigate possible correlations between ORL to CEL temperature/abundance determination discrepancies and other nebular properties, such as metallicity, mean surface brightness, diameter, density, E.C.

##### 4.1 Oxygen abundance

Earlier studies show that the ORL to CEL abundance discrepancy factor varies from target to target. In Fig. 5 we plot total elemental oxygen abundances from ORLs and from CELs against the  $\text{O}^{2+}/\text{H}^+$  ORL to CEL ionic abundance discrepancy factor for a sample of 18 PNe. Fig. 5 shows that over a wide ADF range the total elemental oxygen abundance derived from CELs remains nearly constant, while ORL abundances show a considerable range of over an order of magnitude. There is good positive correlation between  $[\text{O}/\text{H}]_{\text{ORL}}$  and

$$\Delta(\text{O}^{2+}/\text{H}^+) \equiv \log(\text{O}^{2+}/\text{H}^+)_{\text{ORL}} - \log(\text{O}^{2+}/\text{H}^+)_{\text{CEL}}.$$

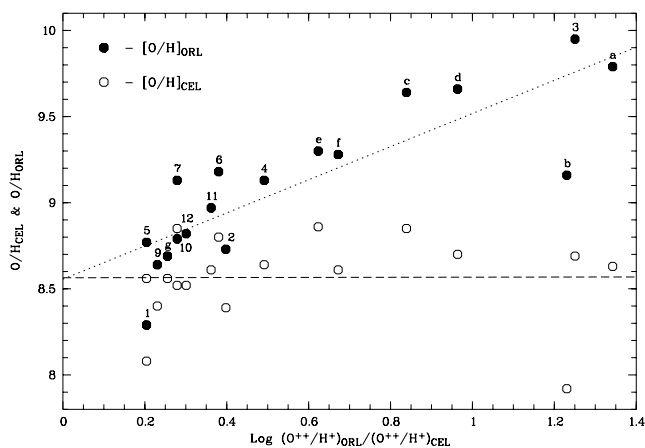


**Figure 5.** Oxygen abundances derived from ORLs (filled circles) and from CELs (open circles) plotted against the ORL to CEL  $\text{O}^{2+}/\text{H}^+$  ionic abundance discrepancy factor. Nebulae are labelled with the ID numbers given in Table 14. Data points with identical abscissa values are for the same PN. The dotted and dashed lines are linear fits to the filled circles and open circles, respectively.

A linear fit yields

$$\left[\frac{\text{O}}{\text{H}}\right]_{\text{ORL}} = (8.56 \pm 0.11) + (0.962 \pm 0.154)\Delta \left(\frac{\text{O}^{2+}}{\text{H}^+}\right),$$

with a linear correlation coefficient of 0.84. Clearly, this tight correlation is a result of variations of ORL oxygen abundances amongst PNe which all have an almost equal CEL oxygen abundance. In fact, a linear fit to  $[\text{O}/\text{H}]_{\text{CEL}}$ , as a function of  $\Delta(\text{O}^{2+}/\text{H}^+)$  (i.e. open circles in Fig. 5) yields

$$\left[\frac{\text{O}}{\text{H}}\right]_{\text{CEL}} = (8.56 \pm 0.11) + (0.003 \pm 0.161)\Delta \left(\frac{\text{O}^{2+}}{\text{H}^+}\right),$$

with a linear correlation coefficient of a mere 0.005.

With an ADF of about 20, the oxygen abundances of NGC 40 and M 1–42 deduced from ORLs are more than an order of magnitude higher than the solar value. Such a high metallicity is very difficult to understand if PNe are descendants of low and intermediate stars and the ORL abundances represent the true metallicity of the bulk material of the ejected envelope during the late evolutionary stages of the star. M 2–24 (Zhang & Liu 2003) also has a large ADF (17) for oxygen. However, the oxygen abundance of M 2–24 derived from CELs is the lowest amongst the PNe plotted in Fig. 5,  $[\text{O}/\text{H}]_{\text{CEL}} = 7.92$ , compared to  $[\text{O}/\text{H}]_{\text{ORL}} = 9.16$ . Zhang & Liu (2003) show that M 2–24 has a dense central emission region and find that it is strongly enhanced in  $\alpha$  elements, suggesting that it was formed in an environment quite different from that of the Sun. For Hu 1–2, both the oxygen abundances derived from ORLs and from CELs are lower by 0.45 dex compared to other PNe with similar ADFs. A recent detailed CEL abundance analysis for Hu 1–2 has been carried out by Pottasch et al. (2003a). The oxygen abundance derived by them was 8.20, compared to our value of 8.08. They find that it also has very low S, Ne and Ar abundances compared to other disc PNe and conclude that the progenitor star of Hu 1–2 is very old, has a low mass and it takes a long time for it to reach the PN stage.

In addition to ADF variations amongst different nebulae, the discrepancy between ORL and CEL abundances has also been found to vary across the nebular surface in NGC 6153 (Liu et al. 2000), NGC 6720 (Garnett & Dinerstein 2001b) and NGC 7009 (Luo & Liu 2003). In all cases, while CEL abundances are found to be nearly constant across the nebula, ORL abundances are strongly peaked towards the nebular centre. Thus again, it seems that the discrepancy between heavy elemental abundances derived from ORLs and from CELs is mainly caused by apparently higher ORL abundances.

##### 4.2 Magnesium abundance

As pointed out by Barlow et al. (2003), the  $\text{Mg II } 4f\text{--}3d$  line at 4481.21 Å is the strongest and easiest to measure ORL from any third-row ion and to a good approximation,  $\text{Mg}/\text{H} = \text{Mg}^{2+}/\text{H}^+$ . We have determined  $\text{Mg}^{2+}/\text{H}^+$  ionic abundances from the  $\text{Mg II } \lambda 4481$  line for 11 PNe in our sample. In Fig. 6, we plot  $\text{Mg}^{2+}/\text{H}^+$  ionic abundance ratios determined from the  $\text{Mg II } \lambda 4481$  ORL against the  $\text{O}^{2+}/\text{H}^+$  ADF for a sample of 18 PNe, including five PNe previously analysed by Barlow et al. (2003), plus M 2–24 from Zhang & Liu (2003) and NGC 7027 from Zhang et al. (in preparation).

As mentioned above, the peculiar bulge PN M 2–24 is strongly enhanced in  $\alpha$  elements, including magnesium. Excluding M 2–24, magnesium abundances determined from the  $\lambda 4481$  ORL are almost constant over a wide range of oxygen ADFs. The average Mg abundance of  $\log(\text{Mg}/\text{H}) + 12 = 7.52_{-0.22}^{+0.14}$  is consistent within the uncertainties with the solar photospheric value, 7.54 (or  $3.45 \times 10^{-5}$  by number; Holweger 2001). As pointed out by Barlow et al. (2003),

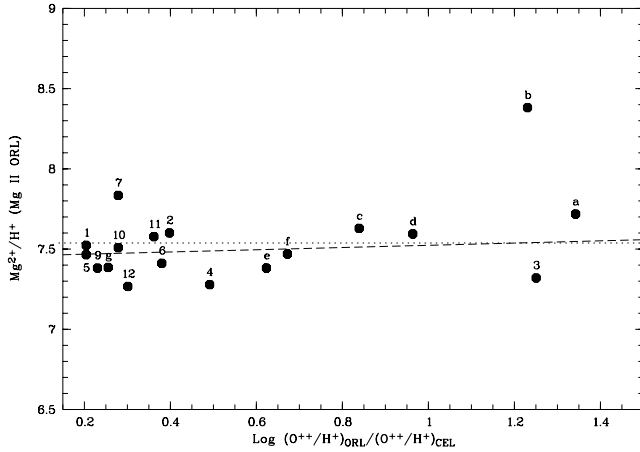


**Figure 6.**  $\text{Mg}^{2+}/\text{H}^+ \sim \text{Mg}/\text{H}$ , derived from the Mg II  $\lambda 4481$  ORL, plotted against the  $\text{O}^{2+}/\text{H}^+$  ADF. Nebulae are labelled with the IDs given in Table 14. The dotted line represents the solar magnesium abundance,  $\text{Mg}/\text{H} = 3.45 \times 10^{-5}$ . The dashed line is a linear fit to all data points excluding Mg 2–24 ('b').

depletion of magnesium on to dust grains is unlikely to be significant in PNe. Clearly, the strong enhancement of ORL abundances relative to CEL values observed in second-row elements, such as carbon, nitrogen, oxygen and neon, is absent for the third-row element magnesium. A linear regression yields

$$\left[ \frac{\text{Mg}^{2+}}{\text{H}^+} \right] = (7.45 \pm 0.07) + (0.069 \pm 0.109) \Delta \left( \frac{\text{O}^{2+}}{\text{H}^+} \right),$$

with a linear correlation coefficient of 0.12.

For the high-excitation PNe Hu 1–2, NGC 6741, 7662 and 7027, [Mg IV] and [Mg V] CELs have been detected in some of them, yielding  $\text{Mg}^{3+}$  and  $\text{Mg}^{4+}$  ionic abundances, respectively. If we make corrections to the magnesium elemental abundances for these high-excitation PNe by allowing for small contributions from  $\text{Mg}^{3+}$  and  $\text{Mg}^{4+}$  ionic stages and assume

$$(\text{Mg}/\text{H})_{\text{sum}} = (\text{Mg}_{\text{ORL}}^{2+} + \text{Mg}_{\text{CELs}}^{3+} + \text{Mg}_{\text{CELs}}^{4+})/\text{H}^+,$$

then, after the corrections, a linear regression yields

$$\left[ \frac{\text{Mg}}{\text{H}} \right]_{\text{sum}} = (7.51 \pm 0.07) + (0.010 \pm 0.152) \Delta \left( \frac{\text{O}^{2+}}{\text{H}^+} \right),$$

with a linear correlation coefficient of 0.02.

### 4.3 Helium abundance

$\text{He}^+$  and  $\text{He}^{2+}$  ionic abundances are traditionally derived from strong and easily observable lines such as He I  $\lambda 4471$ ,  $\lambda 5876$  and  $\lambda 6678$ , and He II  $\lambda 4686$ , all excited by recombination. It is interesting to investigate whether helium ionic abundances derived from these ORLs are also enhanced relative to values indicated by a He I or He II CEL, should such a line be observable. We note that the He I  $2s^3S$  level is metastable. As a consequence, there is a large population built on this level, and excited triplet spectral terms such as  $2p^3P^o$  become accessible by thermal electron collisions. As a result, the He I  $2s^3S-2p^3P^o$  line at  $1.0830 \mu\text{m}$  is strongly enhanced or even dominated by collisional excitation from the  $2s^3S$  metastable level. This line, however, falls in the near-IR and is difficult to observe using an optical spectrograph. X.-W. Liu obtained in 2001 June a high-quality spectrum of NGC 6153 in the far red covering the  $\lambda\lambda 7700-11100$  wavelength region using the Boller & Chivens

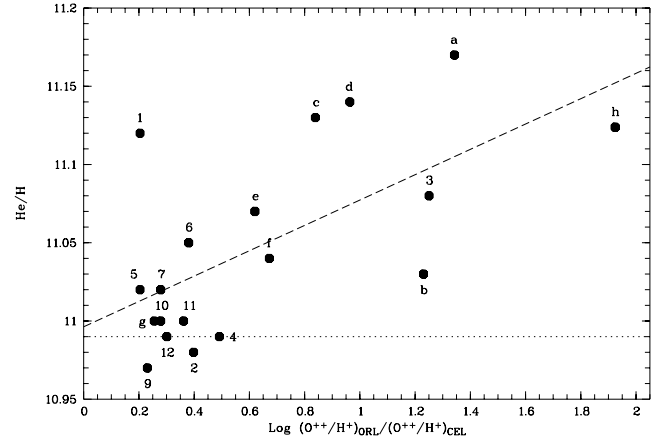


**Figure 7.** Nebular helium abundances [in units such that  $\log N(\text{H}) = 12$ ] plotted against  $\text{O}^{2+}/\text{H}^+$  ADFs for 19 PNe, labelled with the ID numbers listed in Table 14 and 'h' denotes Hf 2–2. The dashed line is a linear fit to the data.

spectrograph mounted on the ESO 1.52-m telescope. The He I  $1.0830\text{-}\mu\text{m}$  line flux measured from this spectrum is found to be in excellent agreement with the prediction of the detailed bi-abundance photoionization model constructed by Péquignot et al. (2003). This implies that if one carries out an empirical abundance analysis assuming a chemically homogeneous nebula, then the  $\text{He}^+/\text{H}^+$  ionic abundance ratio derived from He I ORLs such as He I  $\lambda 4471$ ,  $\lambda 5876$  and  $\lambda 6678$  will be higher than the value yielded by the mainly collisionally excited He I  $1.0830\text{-}\mu\text{m}$  line.<sup>2</sup> Additional measurements of the He I  $1.0830\text{-}\mu\text{m}$  line in other PNe are highly desirable. This line is however strongly affected by optical depth effects, such that detailed radiation transfer and photoionization modelling are required for proper interpretation of its observed intensity.

In Fig. 7, helium abundances in units such that  $\log N(\text{H}) = 12.0$ , are plotted against  $\text{O}^{2+}/\text{H}^+$  ADFs for 19 PNe, including Hf 2–2 (X.-W. Liu, unpublished data). Fig. 7 shows that the He abundance is positively correlated with the  $\text{O}^{2+}/\text{H}^+$  ADF. A linear fit yields

$$\text{He} = (10.997 \pm 0.019) + (8.03 \pm 2.33) \times 10^{-2} \Delta \left( \frac{\text{O}^{2+}}{\text{H}^+} \right),$$

with a linear correlation coefficient of 0.64.

Zhang et al. (2004) find for a large number of PNe that the nebular helium abundance is positively correlated with the difference between the [O III] forbidden-line temperature and the Balmer jump temperature. Because the ADF has been found to be positively correlated with the difference between the two temperatures (Liu et al. 2001b; see also Fig. 4), the positive correlation seen in Fig. 7 comes as no surprise.

It has been known for some time that, in PNe, helium and nitrogen abundances are positively correlated with each other, a fact often attributed to the second dredge-up process. However, as pointed out by Zhang et al. (2004), the very high helium abundance measured in some PNe, including some of the extreme PNe showing very large ADFs, raises the question of whether part, if not all, of the overabundance of helium is caused by physical effects which are responsible for the systematically higher ORL heavy element abundances relative to the corresponding CEL values.

<sup>2</sup> In the bi-abundance model of NGC 6153 constructed by Péquignot et al. (2003), roughly two-thirds of the observed He I  $1.0830\text{-}\mu\text{m}$  line emission is produced by collisional excitation by electron impacts.

#### 4.4 N/O abundance ratio

We have shown in Section 2.3 that if we adopt the new more strict criterion for type I PN of Kingsburgh & Barlow (1994),  $N/O \geq 0.74$ , then three PNe, Hu 1–2, M 1–42 and M 2–24 listed in Table 14 are type I PNe. For the original criterion of Peimbert & Torres-Peimbert (1983),  $He/H \geq 0.125$  and  $N/O \geq 0.5$ , NGC 6741 can be added to the list of type I PN. Here we have adopted the N/O abundance ratio derived from CELs. The new criterion requires the observed N/O abundance ratio to be greater than the average (N+C)/O abundance ratio for H II regions of the host galaxy. Type I PNe are believed to have evolved from more massive progenitor stars, with an initial main-sequence mass  $M > 2.4 M_{\odot}$  (Peimbert & Serrano 1980), and thus to have formed more recently out of a more enriched ISM. In Fig. 8, we plot ADFs for  $O^{2+}/H^{+}$  against the N/O abundance ratio for a sample of 18 PNe. Excluding NGC 40 and Hf 2–2, there is a general trend that the ADF increases for higher N/O abundance ratios, albeit with a large scatter. NGC 40 has a very low E.C. and singly ionized species, such as  $N^{+}$  and  $O^{+}$ , dominate in this nebula. From optical forbidden lines, we find  $N^{+}/O^{+} = 0.16$ , whereas from FIR fine-structure lines measured with the *ISO* Long Wavelength Spectrometer (LWS), we find  $N^{2+}/O^{2+} = 0.70$  (the value from ORLs is 1.0). The total N/O elemental abundance ratio from the CEL analysis is 0.17.

#### 4.5 Surface brightness, diameter and density

The mean surface brightness of a PN can be regarded as an evolutionary parameter. As the nebula ages and expands, the density drops and the surface brightness decreases. Garnett & Dinerstein (2001a) find that  $O^{2+}/H^{+}$  ADFs are greater for larger, lower surface brightness PNe than for compact, dense ones, and suggest that the abundance problem is a function of PN evolution, caused by some physical processes which are related to the evolutionary state of a nebula. A similar trend is found for the current sample of PNe.

**Table 17.** Nebular angular diameters, distances, mean surface brightnesses,  $N_e([S II])$  and E.C.s. Nebular total  $H\beta$  fluxes and optical angular diameters are taken from the Strasbourg–ESO Catalogue of Galactic Planetary Nebulae (Acker et al. 1992) and distances are from Cahn, Kaler & Stanghellini (1992) except for Hf 2–2.

Name	ADF( $O^{2+}$ )	$\log F(H\beta)$ ( $\text{erg cm}^{-2} \text{s}^{-1}$ )	$c(H\beta)$	Diameter (arcsec)	Distance (kpc)	$12 + \log [I(H\beta)/\theta^2]$ ( $\text{erg cm}^{-2} \text{s}^{-1} \text{arcsec}^{-2}$ )	$\log N_e([S II])$ ( $\text{cm}^{-3}$ )	E.C.
Hf 2–2	84.0 <sup>a</sup>	−12.30	0.73 <sup>b</sup>	18.6	4.50 <sup>c</sup>	−1.507	2.52 <sup>b</sup>	0.80
M 1–42	22.0	−11.63	0.70 <sup>d</sup>	9.0	5.46	−0.236	3.09 <sup>d</sup>	2.21
NGC 40	17.8	−10.37 <sup>e</sup>	0.70	48.0	1.24	−0.430	3.24	0.18
M 2–24	17.0	−12.10	0.80 <sup>f</sup>	6.8	9.26	−0.363	3.25 <sup>f</sup>	1.59
NGC 6153	9.2	−10.86	1.30 <sup>g</sup>	24.0	1.28	0.282	3.60 <sup>g</sup>	3.83
M 2–36	6.9	−11.20	0.27 <sup>d</sup>	8.1	6.06	−0.145	3.58 <sup>d</sup>	3.43
NGC 7009	4.7	−9.80	0.20 <sup>h</sup>	28.5	1.20	0.092	3.59 <sup>h</sup>	5.19
NGC 6543	4.2	−9.61	0.10 <sup>i</sup>	19.5	0.98	0.512	3.81 <sup>i</sup>	2.94
NGC 6210	3.1	−10.09	0.13	16.2	2.03	0.223	3.64	4.69
IC 3568	2.5	−10.82	0.26	10.0	2.71	0.042	3.28	4.59
NGC 6720	2.4	−10.08	0.20	76.0	0.87	−1.040	2.70	5.52
NGC 6884	2.3	−11.11	1.00	6.0	2.11	0.936	3.96	5.34
NGC 7662	2.0	−9.99	0.18	17.0	1.16	0.331	3.52	6.79
NGC 6741	1.9	−11.34	1.15	8.0	2.05	0.606	3.30	6.33
NGC 6826	1.9	−9.96	0.06	25.0	1.58	−0.094	3.71	3.26
NGC 7027	1.8	−10.12	1.37 <sup>j</sup>	14.0	0.27	1.560	$\gtrsim 5.00^j$	6.97
NGC 6790	1.7	−10.90	1.10	7.0	1.54	1.112	4.74	6.23
NGC 6572	1.6	−9.82	0.48	10.8	0.71	1.195	4.41	5.26
Hu 1–2	1.6	−11.21	0.51	8.3	1.48	0.064	3.69	9.69

Notes <sup>a</sup>From Liu (2003). <sup>b</sup>From unpublished data. <sup>c</sup>From Maciel (1984). <sup>d</sup>From Liu et al. (2001b). <sup>e</sup>From Carrasco, Serrano & Costero (1983). <sup>f</sup>From Zhang & Liu (2003). <sup>g</sup>From Liu et al. (2000). <sup>h</sup>From Liu et al. (1995). <sup>i</sup>From Wesson & Liu (2004). <sup>j</sup>From Zhang et al. (in preparation).

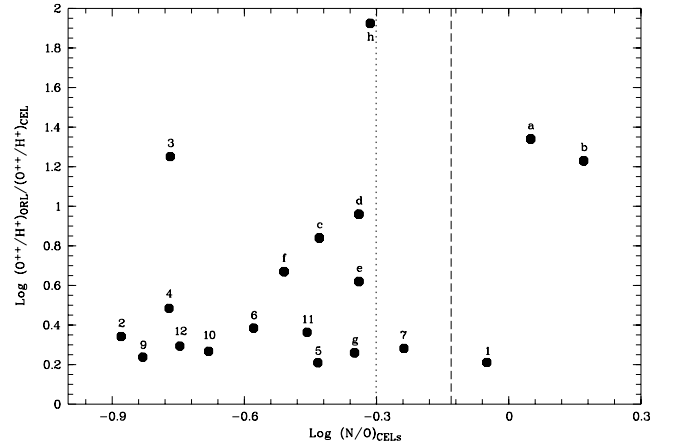


**Figure 8.** Oxygen ADF plotted against  $\log(N/O)$  abundance ratio derived from CELs. Objects are labelled with the ID numbers given in Table 14 and ‘h’ denotes Hf 2–2. The dotted and dashed lines represent, respectively, the classification criteria for type I PN defined by Peimbert & Torres-Peimbert (1983),  $N/O \geq 0.50$ , and by Kingsburgh & Barlow (1994),  $N/O \geq 0.74$ .

In Table 17, we tabulate nebular total  $H\beta$  fluxes, optical angular diameters taken from the Strasbourg–ESO Catalogue of Galactic Planetary Nebulae (Acker et al. 1992), logarithmic extinction coefficients and distances for 19 PNe, including Hf 2–2. Dereddened average nebular surface brightnesses, calculated from total  $H\beta$  flux and angular diameter are also given in the table, in units of  $10^{-12} \text{ erg cm}^{-2} \text{ s}^{-1} \text{ arcsec}^{-2}$ .

In Fig. 9 we plot  $O^{2+}/H^{+}$  ADFs against mean nebular  $H\beta$  surface brightnesses, after correcting for interstellar extinction, for a sample of 19 PNe. Data for 12 PNe previously analysed by Garnett & Dinerstein (2001a) are also plotted. They are generally brighter than PNe in our sample and have lower abundance discrepancies. With the exception of NGC 6720 (labelled as ‘6’), there is a clear trend for the  $O^{2+}/H^{+}$  ADF,  $\Delta(O^{2+}/H^{+})$ , to be anticorrelated with

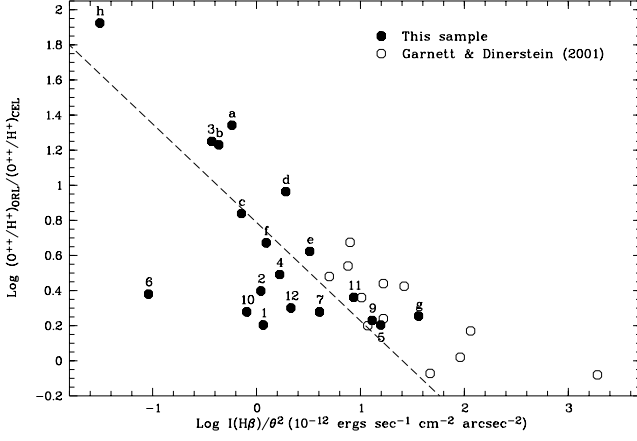


**Figure 9.** ADFs for  $O^{2+}/H^+$  plotted against mean nebular surface brightness for 19 PNe studied by our group and 12 PNe analysed by Garnett & Dinerstein (2001a). Nebulae in our sample are labelled with the ID numbers given in Table 14 and ‘h’ refers to Hf 2–2. The dashed line is a linear fit to all our data points, excluding NGC 6720 (‘6’).

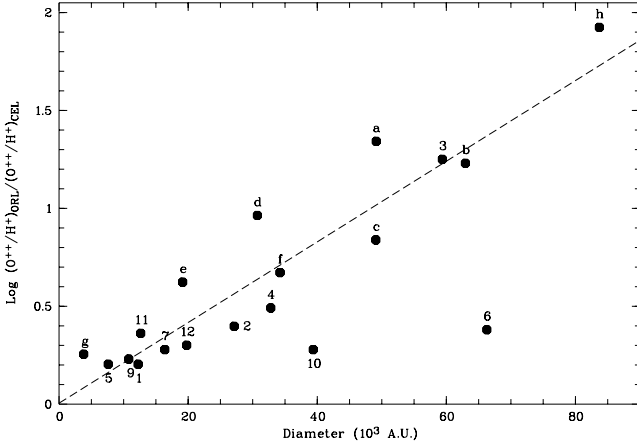


**Figure 10.**  $O^{2+}/H^+$  ADFs plotted against absolute nebular diameters. IDs for individual nebulae are given in Table 14, and ‘h’ is for Hf 2–2. The dashed line is a linear fit to all data points excluding NGC 6720 (‘6’).

nebular mean  $H\beta$  surface brightness,  $\log(I(H\beta)/\theta^2)$ , as first noted by Garnett & Dinerstein (2001a). Excluding NGC 6720, a linear fit to the 18 filled data points yields

$$\Delta \left( \frac{O^{2+}}{H^+} \right) = (0.789 \pm 0.077) - (0.561 \pm 0.106) \log \frac{I(H\beta)}{\theta^2},$$

with a linear correlation coefficient of  $-0.80$ .

NGC 6720, the Ring nebula, has an optical diameter  $\sim 76$  arcsec. A detailed spatially resolved analysis of  $O\text{ II}$  recombination lines across the Ring nebula has been carried out by Garnett & Dinerstein (2001b). They find that the  $O^{2+}$  ADF is larger in the inner, lower surface brightness region than in the outer region of the brighter shell. A similar result has been found previously for NGC 6153 (Liu et al. 2000).

Related to the previous result, Garnett & Dinerstein (2001a) also find that the ADF is positively correlated with absolute nebular diameter,  $D$ ; the larger the PN, the higher the discrepancy. Fig. 10 plots ADFs versus nebular diameters for the same sample of PNe as in Fig. 9. A linear fit to the data, excluding NGC 6720 (‘6’), yields

$$\Delta \left( \frac{O^{2+}}{H^+} \right) = (0.504 \pm 9.14) \times 10^{-2} + (2.06 \pm 0.24) \times 10^{-2} D,$$

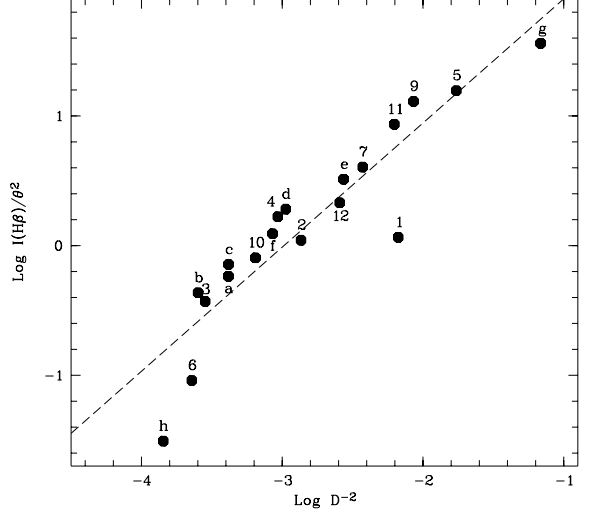


**Figure 11.** Comparison of nebular intrinsic surface brightness,  $I(H\beta)/\theta^2$ , versus  $D^{-2}$ , where  $D$  is the absolute nebular diameter. IDs for individual PNe are listed in Table 14 and ‘h’ is for Hf 2–2. The dashed line is a linear fit to the data points.

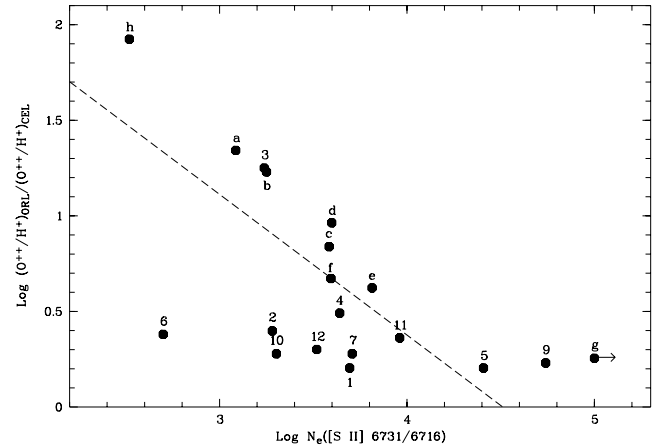


**Figure 12.**  $O^{2+}/H^+$  ADFs plotted against nebular electron density as derived from the  $[S\text{ II}] \lambda 6731/\lambda 6716$  doublet ratio. IDs for individual nebulae are given in Table 14 and ‘h’ is for Hf 2–2. The dashed line is a linear fit to the data points excluding NGC 6720 (‘6’) and NGC 7027 (‘g’).

with a linear correlation coefficient of  $0.91$ . Considering that distances to individual Galactic PNe are notoriously difficult to estimate, and consequently nebular linear diameters, the good correlation seen in Fig. 10 is remarkable.

If we assume that the total mass of ionized gas is a constant and that the nebula expands as a thin shell of constant thickness, then we expect the nebular intrinsic  $H\beta$  surface brightness to be inversely proportional to nebular diameter  $D$  squared,  $I(H\beta)/\theta^2 \propto D^{-2}$ . In Fig. 11, we plot nebular intrinsic surface brightness,  $I(H\beta)/\theta^2$ , against  $D^{-2}$ . The data show a good correlation and can be fitted by

$$\log I(H\beta)/\theta^2 = (2.86 \pm 0.29) + (0.957 \pm 0.101) \log D^{-2},$$

with a linear correlation coefficient of  $0.92$ .

In Fig. 12, we plot  $O^{2+}/H^+$  ADFs against the nebular electron density derived from the  $[S\text{ II}] \lambda 6731/\lambda 6716$  doublet ratio, for 19 PNe, including Hf 2–2 (unpublished data). Nebular  $[S\text{ II}]$  electron densities are listed in Table 17. Fig. 12 shows that the  $O^{2+}$  ADF is

anticorrelated with  $\log N_e([\text{S II}])$ . As in the case of Fig. 9, NGC 6720 shows a large departure from the general trend. For NGC 7027, the  $[\text{S II}] \lambda 6731/\lambda 6716$  ratio gives only a lower limit to the electron density. A linear fit excluding NGC 6720 and 7027 yields

$$\Delta \left( \frac{\text{O}^{2+}}{\text{H}^+} \right) = (3.32 \pm 0.64) - (0.736 \pm 0.176) \log N_e([\text{S II}]),$$

with a linear correlation coefficient of  $-0.73$ .

#### 4.6 Excitation class

E.C.s for the PNe in our sample are given in Table 17, calculated on the classification scheme proposed by Dopita & Meatheringham (1990), which makes use of the observed  $I([\text{O III}]\lambda 5007)/I(\text{H}\beta)$  intensity ratio for low- and intermediate-excitation PNe ( $\text{E.C.} \leq 5$ ) and the  $I(\text{He II}\lambda 4686)/I(\text{H}\beta)$  ratio for higher E.C. PNe. We have adopted the following formulae (Dopita & Meatheringham 1990)

$$\text{E.C.} = 0.45[I([\text{O III}]\lambda 5007)/I(\text{H}\beta)] \quad (\text{E.C.} < 5.1),$$

$$\text{E.C.} = 5.54[I(\text{He II}\lambda 4686)/I(\text{H}\beta) + 0.78] \quad (\text{E.C.} \geq 5.1).$$

For a few nebulae in our sample, the flux of the  $[\text{O III}] \lambda 5007$  line was not available, either because of limited wavelength coverage or CCD saturation. In such cases, the flux of the  $[\text{O III}] \lambda 4959$  line was used instead, assuming  $I(\lambda 5007)/I(\lambda 4959) = 2.88$ .

In Fig. 13,  $\text{O}^{2+}/\text{H}^+$  ADFs are plotted against values of E.C. The figure shows a tight anticorrelation: nebulae of lower E.C. have larger discrepancies between the ORL and the CEL abundances. A linear fit yields

$$\Delta \left( \frac{\text{O}^{2+}}{\text{H}^+} \right) = (1.40 \pm 0.15) - (0.170 \pm 0.029)\text{E.C.},$$

with a linear correlation coefficient of  $-0.82$ .

It is interesting to note that the  $\text{H II} \lambda 4686$  line is clearly present in Hf 2–2, NGC 40, M 1–42 and M 2–24, the four nebulae showing the largest ADFs, with a intensity of a few per cent of that of  $\text{H}\beta$ . Normally, helium starts to be doubly ionized only in PNe with an E.C. higher than about 4 (as determined from the intensity of the  $\lambda 5007$  line), whereas all the above four PNe have an E.C. lower than  $\sim 2$ . Clearly these nebulae have weaker CELs than expected

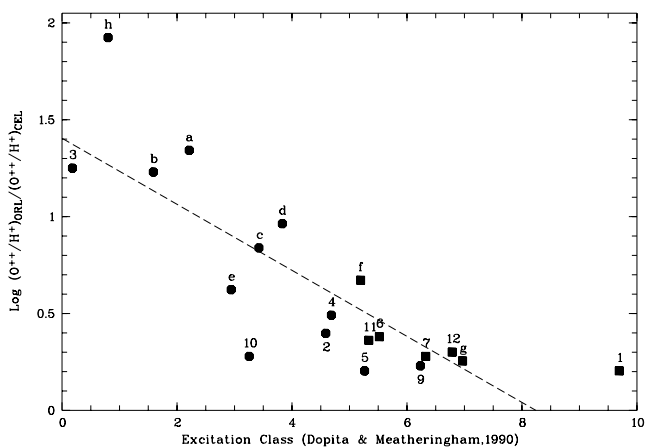


**Figure 13.**  $\text{O}^{2+}/\text{H}^+$  ADFs plotted against the E.C. of Dopita & Meatheringham (1990). ID numbers for individual nebulae are listed in Table 14 and ‘h’ is for Hf 2–2. Solid circles and squares represent E.C. determined from the  $[\text{O III}] \lambda 5007$  line and from the  $\text{He II} \lambda 4686$  line, respectively. The dashed line is a linear fit to the data points.

for these  $\text{He II} \lambda 4686$  intensities, probably as a result of enhanced cooling due to high heavy element abundances.

## 5 POSSIBLE CAUSES OF THE TEMPERATURE AND ABUNDANCE DETERMINATION DISCREPANCIES

### 5.1 Failure of the temperature fluctuation paradigm

Various mechanisms have been proposed to explain the abundance and temperature determination dichotomy. Temperature fluctuations, first proposed by Peimbert (1967) and used by Peimbert (1971) to interpret systematically lower Balmer jump temperatures compared to  $[\text{O III}]$  forbidden-line temperatures, have long been thought as an obvious solution to these two dichotomies. Given the much higher excitation energy of the  $[\text{O III}] \lambda 4363$  auroral line compared to that of the  $\lambda\lambda 4959, 5007$  nebular lines, in an inhomogeneous nebula with large temperature fluctuations, the  $\lambda 4363$  auroral line will be strongly enhanced in hotter regions, leading to a biased electron temperature, which will overestimate the actual average emission temperature of the  $\lambda\lambda 4959, 5007$  nebular lines. As a consequence, an  $\text{O}^{2+}/\text{H}^+$  ionic abundance ratio derived from the observed  $(\lambda 4959 + \lambda 5007)/\text{H}\beta$  intensity ratio, assuming the electron temperature yielded by the  $(\lambda 4959 + \lambda 5007)/\lambda 4363$  nebular to auroral line ratio, will be underestimated.

However, as shown by Liu et al. (2000, 2001b) in their detailed multiwaveband study of NGC 6153, M 1–42 and M 2–36, using high-quality spectra from the UV to the FIR, temperature fluctuations are incapable of explaining the very large differences between the electron temperature and heavy element abundances determined from the two types of emission line, i.e. CELs versus recombination lines/continuum. In particular, they have found that the large discrepancies between the ORL and CEL abundances of carbon, nitrogen, oxygen and neon do not correlate with excitation energy  $E_{\text{ex}}$  nor critical density  $N_{\text{crit}}$  of CELs from which the CEL abundances are derived – whether for IR, optical or UV lines. Very similar results are obtained from the current analysis for a sample of 12 PNe and that of Tsamis et al. (2003a,b, 2004) for a sample of Galactic and Magellanic Cloud  $\text{H II}$  regions and PNe. To summarize, the main evidence against temperature fluctuations as a viable solution to the temperature and abundance determination problem includes the following.

(i) Values of the ADF for different ions are found to be independent of excitation energy of the CELs from which CEL abundances are determined. However, in the scenario of temperature fluctuations, CELs of higher excitation energy, such as the  $[\text{O III}] \lambda\lambda 1661, 1666$  lines will be affected by a greater factor than lines of lower excitation energy, such as the  $[\text{O III}] \lambda\lambda 4959, 5007$  lines, or the  $[\text{O III}] 52\text{- and } 88\text{-}\mu\text{m}$  lines.

(ii) Owing to their very low-excitation energies [ $E_{\text{ex}} \lesssim 1 \times 10^3 \text{ K} \ll T_e([\text{O III}]_{\text{na}}) \sim 1 \times 10^4 \text{ K}$ ], the emissivities of collisionally excited IR fine-structure lines have only a weak dependence on  $T_e$ , thus ionic abundances derived from them should be insensitive to uncertainties in temperature measurement and the possible presence of temperature fluctuations. Yet they all yield ionic abundances comparable to the values given by optical and/or UV CELs. The last two rows of Table 16 and Fig. 3 compare  $\text{O}^{2+}/\text{H}^+$  abundances derived from optical forbidden lines with those deduced from IR fine-structure lines. Fig. 3 shows clearly that there is no evidence that ionic abundances derived from IR lines are systematically higher than values determined from optical forbidden lines and that there

is a good agreement between them, within 0.3 dex in most cases. Table 1 and Figs 2 and 3 show that, while most of the PNe require  $N_e$  derived from optical density-diagnostic lines to be adopted in order for the IR fine-structure lines to give abundances that are in agreement with the optical or UV CELs, for NGC 40 and 6720, it is the use of  $N_e$  deduced from the IR [O III] 88- $\mu\text{m}$ /52- $\mu\text{m}$  ratio (which agrees with  $N_e$  derived from optical lines, both being below the critical density for the IR [O III] 52- $\mu\text{m}$  fine-structure line) that leads to agreement between the IR and optical/UV CEL abundances. Analysis of another low-density nebula NGC 3132 in the sample of Tsamis et al. (2004) shows similar results. The close agreement between the ionic abundances derived from IR fine-structure lines and from optical forbidden lines, both being much lower than the corresponding values derived from ORLs, in these low-density nebulae suggests that temperature fluctuations and/or density inhomogeneities (see below) cannot be the dominant cause of the abundance discrepancies.

(iii) The electron temperature determined from the hydrogen recombination Balmer discontinuity reaches almost an order of magnitude lower than the [O III] forbidden-line temperature in the most extreme nebula Hf 2–2 and is about a factor of 3 lower in M 1–42, indicating two phases of nebular gas with vastly different physical conditions. The existence of two components of ionized gas of distinctively different electron temperatures is physically incompatible with the concept of temperature fluctuations – small, continuous spatial variations around some mean value.

To conclude, while temperature fluctuations may indeed be present in PNe and may be responsible for some of the observed characteristics of PNe (e.g. Zhang et al. 2004), they are unlikely to be the dominant cause of the large discrepancies between the electron temperatures and heavy elemental abundances derived from CELs, on the one hand, and from ORLs and recombination continua, on the other.

## 5.2 Failure of the density inhomogeneity paradigm

Density inhomogeneities with  $N_e \gtrsim 10^6 \text{ cm}^{-3}$  can lead to apparently higher [O III] forbidden-line temperatures, thus mimicking the effects of temperature fluctuations (Viegas & Clegg 1994). Such high-density clumps would also quench the emission of lines with relatively low critical densities, such as the [O III]  $\lambda\lambda 4959, 5007$  nebular lines ( $N_c \sim 10^5 \text{ cm}^{-3}$ ) and the [O III] 52-, 88- $\mu\text{m}$  and [N III] 57- $\mu\text{m}$  fine-structure lines ( $N_c \sim 10^3 \text{ cm}^{-3}$ ). Because the main effects of dense clumps on abundance determinations is mainly through the effects of the artificially overestimated electron temperature, some of the arguments developed in the previous subsection against temperature fluctuations as the major cause of temperature and abundance determination discrepancies also apply here. In particular, no correlation has been found between the ADF and the critical density of collisionally excited abundance diagnostic line. If we assume that the optical [O III] forbidden-line temperature has been overestimated because of the possible presence of dense clumps, and adopt instead the electron temperature determined from the nebular continuum Balmer discontinuity (which is not affected by the dense clumps) as the true value representing the whole nebula, then in nebulae such as NGC 6153, M 1–42 and Hf 2–2, where the Balmer temperature falls to as low as 6100, 3600 and 780 K, respectively, ionic abundances determined from UV and optical CELs become unphysically large, higher than even the values derived from ORLs. In Paper I, we showed that high-order H I Balmer lines yield electron densities comparable to the values derived from a variety of optical

forbidden-line density-diagnostic ratios, suggesting that there is no evidence for a substantial amount of normal abundance ionized gas in dense clumps with densities in excess of, say,  $10^6 \text{ cm}^{-3}$ .

## 5.3 Evidence for a cold, metal-rich, ionized gas component

Abundance gradients as a possible cause for the high ORL abundances observed in PNe were first proposed by Torres-Peimbert, Peimbert & Pena (1990) who showed that by assuming a C-rich inner zone in NGC 4361, the large discrepancy between the carbon abundances deduced from ORLs and from CELs could be reconciled. Liu (1998) mapped the surface brightness distributions of carbon ORLs using deep long-slit spectroscopy and found instead that the ORL abundance of carbon is flat across NGC 4361. Given the limited spatial resolution (a few arcsec), his observation however does not rule out the possibility of small H-deficient inclusions well mixed with the diffuse gas.

At  $T_e \sim 10^4 \text{ K}$ , collisional excitation is several orders of magnitude more efficient than recombination. However, as  $T_e$  drops, the emissivities of UV and optical CELs decrease exponentially, whereas those of ORLs increase. In their empirical analysis of NGC 6153, Liu et al. (2000) found that a two-component nebular model, with H-deficient (metal-rich) inclusions, embedded in diffuse material of ‘normal’ metallicity can account for many of the observed patterns. The metal-rich component was inferred to have a very low temperature, presumably due to enhanced cooling and emits therefore only in ORLs, with essentially no emission from CELs. In contrast, the CELs originate almost entirely from the ‘normal’ component, with a temperature of  $\sim 10^4 \text{ K}$ .

Detailed photoionization models of NGC 6153 and M 1–42, incorporating H-deficient inclusions, have been constructed by Péquignot et al. (2002, 2003) and Tylanda (2003). Because of the enhanced heavy element cooling, dominated by the IR fine-structure lines, models yield an equilibrium  $T_e$  of  $\sim 10^3 \text{ K}$  for the H-deficient component, compared to  $\sim 10^4 \text{ K}$  in the ambient gas, and a density of approximately a factor of 10 higher, so the two components are roughly in pressure equilibrium. The H-deficient inclusions contain only  $\sim 1$  per cent of the total mass and have helium and heavy element abundances similar to those derived from the empirical two-component models of Liu et al. (2000), who estimated that H : He : O  $\sim 1 : 0.4 : 0.04$  by number. The overall metallicity for the whole nebula is close to that of the ambient gas (H : He : O  $\sim 1 : 0.1 : 0.004$  by number).

The two-phase models can be tested (indirectly) if one can measure, by spectroscopy, the average  $T_e$  at which various lines are emitted. The two-phase models predict (Liu 2003)

$$T_e(\text{CNONEORLs}) \lesssim T_e(\text{He I}) \lesssim T_e(\text{BJ}) \lesssim T_e(\text{O III}),$$

with the difference between any two of these temperatures being correlated with the ORL/CEL abundance ratio. Liu (2003) compares values of  $T_e$  derived from the He I  $\lambda 5876/\lambda 4471$  and  $\lambda 6678/\lambda 4471$  ORL ratios, from the H I recombination Balmer discontinuity and from the [O III] optical forbidden-line ratio, for a number of PNe showing particularly large ADFs, including NGC 7009, M 2–36, NGC 6153, M 1–42 and Hf 2–2. He has found that  $T_e(\text{He I}) \lesssim T_e(\text{H I}) \lesssim T_e(\text{O III})$  as predicted. He has also found that O II ORLs yield even lower electron temperature than He I lines,  $T_e(\text{O II}) \lesssim 10^3 \text{ K}$ . These results indicate that ORLs from heavy element ions arise indeed from extremely cold ionized regions, and thus lend strong support to bi-abundance nebular models.

In the following subsections, we present a similar analysis for the PNe in the current sample. Electron temperatures determined from

He I and O II lines are presented and compared to values derived from other diagnostics. Given the weakness of the dependence of ORL relative intensity on electron temperature and the extreme faintness of heavy element ORLs, very accurate measurements are required. The current data set was not optimized for this purpose. The uncertainties are inevitably large. Even so, some interesting conclusions can still be drawn.

### 5.3.1 Electron temperatures from He I ORL ratios

Intensity ratios of ORLs from a given ion, including those of He I lines, have some, albeit weak, dependence on  $T_e$ , and therefore can be used to determine an average electron temperature under which the lines are emitted. The dependence is stronger for ratios involving two lines originating from two separate spectral terms of different orbital angular momentum quantum numbers of the valence electron.

Liu (2003) has determined the average electron  $T_e(\text{He I})$  for the He<sup>+</sup> recombining regions using the He I  $\lambda 5876/4471$  and  $\lambda 6678/4471$  intensity ratios for five extreme PNe previously found to show large ADF values. The two ratios are particularly useful at  $T_e < 5000$  K. He has found that, in all cases,  $T_e(\text{He I}) < T_e(\text{BJ}) < T_e([\text{O III}])$ . Interestingly, the  $\lambda 5876/4471$  ratio observed in Hf 2–2 indicates that, on average, He I ORLs in this nebula must arise from regions of electron density  $\log N_e \lesssim 4.5$  ( $\text{cm}^{-3}$ ).

For the spectra of the PNe in the current sample obtained with the William Herschel Telescope (WHT) ISIS double spectrograph, the  $\lambda 4471$  line and the  $\lambda\lambda 5876, 6678$  lines were recorded in blue-arm and red-arm spectra, respectively, and there was no overlapping in wavelength coverage between the two sets of spectra. As a result, the intensity of a blue-arm line relative to a red-arm line has to be established by either relying on the absolute flux calibration or by using other means. As described in Paper I, we have used photometric  $H\alpha/H\beta$  ratios in the literature that were measured using a large entrance aperture covering the whole nebula. To minimize effects caused by uncertainties in flux calibration, we use the He I  $2p\ ^1P^o - 3s\ ^1S\ \lambda 7281$  line in place of the  $\lambda 4471$  line. Although  $\lambda 7281$  is about a factor of 10 weaker than  $\lambda 4471$ , it has the advantage that it was recorded along with  $\lambda\lambda 5876, 6678$  on the red-arm spectrograph for our WHT observations.

In Fig. 14, we plot the  $\lambda 5876/\lambda 4471$ ,  $\lambda 6678/\lambda 4471$ ,  $\lambda 7281/\lambda 5876$  and  $\lambda 7281/\lambda 6678$  ratios as a function of electron temperature  $T_e$ , for electron densities  $\log N_e = 2, 3, 4$  and  $5$  ( $\text{cm}^{-3}$ ). Case B recombination is assumed and line emissivities are taken from Benjamin et al. (1999) and Smits (1996). Observed line ratios for five extreme PNe previously observed by Liu et al. are marked (see Liu 2003, and references therein). The  $\lambda 7281$  line flux has not been measured in Hf 2–2. Fig. 14 shows that the  $\lambda 7281/\lambda 5876$  and  $\lambda 7281/\lambda 6678$  ratios have a good sensitivity to electron temperature comparable to or even better than the  $\lambda 5876/\lambda 4471$  and  $\lambda 6678/\lambda 4471$  ratios. Except for Hf 2–2, where the  $\lambda 7281$  line has not been measured yet, for each of the other four nebulae, the four He I line ratios yield electron temperatures in good agreement, thus confirming the validity of the method and the good quality of the observations.

Note that the emissivity of the He I  $\lambda 7281$  line is sensitive to optical depths of He I resonance lines – its predicted intensity is about a factor of 2 lower for case A recombination than for case B. Thus, if there is a small departure of the He I singlet recombination spectrum from pure case B recombination towards case A,  $T_e(\text{He I})$  derived from the He I  $\lambda 7281/\lambda 5876$  and  $\lambda 7281/\lambda 6678$  ratios will be underestimated. Thus,  $T_e$  derived from these ratios in pure case

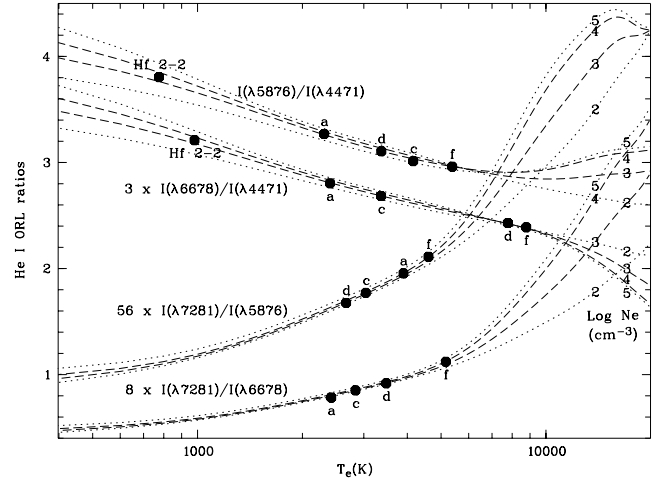


**Figure 14.** He I line ratios,  $\lambda 5876/\lambda 4471$ ,  $3 \times \lambda 6678/4471$ ,  $56 \times \lambda 7281/\lambda 5876$  and  $8 \times \lambda 7281/\lambda 6678$ , as a function of  $T_e$  for  $\log N_e = 2, 3, 4$  and  $5$  ( $\text{cm}^{-3}$ ). Observed line ratios for five extreme PNe previously observed by Liu et al. are marked (see Liu 2003, and references therein). The  $\lambda 7281$  line flux has not been measured in Hf 2–2. Case B recombination is assumed and line emissivities are taken from Benjamin et al. (1999) and Smits (1996). PNe are labelled with the ID numbers given in Table 14.

B can be as a ‘lower limit’ for  $T_e(\text{He I})$ . Liu et al. (2000, 2001a) compared the observed intensities with theoretical predictions for several He I line series in NGC 6153, M 2–36 and M 1–42 and found that the observed intensities of the  $2s\ ^1S - np\ ^1P^o$  and  $2p\ ^1P^o - ns\ ^1S$  series relative to  $\lambda 4471$  are systematically weaker than predicted case B values. They suggest that He I resonance lines are destroyed partly by photoionization of H<sup>0</sup> or absorption by dust, effectively causing a departure of the He I singlet recombination spectrum from pure case B recombination towards case A, even though the nebula is optically thick in the He I Lyman series. It is however interesting to note that in Liu et al. (2000, 2001a) the comparisons were made at much higher electron temperatures,  $T_e = 9100$  K in NGC 6153 and  $T_e = 5000$  K in M 2–36 and M 1–42. At lower temperatures, the discrepancies they noted would have been smaller.

In Fig. 15, variations of the He I  $\lambda 7281/\lambda 5876$  and  $\lambda 7281/\lambda 6678$  ratios as a function of  $T_e$  are plotted for  $\log N_e = 2, 3, 4$  and  $5$  ( $\text{cm}^{-3}$ ). Observed ratios for 14 PNe in our sample are marked. In general, the two ratios yield temperatures in reasonably good agreement. Values of  $T_e(\text{He I})$  derived from the  $\lambda 7281/\lambda 5876$  ratio are presented in Table 18.

### 5.3.2 Electron temperatures from O II ORL ratios

Like He I lines, the relative intensities of O II ORLs have some weak dependence on  $T_e$  and thus can be used to determine the average electron temperature at which the lines are emitted. In Fig. 16 the intensity ratios of the O II  $3s\ ^4P - 3p\ ^4D^o$  multiplet V1 to  $3d\ ^4F_{9/2} - 4f\ G[5]_{11/2}\ \lambda 4089$  as a function of  $T_e$  are plotted for  $\log N_e = 2, 3, 4$  and  $5$  ( $\text{cm}^{-3}$ ). For  $5000 \leq T_e \leq 20\,000$  K, the effective recombination coefficients for the O II  $3s - 3p$  and  $3p - 3d$  transitions have been calculated by Storey (1994) assuming LS-coupling, and those for the  $3d - 4f$  transitions by Liu et al. (1995) in intermediate coupling. These calculations have now been extended to temperatures as low as 100 K (P. J. Storey, private communication) and are used here in generating the curves in Fig. 16. The measured ratios for 17 PNe are marked in the figure and the temperatures yielded by the ratios are presented in Table 18.

**Table 18.** Comparison of electron temperatures derived from: (i) the ratio of O II multiplet V1 to the  $\lambda 4089$  line; (ii) the He I  $\lambda 5876/\lambda 4471$  ratio (for the five PNe previously studied by Liu et al., i.e. NGC 6153, 7009, M 1–42, M 2–36 and Hf 2–2) or the  $\lambda 7281/\lambda 5876$  ratio (for the other 14 PNe); (iii) the H I recombination continuum Balmer jump; (iv) the [O III] optical nebular to auroral line ratio.

Nebula	$T_e(\text{O II})$ (K)	$T_e(\text{He I})$ (K)	$T_e(\text{H I BJ})$ (K)	$T_e([\text{O III}])$ (K)	ADF( $\text{O}^{2+}$ )
Hf 2–2 <sup>a</sup>	2360	775	900	8820	84.0
M 1–42 <sup>a</sup>	450	2310	3560	9220	22.0
NGC 40	–	10 600 <sup>b</sup>	7020	10 600	17.8
M 2–24 <sup>c</sup>	570	2850	16300	–	17.0
NGC 6153 <sup>a</sup>	3200	3370	6080	9120	9.2
M 2–36 <sup>a</sup>	800	4160	5900	8380	6.9
NGC 7009 <sup>a</sup>	1600	5380	8150	9980	4.7
NGC 6543 <sup>d</sup>	16 300	5220	8340	7940	4.2
NGC 6210	1800	6600	9300	9680	3.1
IC 3568	4500	8100	9490	11 370	2.5
NGC 6720	7900	8290	9100	10 630	2.4
NGC 6884	8200	5500	11 550	11 000	2.3
NGC 7662	1650	7280	12 200	13 350	2.0
NGC 6826	9100	8690	9650	9370	1.9
NGC 6741	6600	6830	15 300	12 600	1.9
NGC 7027 <sup>e</sup>	7100	9260	12 800	12 600	1.8
NGC 6790	2200	8590	15 000	12 800	1.7
NGC 6572	9100	7415	11 000	10 600	1.6
Hu 1–2	–	12 560	18 900	19 500	1.6
Mean	4890	6560	10 030	10 980	–

Notes. <sup>a</sup>  $T_e(\text{He I})$ ,  $T_e(\text{BJ})$  and  $T_e([\text{O III}])$  are taken from Liu (2003). <sup>b</sup> The He I  $\lambda 5876/\lambda 4471$  ratio yields  $T_e(\text{He I}) = 6400$  K. <sup>c</sup>  $T_e(\text{BJ})$  is taken from Zhang & Liu (2003). <sup>d</sup>  $T_e(\text{BJ})$  and  $T_e([\text{O III}])$  are taken from Wesson & Liu (2004). <sup>e</sup>  $T_e(\text{BJ})$  and  $T_e([\text{O III}])$  are taken from Zhang et al. (in preparation).

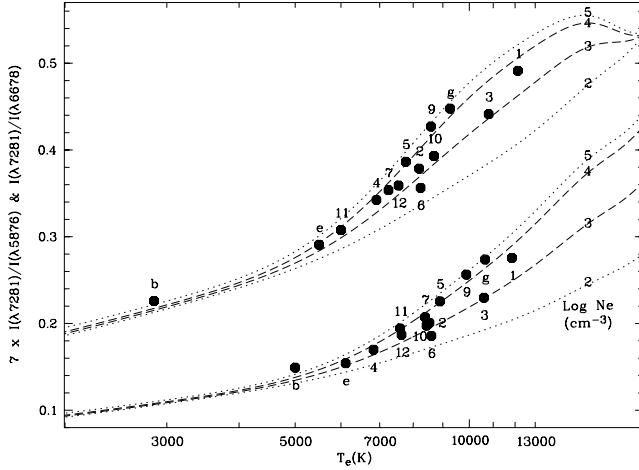


**Figure 15.** He I line ratios  $7 \times \lambda 7281/\lambda 5876$  (upper four curves) and  $\lambda 7281/\lambda 6678$  (lower four curves) as a function of  $T_e$  for  $\log N_e = 2, 3, 4$  and  $5$  ( $\text{cm}^{-3}$ ) (Smits 1996; Benjamin et al. 1999) assuming case B recombination. Observed ratios for 14 PNe in our sample are marked. Nebulae are labelled with the ID numbers given in Table 14.

### 5.3.3 Comparison of the emission temperatures from different emission lines

The values of  $T_e(\text{O II})$  and  $T_e(\text{He I})$ , derived respectively from O II and from He I ORL ratios, are compared in Table 18 to  $T_e(\text{BJ})$  derived from the hydrogen recombination continuum Balmer jump and to  $T_e([\text{O III}])$  derived from the [O III] nebular to auroral line ratio. Also given in the table are  $\text{O}^{2+}/\text{H}^+$  ADFs. As already noted by Liu (2003), Table 18 shows that in general

$$T_e(\text{CNONE ORLs}) \lesssim T_e(\text{He I}) \lesssim T_e(\text{BJ}) \lesssim T_e([\text{O III}]).$$

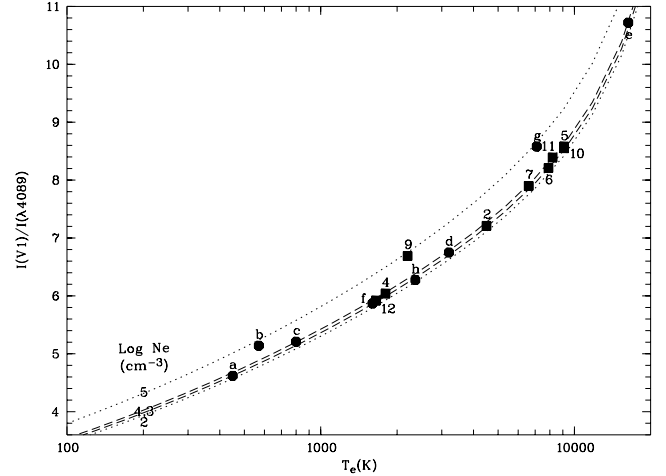


**Figure 16.** Intensity ratio of O II multiplet V1 to the 3d–4f transition  $\lambda 4089$  as a function of  $T_e$  for  $\log N_e = 2, 3, 4$  and  $5$  ( $\text{cm}^{-3}$ ) (Storey 1994; Liu et al. 1995). The observed ratios for 17 PNe are marked. Nebulae are labelled with the ID numbers given in Table 14 plus ‘h’ for Hf 2–2.

There are, however, some notable exceptions to this general pattern in Table 18. The He I temperature  $T_e(\text{He I}) = 10\,600$  K derived from the  $\lambda 7281/\lambda 5876$  ratio for NGC 40 is identical to  $T_e([\text{O III}])$  and is about 3600 K higher than the Balmer jump temperature, which is at odds with the very large ADF observed in this nebula. A comparable He I temperature of 10 800 K was obtained from the  $\lambda 7281/\lambda 6678$  ratio. On the other hand,  $\lambda 5876/\lambda 4471$  and  $\lambda 6678/\lambda 4471$  yield temperatures of 6400 and 8150 K, respectively. It seems that we may have overestimated the intensity of the  $\lambda 7281$  line in NGC 40, caused for example by dust-scattering of the WC 8 central star  $\lambda 7281$

feature. Another exception is that the O II temperature derived from the intensity ratio of multiplet V1 to  $\lambda 4089$  for Hf 2–2, while nearly 6500 K lower than the [O III] forbidden-line temperature, is about a factor of 2 higher than He I and H I Balmer jump temperatures. We note that if we use only the intensity of the strongest component of multiplet V1,  $\lambda 4649.13$ , then its ratio to  $\lambda 4089$  yields a temperature of 630 K. A similarly low temperature of 540 K is derived from the ratio of the strongest component of multiplet V10,  $\lambda 4075.86$ , to  $\lambda 4089$ . It is possible that line blending affecting the other components of multiplet V1 may have caused the high temperature yielded by the ratio of the total intensity of multiplet V1 to that of the  $\lambda 4089$  line. Alternatively, the apparently too high V1/ $\lambda 4089$  temperature may also be caused by departures of the level populations of the three fine-structure levels  $^3P_{0,1,2}$  of the ground term of the recombining  $O^{2+}$  ion from their thermalized values, leading to the underpopulation of the  $^3P_2$  level (Liu 2003). A detailed discussion of this process has been presented by Esteban et al. (2002) and Tsamis et al. (2003a). A full discussion of the extraordinary PN Hf 2–2 will be presented elsewhere.

The very low electron temperatures deduced from O II and He I ORL ratios, as first noted by Liu (2003) and shown in Table 18 (see also Wesson et al. 2003; Tsamis et al. 2004), provides strong evidence for the bi-abundance nebular model first proposed by Liu et al. (2000) for NGC 6153 and studied in some detail by Péquignot et al. (2002, 2003) and Tylanda (2003). In this scenario, a small amount of ionized H-deficient material embedded in a diffuse nebula of ‘normal’ composition emits copiously in the ORLs of helium and heavy element ions but emits essentially nothing in UV and optical CELs. This is because of the very low  $T_e$  ( $\lesssim 10^3$  K) prevailing in this metal-rich gas component, resulting in a much enhanced cooling rate controlled by the low-excitation IR lines. In other words, there are two completely different phases of ionized gas in the nebula, one of ‘normal’ composition (i.e. composition traditionally found from CEL abundance analysis) and another with much enhanced helium and heavy elemental abundances relative to hydrogen. The two gas components have radically different electron temperatures, a physical picture which differs fundamentally from that depicted by the temperature fluctuation scenario proposed originally by Peimbert (1967).

Liu et al. (2001b) showed that the ORL to CEL abundance discrepancy factor is strongly correlated with the difference between the [O III] forbidden-line temperature and the H I Balmer jump temperature. The linear fit that they obtained between the two quantities using data available at that time has already been shown in Fig. 4. In Fig. 17 we plot the  $O^{2+}/H^+$  ADF as a function of (i)  $T_e([O III]) - T_e(BJ)$ ; (ii)  $T_e([O III]) - T_e(He I)$ ; (iii)  $T_e([O III]) - T_e(O II)$ . While there is a large scatter, especially in the cases of  $T_e([O III]) - T_e(He I)$  and  $T_e([O III]) - T_e(O II)$  and for small values of ADF, a positive correlation is seen in all cases.

A linear fit between  $\Delta(O^{2+}/H^+)$  and  $\Delta T_{BJ} \equiv T_e([O III]) - T_e(BJ)$  for all the data points of the 18 PNe plotted in the figure yields

$$\Delta\left(\frac{O^{2+}}{H^+}\right) = (0.396 \pm 0.056) + (16.6 \pm 2.0) \times 10^{-5} \Delta T_{BJ},$$

with a linear correlation coefficient of 0.89. The fit is shown as a dashed line in Fig. 17.

Similarly, after excluding a few outlying points from NGC 40, 6741, 6884, 7662 and Hu 1–2, a linear fit between  $\Delta(O^{2+}/H^+)$  and  $\Delta T_{HeI} \equiv T_e([O III]) - T_e(He I)$  for the remaining 13 data points

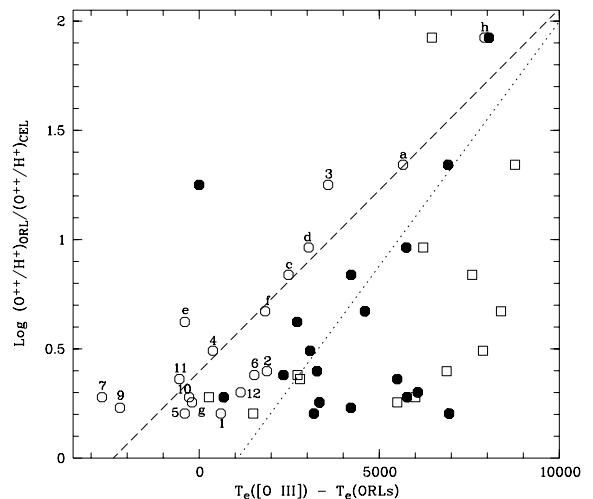


**Figure 17.**  $O^{2+}/H^+$  ADFs plotted against (i) the difference between the [O III] and Balmer jump temperatures (open circles); (ii) the difference between the [O III] and He I temperatures (filled circles); (iii) the difference between the [O III] and O II temperatures (open squares). Nebulae are labelled with the ID numbers given in Table 14 plus ‘h’ for Hf 2–2. Data points with identical ordinate values are for the same PN. The dashed and dotted lines are linear fits to the open and filled circles, respectively, but excluding NGC 40 (‘3’), NGC 6741 (‘7’), NGC 6884 (‘11’), NGC 7662 (‘12’) and Hu 1–2 (‘1’) in the latter case.

yields

$$\Delta\left(\frac{O^{2+}}{H^+}\right) = (-0.240 \pm 0.171) + (22.4 \pm 3.8) \times 10^{-5} \Delta T_{HeI},$$

with a linear correlation coefficient of 0.86. The fit is shown as a dotted line in Fig. 17. No linear regression was attempted between  $\Delta(O^{2+}/H^+)$  and  $\Delta T_{OII} \equiv T_e([O III]) - T_e(O II)$ , due to the large scatter of data. Better measurements are needed.

### 5.3.4 Nature and origin of the postulated H-deficient inclusions

We have shown that there is good evidence pointing to the existence of a metal-rich component of ionized gas, which has a very low electron temperature and produces most of the ORL emission from heavy element ions that have been observed in many PNe. The nature and origin of this new H-deficient gas component is not at all clear at the moment. H-deficient knots have been known to exist in a small number of so-called ‘born-again’ PNe, such as Abell 30 and Abell 78 (Iben et al. 1983; Jacoby & Ford 1983). Detailed ORL observations and modelling of the knots J 1 and J 3 in Abell 30 (Ercolano et al. 2003; Wesson et al. 2003) show that they share many of the observed patterns seen in extreme PNe such as Hf 2–2 (Liu 2003), M 1–42 (Liu et al. 2001b) and NGC 6153 (Liu et al. 2000), where direct observations have yet to discover the existence of such H-deficient knots. The nature of ‘born-again’ PNe and the origin of H-deficient knots detected in them remains a matter of debate (Harrington 1996). In particular, Wesson et al. (2003) show that the H-deficient knots in Abell 30 are oxygen-rich, contrary to current theoretical predictions for born-again nebulae.

Given the weakness of ORLs, spatially resolved measurements of ORLs in PNe have been carried out for only a few nebulae, including NGC 4361 (Liu 1998), NGC 6153 (Liu et al. 2000), NGC 6720 (Garnett & Dinerstein 2001b) and NGC 7009 (Luo & Liu 2003). Except for NGC 4361, heavy element abundances derived from

ORLs are found to show large radial gradients, peaking strongly at the nebular centre. In other words, the degree of discrepancy between the ionic abundances derived from these two types of emission line is also found to vary within a given nebula, and is generally largest close to the nebular centre. ORL abundances of C, N and Ne are also found to show spatial variations similar to oxygen. In NGC 7009, in addition to the central peaking, a second peak in ORL abundances has been observed at  $\sim 18$  arcsec from the central star along the major axis, near a region of very low surface brightness, approximately halfway between the bright shell and the two outlying ansae.

Recently, Ruiz et al. (2003) and Peimbert et al. (2004) have presented deep optical spectroscopy of the PNe, NGC 5307 and 5315, using an echelle spectrograph. Both nebulae are found to show modest abundance discrepancies – the ADFs for  $O^{2+}/H^{+}$  ionic abundance ratio are 1.95 and 1.74 for NGC 5307 and 5315, respectively. At a spectral resolution of  $34 \text{ km s}^{-1}$ , these authors find that in both PNe O II ORLs and [O III] CELs have comparable widths and radial velocities. Based on this, they have argued that these two nebulae cannot harbour high-velocity H-deficient knots of the type found in, for example, ‘born-again’ PN Abell 30 (Wesson et al. 2003). Interestingly, using the fibre-fed echelle spectrograph Feros mounted on the ESO 1.52-m telescope, X.-W. Liu secured in 2001 June a high-resolution spectrum of NGC 7009, which shows a large ADF of  $\sim 5$  (Liu et al. 1995). The spectrum has a spectral resolution of  $\sim 48\,000$  and an entrance aperture  $2.7$  arcsec in diameter positioned at the north-western part of the bright shell of the nebula. A preliminary analysis of the spectrum shows that both O II ORLs and [O III] CELs exhibit at least three partially resolved velocity components. The ORL to CEL intensity ratio varies significantly amongst the components. In addition, the O II ORLs are definitely narrower than [O III] CELs. These results are in strong contrast to those found by Ruiz et al. (2003) and Peimbert et al. (2004) for NGC 5307 and 5315.

Liu (2003) suggests that the hypothesized H-deficient inclusions could come from evaporation of the planetary system (planets, asteroids, comets, etc.) of the progenitor star. Given that the postulated H-deficient inclusions contain only a few Jupiter masses (Liu et al. 2000; Péquignot et al. 2002), this may not be so exotic as it sounds. After all, many stars are now known to harbour planets. If so, it may also provide an explanation for the high ORL/CEL abundance ratios observed in some H II regions (Tsamis 2002; Tsamis et al. 2003a), where protoplanetary discs around newly formed stars in the very vicinity of hot, massive young stars, which ionize the H II regions, have been found to be evaporating by the strong UV radiation fields and stellar winds from the hot stars.

The strong correlations that have been revealed in the current work and by others (Garnett & Dinerstein 2001a; Tsamis et al. 2004) indicate that the discrepancy between abundances derived from ORLs and CELs is a strong function of nebular evolution, and is most prominent in large, evolved, low-excitation PNe. Further detailed observations and analyses of those extreme PNe that show particularly large ADF values, in particular the density, mass, composition and dynamics of this postulated new H-deficient component, will be extremely useful.

## ACKNOWLEDGMENTS

We would like to thank Dr R. Rubin for a critical reading of the manuscript prior to its submission. YL thanks Y. Zhang for helpful comments.

## REFERENCES

- Acker A., Marcout J., Ochsenbein F., Stenholm B., Tylenda R., 1992, Strasbourg–ESO Catalogue of Galactic Planetary Nebulae, Parts 1 and 2. European Southern Observatory, Garching bei München
- Aller L. H., Czyzak S. J., 1983, *ApJS*, 51, 211 (AC83)
- Aller L. H., Keyes C. D., 1987, *ApJS*, 65, 405 (AK87)
- Aller L. H., Keyes C. D., Czyzak S. J., 1985, *ApJ*, 296, 492 (AKC85)
- Aller L. H., Hyung S., Feibelman W. A., 1996, *PASP*, 108, 488 (AHF96)
- Allende Prieto C., Lambert D. L., Asplund M., 2001, *ApJ*, 556, L63
- Allende Prieto C., Lambert D. L., Asplund M., 2002, *ApJ*, 573, L137
- Baessgen M., Maluck G., Grewing M., Kraemer G., 1983, *MitAG*, 60, 331 (BMGK83)
- Balick B., Perinotto M., Maccioni A., Terzian Y., Hajian A., 1994, *ApJ*, 424, 800 (BPMT94)
- Barker T., 1978a, *ApJ*, 220, 193 (B78a)
- Barker T., 1978b, *ApJ*, 221, 145 (B78b)
- Barker T., 1980, *ApJ*, 240, 99 (B80)
- Barker T., 1982, *ApJ*, 253, 167 (B82)
- Barker T., 1986, *ApJ*, 308, 314 (B86)
- Barker T., 1987, *ApJ*, 322, 922 (B87)
- Barker T., 1988, *ApJ*, 326, 164 (B88)
- Barlow M. J., Liu X.-W., Péquignot D., Storey P. J., Tsamis Y. G., Morisset C., 2003, in Kwok S., Dopita M., Wood P. R., eds, *IAU Symp. 209, Planetary Nebulae: Their Evolution and Role in the Universe*. Astron. Soc. Pac., San Francisco, p. 373
- Benjamin R. A., Skillman E. D., Smits D. P., 1999, *ApJ*, 514, 307
- Cahn J. H., Kaler J. B., Stanghellini L., 1992, *A&AS*, 94, 399
- Carrasco L., Serrano A., Costero R., 1983, *Rev. Mex. Astron. Astrofis.*, 8, 187
- Clegg R. E. S., Seaton M. J., Peimbert M., Torres-Peimbert S., 1983, *MNRAS*, 205, 417 (CSPT83)
- Dopita M. A., Meatheringham S. J., 1990, *ApJ*, 357, 140
- Ercolano B., Barlow M. J., Storey P. J., Liu X.-W., Rauch T., Werner K., 2003, *MNRAS*, 344, 1145
- Esteban C., Peimbert M., Torres-Peimbert S., Rodríguez M., 2002, *ApJ*, 581, 241
- Feibelman W. A., Aller L. H., Hyung S., 1992, *PASP*, 104, 339
- Garnett D. R., Dinerstein H. L., 2001a, *Rev. Mex. Astron. Astrofis. Ser. Conf.*, 10, 13
- Garnett D. R., Dinerstein H. L., 2001b, *ApJ*, 558, 145
- Grandi S. A., 1976, *ApJ*, 206, 658
- Grevesse N., Noels A., Sauval A. J., 1996, in *ASP Conf. Ser. 99, Cosmic Abundances*. Astron. Soc. Pac., San Francisco, p. 117
- Guerrero M. A., Machado A., Chu Y.-H., 1997, *ApJ*, 487, 328 (GMC97)
- Harrington J. P., 1996, in *ASP Conf. Ser. 96, Hydrogen Deficient Stars*. Astron. Soc. Pac., San Francisco, p. 193
- Harrington J. P., Feibelman W. A., 1983, *ApJ*, 265, 258 (HF83)
- Harrington J. P., Seaton M. J., Adams S., Lutz J. H., 1982, *MNRAS*, 199, 517 (HSAL82)
- Hawley S. A., Miller J. S., 1977, *ApJ*, 212, 94 (HM77)
- Holweger H., 2001, in *AIP Conf. Proc. 598, Joint SOHO/ACE Workshop on Solar and Galactic Composition*. American Institute of Physics, New York, p. 23
- Hyung S., Aller L. H., 1997a, *ApJ*, 491, 242 (HA97a)
- Hyung S., Aller L. H., 1997b, *MNRAS*, 292, 71 (HA97b)
- Hyung S., Aller L. H., Feibelman W. A., 1994, *MNRAS*, 269, 975 (HAF94)
- Hyung S., Aller L. H., Feibelman W. A., 1997, *ApJS*, 108, 503 (HAF97)
- Iben I. J., Kaler J. B., Truran J. W., Renzini A., 1983, *ApJ*, 264, 605
- Jacoby G. H., Ford H. C., 1983, *ApJ*, 266, 298
- Kaler J. B., 1972, *ApJ*, 173, 601
- Kaler J. B., Shaw R. A., Kwitter K. B., 1990, *ApJ*, 359, 392 (KSK90)
- Kingsburgh R. L., Barlow M. J., 1994, *MNRAS*, 271, 257
- Kisielius R., Storey P. J., 2002, *A&A*, 387, 1135
- Kwitter K. B., Henry R. B. C., 1998, *ApJ*, 493, 247 (KH98)
- Liu X.-W., 1998, *MNRAS*, 295, 699

- Liu X.-W., 2003, in Kwok S., Dopita M., Sutherland R., eds, IAU Symp. 209, Planetary Nebulae: Their Evolution and Role in the Universe. Astron. Soc. Pac., San Francisco, p. 339
- Liu X.-W., Danziger J., 1993, MNRAS, 263, 256
- Liu X.-W., Storey P. J., Barlow M. J., Clegg R. E. S., 1995, MNRAS, 272, 369
- Liu X.-W., Barlow M. J., Danziger I. J., Storey P. J., 1999, in Walsh J. R., Rosa M. R., eds, ESO Workshop on Chemical Evolution from Zero to High Redshifts. Springer-Verlag, Berlin, p. 39
- Liu X.-W., Storey P. J., Barlow M. J., Danziger I. J., Cohen M., Bryce M., 2000, MNRAS, 312, 585
- Liu X.-W. et al., 2001a, MNRAS, 323, 343
- Liu X.-W., Luo S.-G., Barlow M. J., Danziger I. J., Storey P. J., 2001b, MNRAS, 327, 141
- Liu Y., Liu X.-W., Luo S.-G., Barlow M. J., 2004, MNRAS, in press (doi:10.1111/j.1365-2966.2004.08155.x) (Paper I) (this issue)
- Luo S.-G., Liu X.-W., 2003, in Kwok S., Dopita M., Wood P. R., eds, IAU Symp. 209, Planetary Nebulae: Their Evolution and Role in the Universe. Astron. Soc. Pac., San Francisco, p. 393
- Luo S.-G., Liu X.-W., Barlow M. J., 2001, MNRAS, 326, 1049
- Maciel W. J., 1984, A&AS, 55, 253
- Mal'Kov Y. F., 1998, Astron. Rep., 42, 293 (M98)
- Manchado A., Pottasch S. R., 1989, A&A, 222, 219 (MP)
- Mathis J. S., Torres-Peimbert S., Peimbert M., 1998, ApJ, 495, 328
- Mendez R. H., Manchado A., Herrero A., 1988, A&A, 207, L5
- Middlemass D., Clegg R. E. S., Walsh J. R., 1989, MNRAS, 239, 1 (MCW89)
- Péquignot D., Amara M., Liu X.-W., Barlow M. J., Storey P. J., Morisset C., Torres-Peimbert S., Peimbert M., 2002, Rev. Mex. Astron. Astrofis. Ser. Conf., 12, 142
- Péquignot D., Liu X.-W., Barlow M. J., Storey P. J., Morisset C., 2003, in Kwok S., Dopita M., Wood P. R., eds, IAU Symp. 209, Planetary Nebulae: Their Evolution and Role in the Universe. Astron. Soc. Pac., San Francisco, p. 347
- Peimbert M., 1967, ApJ, 150, 825
- Peimbert M., 1971, Bol. Obs. Tonantzintla Tacubaya, 6, 29
- Peimbert M., Serrano A., 1980, Rev. Mex. Astron. Astrofis., 5, 9
- Peimbert M., Torres-Peimbert S., 1983, in Planetary Nebulae. D. Reidel, Dordrecht, p. 241
- Peimbert M., Torres-Peimbert S., 1987, Rev. Mex. Astron. Astrofis., 14, 540 (PTP87)
- Peimbert M., Storey P. J., Torres-Peimbert S., 1993, ApJ, 414, 626
- Peimbert M., Peimbert A., Ruiz M. T., Esteban C., 2004, ApJS, 150, 431
- Pottasch S. R., Beintema D. A., Bernard Salas J., Feibelman W. A., 2001, A&A, 380, 684 (PBBF01)
- Pottasch S. R., Hyung S., Aller L. H., Beintema D. A., Bernard-Salas J., Feibelman W. A., Klöckner H.-R., 2003a, A&A, 401, 205 (PHAB03)
- Pottasch S. R., Bernard-Salas J., Beintema D. A., Feibelman W. A., 2003b, A&A, 409, 599 (PBBF03)
- Rubin R. H., 1986, ApJ, 309, 334
- Ruiz M. T., Peimbert A., Peimbert M., Esteban C., 2003, ApJ, 595, 247
- Sabbadin F., Cappellaro E., Turatto M., 1987, A&A, 182, 305 (SCT87)
- Sawey P. M. J., Berrington K. A., 1993, Atom. Data Nucl. Data Tables, 55, 81
- Smits D. P., 1996, MNRAS, 278, 683
- Storey P. J., 1994, A&A, 282, 999
- Torres-Peimbert S., Peimbert M., Pena M., 1990, A&A, 233, 540
- Tsamis Y. G., 2002, PhD thesis, Univ. London
- Tsamis Y. G., Barlow M. J., Liu X.-W., Danziger I. J., Storey P. J., 2003a, MNRAS, 338, 687
- Tsamis Y. G., Barlow M. J., Liu X.-W., Danziger I. J., Storey P. J., 2003b, MNRAS, 345, 186
- Tsamis Y. G., Barlow M. J., Liu X.-W., Danziger I. J., Storey P. J., 2004, MNRAS, in press
- Tylenda R., 2003, in Kwok S., Dopita M., Sutherland R., eds, IAU Symp. 209, Planetary Nebulae: Their Evolution and Role in the Universe. Astron. Soc. Pac., San Francisco, p. 389
- Viegas S. M., Clegg R. E. S., 1994, MNRAS, 271, 993
- Wesson R., Liu X.-W., 2004, MNRAS, 351, 1026
- Wesson R., Liu X.-W., Barlow M. J., 2003, MNRAS, 340, 253
- Zhang Y., Liu X.-W., 2003, A&A, 404, 545
- Zhang Y., Liu X.-W., Wesson R., Storey P. J., Liu Y., Danziger I. J., 2004, MNRAS, 351, 935

This paper has been typeset from a  $\text{\TeX}/\text{\LaTeX}$  file prepared by the author.